NITROGEN EVOLUTION AND SOOT FORMATION DURING SECONDARY COAL PYROLYSIS

by

Haifeng Zhang

A dissertation submitted to the faculty of

Brigham Young University

in partial fulfillment of the requirements for the degree of

Doctor of Philosophy

Department of Chemical Engineering

Brigham Young University

April 2001

BRIGHAM YOUNG UNIVERSITY

GRADUATE COMMITTEE APPROVAL

of a dissertation submitted by

Haifeng Zhang

This dissertation has been read by each member of the following graduate committee and by majority vote has been found to be satisfactory.

Date	Thomas H. Fletcher, Chair
Date	L. Douglas Smoot
Date	Ronald J. Pugmire
Date	Kenneth A. Solen
Date	Merrill W. Beckstead

BRIGHAM YOUNG UNIVERSITY

As chair of the candidate's graduate committee, I have read the dissertation of Haifeng Zhang in its final form and have found that (1) its format, citations, and bibliographical style are consistent and acceptable and fulfill the university and department style requirements; (2) its illustrative materials including figures, tables, and charts are in place; and (3) the final manuscript is satisfactory to the graduate committee and is ready for submission to the university library.

_____ _____

Date

Thomas H. Fletcher
Chair, Graduate Committee

Accepted for the Department

_____

Kenneth A. Solen
Department Chair

Accepted for the College

_____

Douglas M. Chabries
Dean, College of Engineering and Technology

ABSTRACT

NITROGEN EVOLUTION AND SOOT FORMATION DURING SECONDARY COAL PYROLYSIS

Haifeng Zhang

Department of Chemical Engineering

Doctor of Philosophy

Economical NO_x control techniques used in pulverized coal furnaces, such as air/fuel staging, promote secondary reactions of the primary coal volatiles. Secondary reactions significantly influence the nitrogen transformations among different combustion products and the ultimate NO_x production. The major objectives of this study are to investigate the nitrogen evolution and soot formation mechanisms at high temperature, high heating rate conditions.

A $CO/H_2/O_2/N_2$ flame was operated under fuel-rich conditions in a flat flame reactor to provide a high temperature, oxygen-free post-flame environment to study secondary reactions of coal volatiles. Effects of temperature, residence time and coal rank on nitrogen evolution and soot formation were examined. Elemental compositions of the char, tar and soot were determined by elemental analysis, gas species distributions were determined using FTIR, and the chemical structure of the tar and soot was analyzed

by solid-state ^{13}C NMR spectroscopy.

Both temperature and residence time have a significant impact on the secondary reactions of tar. Coal-derived soot exhibited loss of aliphatic side chains and oxygen functional groups prior to significant growth in average aromatic ring size. Polymerization reactions accelerated at temperatures above 1400 K, leading to a larger and more interconnected cluster.

Experiments were performed on the model compounds of biphenyl and pyrene to study soot formation mechanisms for aromatic hydrocarbons. Ring opening reactions were shown to constitute the first step in the soot formation process for biphenyl, followed by ring size growth and cluster crosslinking. Little evidence of ring opening reactions was observed during the pyrolysis of pyrene.

A simple model was devised to describe the secondary reactions of coal volatiles based on the chemical structure analysis.

During secondary pyrolysis, an enrichment of nitrogen in tar was first observed, followed by a subsequent fast nitrogen release, finally decreasing at a much slower rate at high temperatures. The decay of the nitrogen functionalities in the tar is similar for all the coals in this study, indicating that reactivity of the tar nitrogen functionalities show very little rank dependence. As pyrolysis proceeded, the clusters in soot became larger and more interconnected, which retarded the further release of nitrogen. Some types of quaternary nitrogen are thought to be responsible for the earlier release of NH_3 than HCN at low temperatures. However, additional NH_3 can be formed through the interactions of HCN and other oxygen radicals in the gas phase or on a specific surface.

ACKNOWLEDGMENT

I would like to thank my academic advisor, Dr. Thomas H. Fletcher, for introducing me into the inspiring world of combustion. His guidance, support and encouragement during my studies at Brigham Young University are indeed a blessing for me. Special thanks to Dr. Philip Hanst, President of Infrared Analysis, Inc. and Ms. Jovette Caron, at ABB Bomem, Inc., for their assistance during the FTIR analysis. Appreciation is also extended to Dr. Mark Solum and Dr. Ronald J. Pugmire at the University of Utah who performed all the ^{13}C NMR analyses on the tar and soot samples, and to Dr. Bruce L. Webb at Brigham Young University who helped me with the ICP analysis.

I am grateful to Paul and Mary Goodman and Josh Wang who assisted me in the experiments in the first year. Useful discussions with Steve Perry, Jianhui Hong and Qirong Wu (Chemistry department) made this dissertation more refined and more elegant in several ways.

I gratefully acknowledge the financial support provided by the US Department of Energy through the DOE/UCR program. Funding contributed through the Advanced Combustion Engineering and Research Center (ACERC) is also appreciated.

Special thanks are expressed to my beloved parents and my sister for their unwavering support, financially and spiritually, during my 22-year journey to achieve the degree of Doctor of Philosophy. I believe this dissertation is a blessing not only for me but also for my family.

Table of Contents

List of Figures

List of Tables

Nomenclature

English Symbols

A	absorbance (unitless)
a	absorption coefficient (m^2 mole)
a	acceleration (m s^{-1})
A_a	pre-exponential factor in rate constant for additional soot formation from hydrocarbons (sec^{-1})
A_c	pre-exponential factor in rate constant for tar cracking (sec^{-1})
Al	aluminum
A_N	pre-exponential factor in rate constant for N_r decay (sec^{-1})
A_p	pre-exponential factor in rate constant for tar polymerization (sec^{-1})
Ar	Argonne
ASTM	American Society for Testing Materials
B. L.	bridges and loops per cluster
bit.	bituminous coal
BYU	Brigham Young University
C	carbon
c	concentration (mole m^{-3})
C_2H_2	acetylene
C_2H_4	ethylene
C_3H_6	propylene
C_4H_6	1,3-butadiene
C_6H_6	benzene
C_{cl}	aromatic carbons per cluster
CH_4	methane
CO	carbon monoxide
CO_2	carbon dioxide

COS	carbonyl sulfide
CPD	chemical percolation devolatilization model
CPMAS	cross-polarization and magic angle spinning
CS_2	carbon disulfide
D*	detectivity (cm $Hz^{0.5}$ W^{-1})
daf	dry, ash free basis
DOE/UCR	Department of Energy/University Coal Research
D_p	particle diameter (m)
E_a	activation energy in rate constant for additional soot formation from hydrocarbons (KJ $mole^{-1}$)
E_c	activation energy in rate constant for tar cracking (KJ $mole^{-1}$)
E_N	activation energy in the rate constant for N_r decay (KJ $mole^{-1}$)
E_p	activation energy in rate constant for tar polymerization (KJ $mole^{-1}$)
FFB	flat flame burner
FG-DVC	functional group-depolymerization, vaporization, and crosslinking model
FIMS	Field-ionization Mass Spectrometry
f_a	fraction of total sp^2-hybridized carbon
f_a'	fraction of aromatic carbon
f_a^B	fraction of carbon as aromatic bridgehead
f_a^C	fraction of carbonyl carbon
f_a^H	fraction of aromatic carbon with proton attachment
f_{al}	fraction of aliphatic carbon
f_{al}^*	fraction of carbon as CH_3 or nonprotonated carbon
f_{al}^H	fraction of carbon as CH or CH_2
f_{al}^O	fraction of carbon bonded to oxygen
f_a^N	fraction of nonprotonated aromatic carbon
f_a^P	fraction of phenolic or phenolic ether aromatic carbon
f_a^S	fraction of alkylated aromatic carbon
$f_{soot,a}$	mass fraction of total additional soot from hydrocarbons
$f_{soot,a}^*$	ultimate mass fraction of additional soot from hydrocarbons
f_{tar}	mass fraction of primary tar

$f_{tar,c}$	mass fraction of primary tar that participates in tar cracking
$f_{tar,c}^{*}$	ultimate mass fraction of primary tar eventually converted to secondary gases
$f_{tar,p}$	mass fraction of primary tar that participates in tar polymerization
$f_{tar,p}^{*}$	ultimate mass fraction of primary tar eventually converted to soot
FTIR	Fourier Transform Infrared Spectroscopy
g/cm^2-sec	gram per square centimeter per second
GC	Gas Chromatography
GRAMS/32	FTIR software developed at Galactic Industries Corporation
H	hydrogen
H_2	molecular hydrogen
H_2O	water
H_2O_2	hydrogen peroxide
HCN	hydrogen cyanide
HNCO	isocyanic acid
HP	Hewlett Packard, Inc.
hvBb	high volatile B bituminous coal
hvCb	high volatile C bituminous coal
I	intensity (W m^{-2} μm^{-1} sr^{-1})
I. D.	inner diameter (m)
I_0	incident intensity (W m^{-2} μm^{-1} sr^{-1})
ICP	Inductively Coupled Plasma
IR	Infrared
K	Kelvin
L	path length
Leco	Leco corporation, Inc.
$\dot{m}$	total mass flow rate (Kg m^{-2})
M	molecular weight
M_δ	the average molecular weight of the cluster attachments
M_{cl}	the average molecular weight of an aromatic cluster
MCT	Mercury Cadmium Telluride
mm	millimeter

ms	millisecond
$[N]_{coal}$	nitrogen content in coal
$[N]_{tar}$	nitrogen content in tar or soot
N	nitrogen
N_2	molecular nitrogen
NH_3	ammonia
NMR	Nuclear Magnetic Resonance
NO	nitrogen oxide
NO_2	nitrogen dioxide
NO_x	nitrogen oxides (including NO, NO_2 and N_2O)
NPAC	N-containing PAC
O	oxygen radical
O_2	molecular oxygen
P_0	fraction of attachments that are bridges
PAH	polycyclic aromatic hydrocarbons
PPB	parts per billion
ppm	parts per million
psi	pounds per square inch
R_∞	ultimate nitrogen ratio for tar or soot during secondary pyrolysis
r_a	reaction rate of additional soot formation from hydrocarbons
r_c	reaction rate of tar cracking
RIAS	Region Integration and Subtraction
R_N	ratio of the nitrogen content in tar over the nitrogen content in coal
r_p	reaction rate of tar polymerization
S	sulfur
S. C.	side chains per cluster
SEC	size exclusion chromatography
SEM	Scanning Electron Microscopy
Si	silicon
SiO_2	silicon oxide
SO_2	sulfur dioxide
subbit.	subbituminous coal

subC	subbituminous C coal
T	temperature
t	time
tar_N	fraction of nitrogen incorporated into tar or soot
THF	tetrahydrofuran
T_i	titanium
U. V.	Ultraviolet and Visible Spectrometry
v_∞	slip velocity between the particle and the entraining gas
wt%	weight percentage
XANES	X-ray Absorption Near-Edge Spectroscopy
XPS	X-ray Photoelectron Spectroscopy
y_{soot}	mass fraction of soot as dry, ash free coal
y_{soot}^{a}	mass fraction of ultimate additional soot formation as dry, ash free coal
y_{tar}	mass fraction of tar as dry, ash free coal
y_{tar}^{0}	mass fraction of primary tar as dry, ash free coal
z	distance (m)

Greek Symbols

$\sigma+1$	total attachments per cluster
χ_b	fraction of bridgehead carbons
μ_g	gas viscosity (Kg m^{-1} sec^{-1})
μm	micron
ρ_p	particle density (Kg m^{-3})

1. Introduction

The consumption of coal for power generation is projected to increase steadily into the new century. Coal combustion produces more NO_x per unit of energy than any other major combustion technology (Smoot, 1993). Therefore, pollutant emission associated with coal combustion will have a huge impact on the environment. NO_x (nitrogen oxides), a major pollutant from coal fired furnaces, can cause a variety of environmental and health problems such as stratospheric ozone depletion and urban smog. Consequently, the reduction of NO_x emissions is currently a major topic of coal research.

The major source of NO_x from coal combustion is the nitrogen present in the coal itself, since the production by the thermal mechanism (thermal NO_x) is effectively inhibited by regulating flame temperatures (Niksa, 1994). In commercial pulverized coal furnaces, coal nitrogen is released in three stages, as shown in Figure 1.1. Nitrogen is initially liberated with the volatiles during primary devolatilization. Primary devolatilization involves the thermal decomposition of the coal's organic structure and the release of low molecular weight volatiles. These volatiles can be divided into two parts: (a) light gases which *do not condense* at ambient temperature and pressure; and (b) tars which are comprised of relatively heavy, aromatic structures that *do condense* at ambient temperature and pressure. During primary devolatilization, nearly all the volatile-N is released with the tar (Chen and Niksa, 1992a). In the second stage of nitrogen

transformation, the volatiles undergo secondary reactions (secondary pyrolysis) in hot, fuel-rich conditions that convert part of the nitrogen in the tar into HCN (Nelson, et al. 1990; Chen, 1991; Ledesma, 1998). Since tar has a strong propensity to form soot at high temperatures and long residence times, some of the nitrogen in the tar will be incorporated into the soot. At the same time, nitrogen trapped in the char, i.e., the organic solid remaining after the initial stage of devolatilization, is expelled by thermal dissociation induced by higher particle temperatures. In the third stage, oxygen reacts with char, liberating all additional nitrogen by chemical conversion to NO_x (Pershing, 1977). All of the nitrogen released will end up in the combustion products. However, volatile-N, unlike char nitrogen, is amenable to reduction to N_2 through inexpensive techniques such as burner configuration modifications and aerodynamic control, which can reduce NO_x emission by 50-80% (Smoot, 1993).

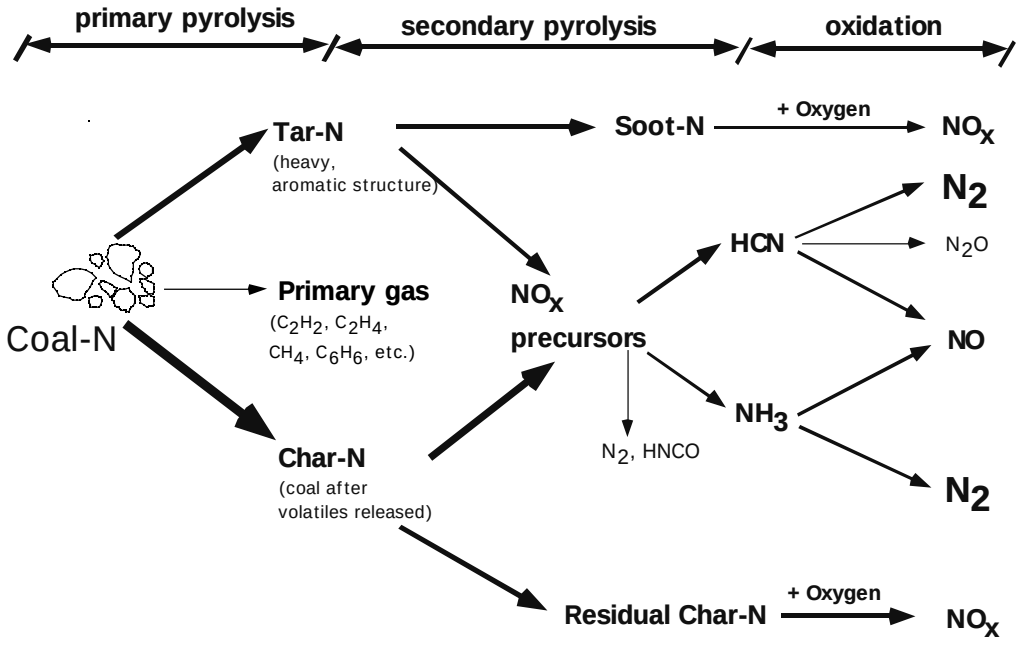

Figure 1.1. Three stages of nitrogen release during coal combustion.

The most economical combustion modification to reduce NO_x is air staging. In air staging, the combustion air is distributed at different elevations along the furnace wall to establish alternating fuel-rich and fuel-lean zones (Man, et al. 1998). Air staging promotes the conversion of volatile-N to N_2, hence minimizing NO_x formation by delaying the mixing of the air (oxygen) supply with volatile-N (Van der Lans, et al., 1997). Such delayed mixing therefore gives the primary coal volatiles (tar and light gas) ample time to undergo secondary reactions. Since aerodynamic control methods such as air staging totally rely on the availability of volatile nitrogen in the gas phase, the incorporation of tar nitrogen into soot has an adverse effect on NO_x reduction. It is clear that secondary pyrolysis significantly influences the ultimate NO_x production in industrial furnaces. Consequently, a detailed investigation into the nitrogen transformations during secondary pyrolysis and the effects of the tar-soot transition on nitrogen release is critical for design and implementation of new pollution control strategies.

Current nitrogen release models, including the CPD model at BYU (Fletcher, et al. 1992), only simulate the nitrogen release during primary pyrolysis, which occurs at relatively low temperatures (below 1200 K). However, the temperatures in the pyrolysis zones of industrial furnaces are usually much higher (1800 K). The form and partitioning of nitrogen species at high temperatures, after they are released from the char, directly determine the NO_x production in the furnace. This project intends to investigate the nitrogen transformations during secondary pyrolysis and to build a more extensive model that accounts for nitrogen release and transformations at conditions more relevant to industrial furnaces.

2. Literature Review

Previous studies on pulverized coal pyrolysis are reviewed here with emphasis on the secondary reactions of coal volatiles, the formation of NO_x precursors in the gas phase, and the effects of secondary reactions on nitrogen transformations.

General Mechanism of Coal Devolatilization

Coal pyrolysis is the first step in coal combustion and gasification. Although coal pyrolysis occurs on a time scale (up to several hundreds milliseconds) much shorter than the subsequent char oxidation process (0.5 to 2 seconds for pulverized coal), it has a huge impact on the overall combustion efficiency and pollutant production in industrial furnaces. Coal pyrolysis has been studied extensively for more than a century. However, no general mechanism is universally accepted, nor can all observations be accounted for by any single model (Chen, 1991). This is probably because of the numerous chemical and transport processes that occur simultaneously in the coal flame, making them very difficult to distinguish and interpret. In addition, coal pyrolysis is very sensitive to specific properties of coal type, which vary substantially among coal rank. In this section, fundamentals needed to interpret pyrolysis experimental data are reviewed, starting with a brief description of the chemical structure of coal, and followed by a discussion of the sequence in coal pyrolysis. Finally, previous studies on secondary reactions of coal volatiles are reviewed in detail.

Chemical Structure of Coal

Coal is mainly composed of a variety of organic structures. Coal can be viewed as a complex organic polymer consisting of large polycyclic aromatic clusters of several fused rings linked together by assorted hydrocarbon chains and bridges of varying lengths. Modern analytical techniques (NMR, FTIR, etc.) have established four major structures in coal: aromatic clusters; aliphatic bridges and loops; side chains; and oxygen groups (Chen, 1991; Smith, et al. 1994). These structures are shown in Figure 2.1.

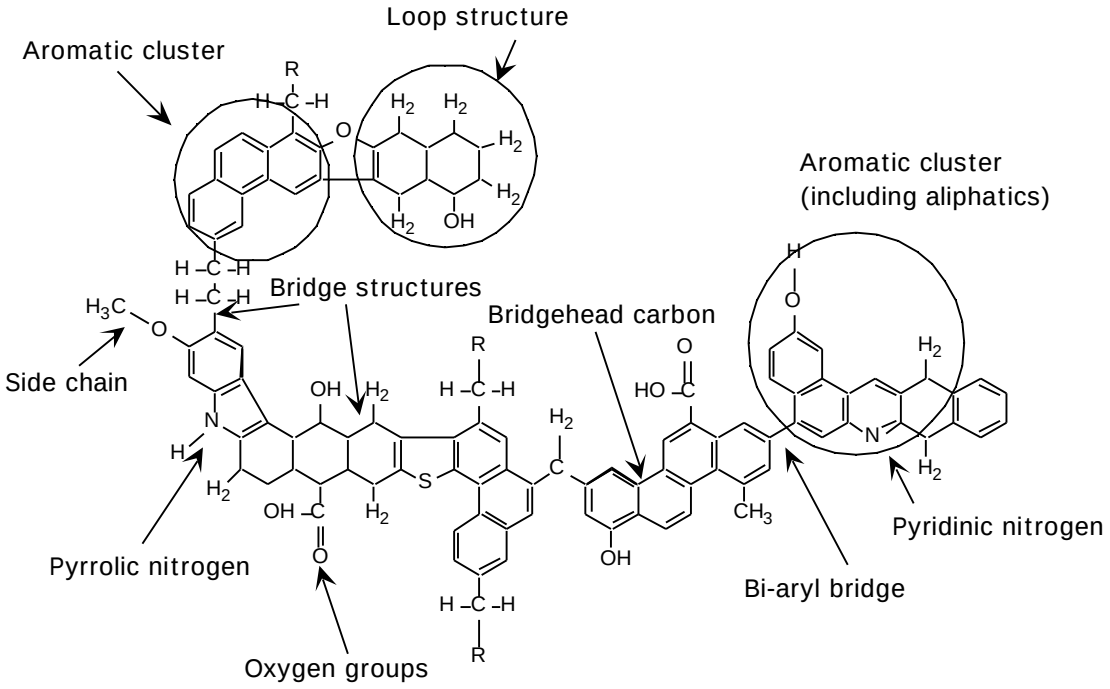

Figure 2.1. The structure of a hypothetical coal molecule (adapted from Solomon, et al. 1988).

^{13}C NMR analysis of coals has shown that the majority of the carbon in coal is aromatic (Solum, et al. 1989). The percentage of aromatic carbon (aromaticity) usually

increases with coal rank. Aromatic carbons are incorporated into various sizes of condensed rings, ranging from one to three condensed rings for lignites and subbituminous coals to two to four condensed rings for bituminous coals (Pugmire, et al. 1990). There are also aliphatic side chains and oxygen-containing functional groups at the edges of these aromatic clusters. These aromatic clusters are linked together by the aliphatic bridges or ether bridges to make a large three-dimensional macromolecular network.

Other important heteroatoms in coal are sulfur and nitrogen. Those elements generally comprise a small fraction of the organic materials, but they account for almost all the pollutants formed during coal combustion. A detailed description of the nitrogen forms in coal is presented in a later section.

Coal Pyrolysis

The observed phenomena during coal pyrolysis are not only determined by the chemical structure of the coal, but are also influenced by physical properties (particle size, moisture content) and operating conditions. Nevertheless, three main processes can be identified during coal devolatilization. (1) Upon heating, coal undergoes mild changes, including the disruption of hydrogen bonds, vaporization and release of certain noncovalently bonded molecules, and low temperature crosslinking (large aromatic fragments attaching together) in low rank coals with more than 10% oxygen (Solomon, et al. 1992). These early reactions usually occur at temperatures lower than 500 K, and are generally not very important in the whole pyrolysis process. (2) During primary pyrolysis at higher temperatures (500 K-1000 K), the weak aliphatic bridges connecting large aromatic clusters in the coal matrix are cleaved to produce molecular fragments.

Those fragments containing one to several aromatic ring structures will be released as tar if their vapor pressure is sufficiently high to escape the coal matrix. The larger fragments, too large to vaporize, will eventually undergo moderate temperature "crosslinking" reactions to attach to the char. At the same time, release of some of the functional groups attached to the aromatic clusters and some labile bridges leads to the formation of light gases, including CO, CO_2 and light hydrocarbons. (3) Secondary pyrolysis initiates when the tar and certain light gases (such as benzene and acetylene) begin to undergo further reactions in the gas phase. There are ambiguous and contradictory definitions for secondary pyrolysis in the literature (Haussmann and Kruger, 1989; Chen, 1991; Solomon, et al. 1992). In this dissertation, secondary pyrolysis is referred to as any reaction of volatiles after they leave the char particles. Figure 2.2 shows the major reaction pathways of coal during pyrolysis.

Tar is the major reactant in secondary reactions, although certain light hydrocarbons are also believed to participate in secondary pyrolysis at high temperatures. At temperatures from about 1000 K to1300 K, functional groups and side-chains attached to the aromatic rings in the tar will thermally decompose to release additional gases, usually comprising CO, CO_2, light hydrocarbons, H_2 and heteroatom species (HCN, NH_3, SO_2, COS, etc.) (Doolan, et al. 1986; Serio, et al. 1987; Xu and Tomita, 1989; Bassilakis, et al. 1993). At temperatures higher than 1200 K and prolonged residence time, the aromatic rings in the tar will attach together to form larger clusters in a process similar to the crosslinking reactions in the char. The size of the clusters will continue to grow until the identifiable soot nuclei form in the flame. It is the generation of such nuclei from the initial gas-phase reactants that initiates the soot particle inception process. These nuclei

will serve as seeds to form large soot particles through process of coagulation, agglomeration, and aggregation (Ma, 1996). The molecular weight of the final soot particles can be as high as several million amu. The hypothetical molecule of the parent coal and the succeeding pyrolysis stages from a molecular point of view are demonstrated in Figure 2.2.

Secondary Reactions of Coal Volatiles

As mentioned in the first chapter, secondary reactions play an important role in the overall coal combustion process. However, most of the previous research in the field has been devoted to primary pyrolysis. The limited studies on the secondary reactions of coal volatiles will be reviewed here in two parts: the first part discusses the formation and distribution of various gases from tar cracking reactions; the second part emphasizes soot formation in coal pyrolysis or combustion systems. Although these two parts are reviewed separately here, it should be pointed out that these two processes significantly overlap during secondary pyrolysis. It is believed that soot formation is favored at higher temperatures (Doolan, et al. 1986; Solomon, et al. 1992). The effects of secondary reactions on nitrogen release will be reviewed in the next section.

Gas Phase Cracking Reactions

The kinetics of vapor-phase secondary reactions for coal tar were studied by Serio and coworkers (Serio, et al. 1987). Their experiment consisted of two independently-heated tubular chambers connected in series. The first chamber was a fixed-bed reactor used to pyrolyze a Pittsburgh bituminous coal at a low heating rate (3^{o}C/min) to a maximum temperature of 550^{o}C. The freshly generated tar and other volatiles were pyrolyzed in the second chamber at temperatures ranging from 500-900^{o}C and residence

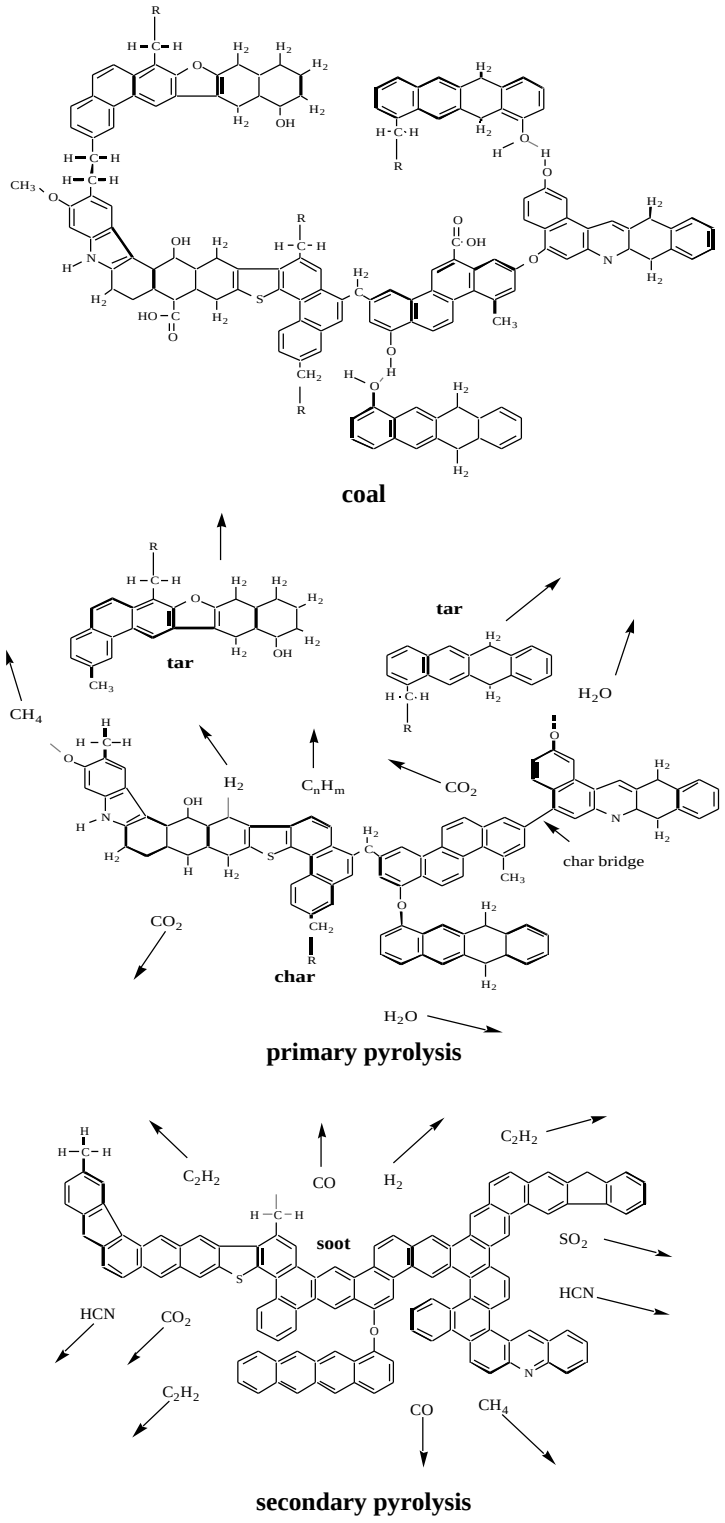

Figure 2.2. Stages of pyrolysis viewed at the molecular level (adapted from Solomon, et al. 1988).

times ranging from 0.6-3.9 s. The major products from the tar cracking were light gases (CH_4, C_2H_4, C_2H_2, etc.), light oils and some transformed tar. Higher temperatures promoted higher conversion of the tar vapors in the second reactor. Kinetic parameters for the cracking reactions were reported based on the measured data.

In a similar study, tar was generated by a fluidized-bed flash pyrolyzer from an Australian coal (Doolan, et al. 1986). The tar vapor and other gases were then cracked in two reaction systems, one using tar vapor in tubular quartz reactors at 900-1400 K and residence times of ~0.2 and ~1 s, the other using tar aerosol in a shock tube at 1100-2000 K and a residence time of 1 ms. Yields of CO and light hydrocarbons including CH_4, C_3H_6, C_2H_2, C_6H_6, were determined as a function of temperature. All of the measured gases reached a maximum yield with temperature and then declined, with the exception of C_2H_2, which increased dramatically in the temperature range 1200 K-1400 K. Pyrolytic carbon (soot) was also identified starting at about 1300 K, which is coincident with the depletion of hydrogen in the tar.

Nelson et al. (1988) investigated the pyrolysis of coal at high temperatures in fluidized bed reactors and in a shock tube. The experiments were compared with results from an experiment where tar was produced at 600^{o}C in a fluidized-bed reactor and where the tar subsequently flowed into a shock tube that operated between 600 and 800^{o}C. The gaseous hydrocarbon yields observed from secondary cracking of the tar were similar to those observed for direct pyrolysis of the same coal in a fluidized-bed pyrolyzer at 600-800^{o}C. The kinetic parameters obtained for the production of C_2H_4 and C_3H_6 from tar pyrolysis were similar to those obtained from model compounds like

hexadecane. However, the activation energies obtained for the formation of these products by direct pyrolysis of coal were much lower than from the model compounds.

A more detailed study was carried out by Xu and Tomita (1989) who treated the effects of temperature and residence time on secondary reactions separately. The distributions of inorganic gases, hydrocarbon gases and liquids by pyrolyzing nascent volatiles were carefully measured using gas chromatography. It was found that temperature and residence time exerted the most influence on secondary reactions of volatiles. Tar started to decompose at 600°C, forming aliphatics, aromatics and coke, but the yield of CO_x remained constant. At 800°C, the nature of the secondary reactions changed considerably due to soot-forming reactions. The conversion of tar to aliphatics became negligible above 800°C. The decomposition of aliphatic hydrocarbons and small aromatic oils became significant at 900°C, resulting in a continuous increase of coke formation. At this high temperature, the reported coke and soot yields were not distinguished. The kinetic parameters derived from curve-fitting their experimental data showed agreement with those observed in the pyrolysis of coal itself or in the tar pyrolysis, implying that the formation rates of hydrocarbons were similar in the above cases. This is in agreement with the findings of Nelson (1988).

The changes in molecular structure of flash pyrolysis tar generated from a subbituminous coal in a fluidized-bed reactor were analyzed by Field-Ionization Mass Spectrometry (FIMS) (Hayashi, et al. 1992). The extent of secondary reactions was regulated by an independent temperature-controlled freeboard zone in the reactor. The H/C ratio of tar was found to decrease with the increasing freeboard temperature, and the yields of CO, CO_2 and light hydrocarbons increased monotonically up to 800°C.

Analysis of the tar showed that the yields of pure aromatics and nitrogen-containing compounds increased monotonically with temperature, while hydroxyl compounds decreased.

Soot Formation Reactions

Soot can be found in almost all combustion and pyrolysis systems. Extensive research on soot formation demonstrated that soot is usually formed when the local environment is sufficiently fuel-rich to allow condensation or polymerization reactions of the fuel to compete with oxidation (Ma, 1996). In pulverized coal furnaces with staged combustion, the high temperature and the lack of oxygen by the delayed mixing promote the formation of soot. Soot impacts coal combustion in two ways. First, soot particles suspended in the combustion flame will significantly enhance radiative heat transfer due to their large surface area, small size (submicron for young soot and several hundred microns for the mature soot) and spectrally continuous radiation characteristics (Rigby, 1996). Calculations have shown that the near-burner flame temperature could be lowered up to 300 K due to the radiative heat transfer between the soot and the wall (Brown, 1998). It is therefore important to include the effects of soot in combustion models, since kinetic predictions are a strong function of temperature. Second, part of the nitrogen released from coal during devolatilization will be reincorporated into the soot, which complicates models of nitrogen transformation and NO_x production.

The limited studies on coal-derived soot are reviewed here, including the hypothesized precursors, proposed soot formation mechanisms, and the influence of local combustion parameters on soot formation.

The formation of soot from electrically-heated entrained flow pyrolysis of different coal ranks was studied by Nenninger (1986). The aerosols from the collection system were analyzed for tar and condensed ash by both extraction with methylene chloride and neutron activation analysis. The soot yields were calculated by difference. The sum of tar plus soot was reported to be constant while the soot yield increased dramatically at temperatures above 1200 K (with an equally dramatic decline in tar yield). This was the first direct evidence that tar, whose main components are polycyclic aromatic hydrocarbons, or PAH, is the soot precursor in coal systems.

Wornat and coworkers (1988a) determined the comprehensive compositions of PAH from the pyrolysis of a high-volatile bituminous coal in a drop tube reactor under sooting conditions. The results suggested that ring size and the presence of attached functional groups determine the reactivities of the PAH. Compounds with more complex attachments were more reactive than compounds with simple or no attachments. In addition, it was found that the increases in soot yield occurred at the expense of PAH yield, suggesting that PAH serves as a precursor to soot. About 20 wt% of the coal (daf) was converted to soot at high temperatures and long residence times, which is comparable with the data reported by Nenniger (20 wt%, daf) at 2200 K for a high-volatile bituminous coal.

FTIR spectra of the tar produced at high temperatures in a fluidized bed reactor showed the existence of peaks characteristic of the stretching frequency of the carbon-carbon triple bond, suggesting that alkynes generated from tar cracking reactions may participate in soot formation during higher temperatures.

A systematic characterization of temperature-induced secondary reactions of coal volatiles from a subbituminous coal and a hva bituminous coal was carried out in a radiant entrained-flow reactor (Chen, 1991). The soot formation from secondary reactions of coal volatiles was examined under inert conditions. Again, the yields of tar/oils plus soot in the high temperature experiments were reported to be relatively constant with temperature. It was hypothesized that the weight loss due to expelling CO and other gases from tars was compensated by the addition of light hydrocarbons.

Coal-derived soot was analyzed from entrained-flow pyrolysis in a post-flame environment by Ma (1996). The total soot yields decreased slightly with increased temperature for coals ranging from lignite to hva bituminous, which is inconsistent with the observations of other researchers (Nenniger, 1986; Wornat, et al. 1988a; Chen, 1991). It should be pointed out that the other three experiments were conducted in inert conditions (N_2 or argon). Certain types of oxygen-containing species in the post flame may have altered the soot yield in Ma's experiment. Because coal combustion in industrial furnaces does not occur under inert conditions, Ma's results may be more useful in evaluating soot formation mechanisms in coal systems. A more comprehensive review of soot in coal combustion systems was published by Fletcher et al. (1997), describing various experiments on coal-derived soot, measured optical properties of soot, and existing models of soot formation and oxidation.

Nitrogen Transformations during Pyrolysis

Nitrogen Functionalities in Coal

Coal-bound nitrogen resides principally in heterocyclic ring moieties (Smith, et al. 1994). The results of X-ray Photoelectron Spectroscopy (XPS) studies reveal that most

coal-N is present in pyrrolic (five-membered ring) and pyridinic (6-membered ring) groups. It was observed that pyrrolic functionalities in coals are present in much higher concentrations than pyridinic forms, and that the proportion of pyridinic-N seems to increase with coal rank (Kelemen, et al. 1993). In the XPS studies, an additional component, corresponding to quaternary nitrogen (Kelemen, et al. 1994), was often found necessary to achieve an acceptable fit to the measured XPS spectra. However, the exact nature of this functionality is still poorly understood. The XPS analysis of Argonne Premium Coals showed that quaternary nitrogen is only a small fraction of the total coal-N, and that the quaternary nitrogen content seems to decrease with coal rank (Figure 2.3).

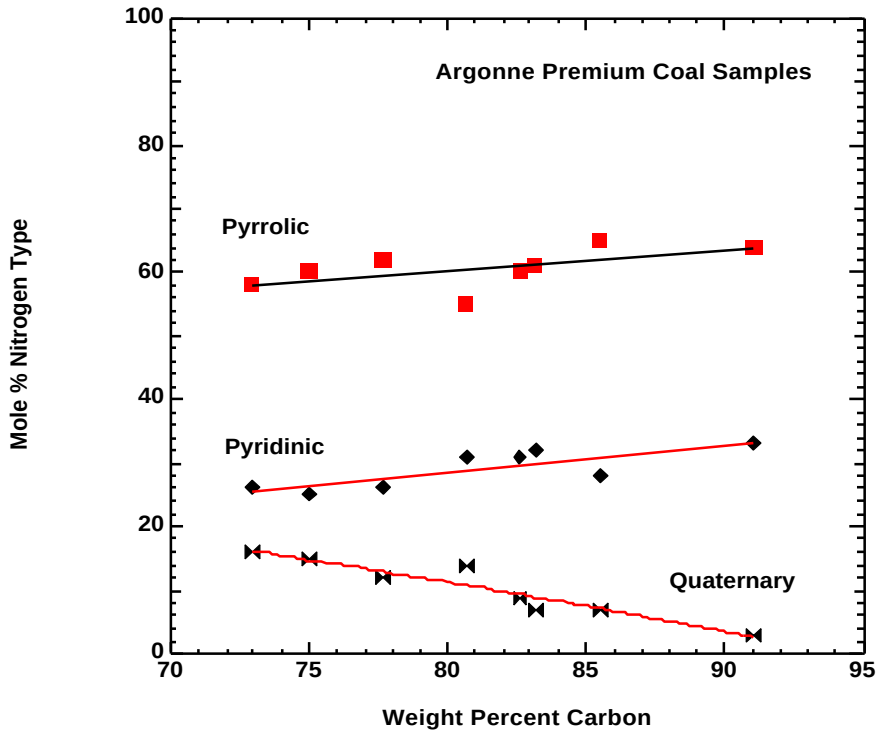

Figure 2.3. Nitrogen functional groups by XPS curve resolution analysis (adapted from Kelemen 1993).

It has been argued that quaternary nitrogen may be formed due to the oxidation of the pyridinic nitrogen to N-oxide (Nelson, et al. 1992). XPS analysis of the coal surfaces prepared by conventional wet polishing had been observed to produce an appreciable increase in the intensity of the quaternary nitrogen and a corresponding decrease in the intensity of the pyridinic nitrogen. Further studies are still required to verify the genuine structures of this class of nitrogen compounds.

Nitrogen Partitioning during Primary Pyrolysis

Primary pyrolysis is the first step during coal combustion, therefore the nitrogen release during primary pyrolysis has a huge impact on the subsequent secondary reactions. The amount of coal nitrogen released as light gases is negligible at low temperatures (Freihaut, et al. 1993; Kelemen, et al. 1993). This is probably because nearly all forms of nitrogen in coal are incorporated into aromatic ring structures, which require higher energies to react. Pyrolysis studies on N-containing aromatic model compounds have demonstrated that significant thermal decomposition would only take place at temperatures higher than 800^{o}C.

Tar is the major transport mechanism for fuel nitrogen during the initial stage of pyrolysis (Solomon and Colket, 1978; Chen, 1991). Heated grid experiments on a lignite and 12 bituminous coals at a heating rate of 600 K/s showed that for temperatures up to 600^{o}C, no significant amount of nitrogen were released. The striking similarity between the tars and the corresponding parent coals by ^{13}C NMR and infrared analysis suggested that tar-N occurs in the same structures as in the parent coal in the initial stage of devolatilization.

The effects of heating rate on both tar yield and nitrogen partitioning between various products were examined on two bituminous coals without the interference of secondary reactions (Cai, et al. 1992). The tar-N fraction increased with heating rate, since the tar yield experienced a similar increase. This may suggest that the nitrogen content in the tar is independent of heating rate and that the nitrogen structure remains almost intact during primary pyrolysis.

A detailed study of primary nitrogen release in an entrained-flow system was conducted on four coals of different rank (Chen and Niksa, 1992b). It was found that the nitrogen was initially released almost entirely in the tar. His study also demonstrated the dependence of tar nitrogen release on coal type: high rank coal, with a higher tar yield, produced more tar-N than low rank coal.

Freihaut and coworkers (1993) used a heat grid reactor and an entrained-flow reactor to examine the influence of temperature, residence time, pressure, and particle size, on coal nitrogen release. In the entrained flow experiments, the low rank coal tar contained significantly less nitrogen on a mass fraction basis than the parent coal during the initial, primary tar evolution phases. Their results showed that the nitrogen evolution behavior of low rank coals differs from that of bituminous coals both with respect to tar yield potential and intrinsic nitrogen concentration in the tar.

XPS analysis of the chars and tars obtained from pyrolyzing Argonne Premium coals showed some interesting results regarding nitrogen transformations. Pyrrolic and pyridinic species were the dominant nitrogen forms in chars and tars obtained from low temperature, low heating rate pyrolysis. However, an additional band corresponding to amino nitrogen or nitrile species was found necessary to obtain a good fit to the XPS

nitrogen spectrum for low rank coals (Kelemen, et al. 1998). Pyrolysis studies in fluidized bed reactors reported significant amount of nitrile species in the high rank coal tar, but the tars generated from an entrained-flow system did not show a nitrile band. Because it is generally believed that amino species tend to form ammonia during thermal decomposition while nitrile compounds are the main source for HCN release, further studies on the genuine nature of this additional nitrogen form are needed.

Nitrogen Transformations during Secondary Reactions

At temperatures above 1000 K and at long residence times, the volatiles released during primary pyrolysis will undergo secondary reactions. Under fuel-rich conditions, thermal cracking of the tar molecules will cause ring opening reactions, leading to the release of nitrogen in the form of light gases such as HCN (Chen, 1991). When soot formation begins at 1300 K, a portion of the nitrogen in the tar is incorporated into the soot matrix. The nitrogen incorporated into the soot is not easily reduced by the aerodynamic technologies such as air/fuel staging. The study of soot nitrogen is complicated by the nitrogen released from char at similar temperatures. As mentioned earlier, the high temperature nitrogen release from the char is considered primary pyrolysis, since it has not reacted in the gas phase.

Experiments on a hv bituminous coal showed that the N/C ratio was quite different for the tar and soot, indicating that soot is not a simple accumulation of PAH's in the tar (Wornat, et al. 1988a). Incorporation of the N-containing PAH into the soot was faster than the non N-containing PAH during the initial soot formation process. The nitrogen content of the soot was found to decrease with increasing temperature. Two mechanisms were suggested for such a decrease, including the liberation of N-containing

gas species from the soot and the incorporation of PAH with successively lower nitrogen content during soot growth. The second aspect was suggested to have a larger effect on reducing the soot N/C ratio.

As much as 25% of the volatile-N was reported to be incorporated into soot for a hv bituminous coal and 10% for a subbituminous coal (Chen and Niksa, 1992b). It was also observed that nitrogen incorporation into soot occurred early during secondary pyrolysis, and that the fraction of coal nitrogen integrated into the soot remained constant, even though the soot yield increased steadily with increasing temperature. Consequently, the nitrogen content of the soot decreased throughout secondary reactions, which is consistent with Wornat's observation. The major N species in the gas phase was found to be HCN. Haussmann et al. (1989) also reported about 20-30% of volatile-N trapped in the soot for a bituminous coal. However, pyrolysis experiments in a flat flame burner showed much less nitrogen fraction trapped in the soot, and no significant changes of nitrogen composition in the soot with residence time were noticed (Rigby, 1996).

The nitrogen functionality of the tar was examined by pyrolyzing a German bituminous coal in a fluidized bed and performing size exclusion chromatography (SEC) on different molecular mass fractions (Li, et al. 1997). The nitrile group, not present in the raw coal and the tars produced at 600 and 700^{o}C, appeared in the SEC fractions of the tar produced at 800^{o}C, which coincides with the temperature at which N-containing model compounds begin to decompose. XPS analysis of the tars also indicated the conversion of pyridinic nitrogen to nitrile nitrogen in the range of 600-800^{o}C. The presence of reactive species and H was suggested as a reason for the earlier release of

nitrogen gas species (HCN, NH_3, HNCO, etc.) from the coal than from the model compounds.

Heated grid experiments on some bituminous coals demonstrated the different nitrogen release patterns during high temperature pyrolysis (Man, et al. 1998). At relatively low temperatures (1000-1200^{o}C), volatile nitrogen (mostly contained in tar) fractional yields were approximately equal or slightly less than the total volatile yields. However, at higher temperatures (1400^{o}C above), there was additional release of nitrogen with very little total mass loss. The "secondary" nitrogen release (defined by these authors to be any reactions occurring after the primary tar release) occurred at a much slower rate than the "primary" nitrogen release. This "secondary release" was associated with a reduction of hydrogen content in the char.

Ledesma's (1998) experiment on the thermal cracking of coal tars is the only study of nitrogen release from tars free from the effects of residual char and from transport effects from the coal surface. Primary tars were generated at 600^{o}C in a fluidized reactor and subsequently thermally decomposed in a tubular reactor connected with the fluidized reactor. HCN was found to be the dominant nitrogen species from tar cracking. A considerable amount of NH_3 and HNCO was also identified. This is the only experiment where a significant amount of HNCO has been reported. The fraction of soot-N was not reported, but was likely less than 10% based on the nitrogen balance.

Recently, the N-containing PAH (NPAH) in the tars of a bituminous coal and a subbituminous coal were characterized according to their fused aromatic ring numbers using gas chromatography coupled with a chemiluminescence detector (Yu, et al. 1999). It was found that the initial depletion of N-containing species was mainly attributed to

direct conversion to soot during the early stage of secondary pyrolysis. Neutralization and mass transformation of polar compounds (carboxyl-substituted NPAH) appear to be responsible for an observed increase of NPAC in the middle stage of secondary reactions. The decrease of NPAC, after reaching a maximum at the late stage of secondary pyrolysis, indicates the successive predominance of polymerization and ring rupture reactions, which lead to the release of HCN. Yu's results also confirm the findings of Axworthy (1978), in that the stability of NPAC does not necessarily correspond to the activation energy associated with a given pyrolysis condition. 2-ring NPAC (such as quinoline) in the coal tars, assumed to form from the reaction of pyridine and acetylene, appear to be the most stable species during severe secondary pyrolysis.

Noncondensible Nitrogen Gases

Secondary reactions of tar and thermal decomposition of char at high temperatures will result in the release of nitrogen species into the gas phase. The major gas species are identified as HCN, NH_3, HNCO and N_2 (Xu and Tomita, 1989; Chen and Niksa, 1992b; Bassilakis, et al. 1993; Freihaut, et al. 1993; Li, et al. 1997; Ledesma, et al. 1998). HCN and NH_3 are by far the most important nitrogen species in pulverized coal burners and fluidized reactors, although some slow heating pyrolysis experiments on fixed bed did show N_2 as the dominant species (Axworthy, et al. 1978; Leppalahti, 1995; Takagi, et al. 1999). HNCO yields corresponding to 15% of the total volatile-N were reported in a fluidized bed pyrolysis experiment (Li, et al. 1997).

There is still controversy over the origins and interactions of HCN and NH_3 during coal pyrolysis. Some researchers believe HCN and NH_3 are generated from a similar source since the temperature of initial HCN and NH_3 formation is very close

(Nelson, et al. 1992); others assume that NH_3 is converted to HCN under severe conditions (Chen 1991; Brill, et al. 1992). Recently, more and more researchers have begun to believe that HCN may be the primary nitrogen species during pyrolysis and that NH_3 is partly formed from HCN through hydrogenation (Bassilakis, et al. 1993; Leppalahti, 1995; Rudiger, et al. 1997; Ledesma, et al. 1998; Friebel and Kopsel, 1999; Schafer and Bonn, 2000). The absence of NH_3 from the decomposition products of N-containing model compounds was explained by the lack of donatable hydrogen atoms in these aromatic compounds (Mackie, et al. 1990; Mackie, et al. 1991). Enhanced HCN conversion to NH_3 by adding small amounts of water (hydrogen donor) was also reported (Schafer, 2000). The hydrogenation of HCN to NH_3 is further complicated by the fact that more NH_3 has been found in experiments with relatively high concentrations of oxygen-containing species (O_2, O, OH, etc.) (Van der Lans, et al. 1997). The relatively higher NH_3 yield associated with low rank coals under inert conditions may be somewhat correlated with the higher oxygen content in the parent coal.

The relative amounts of HCN and NH_3 can be affected by many factors such as coal rank, heating rate, temperature, local stoichiometry and even experimental apparatus. Table 2.1 shows the list of reported HCN and NH_3 yields from different coal pyrolysis experiments.

These results can be summarized as follows: HCN is predominant in high temperature, high heating rate entrained-flow systems; however, in slow heating rate fixed bed experiments, more NH_3 is identified. Strong rank dependence of HCN and NH_3 release is demonstrated in entrained flow systems and fluidized bed experiments, with more NH_3 release for low rank coals than for high rank coals. The large variation in the

Table 2.1. Noncondensible Nitrogen Products under Pulverized Coal Combustion Conditions.

Nitrogen Products	Apparatus	Conditions
HCN is the dominant product	arc-jet fired entrained flow reactor (Haussmann, 1989)	900 ppm O_2, bit. and subbit. coal
	heated grid (Freihaut, et al. 1989)	in N_2, 14 coals
	radiant flow reactor (Chen, 1991)	inert atmosphere, 6 coals
	entrained flow reactor (Freihaut, et al. 1993)	inert atmosphere, 14 coals
	entrained flow reactor (Bassilakis, et al. 1993)	inert atmosphere, Argonne Premium coals
both HCN and NH_3 detected; HCN is the primary components with small amount of NH_3 for lower rank coals	entrained flow reactor (Blair, et al. 1976)	inert atmosphere, 20 coals
	laboratory-scale combustor (Rees, et al. 1981)	substoichiometric; bit. coals
	drop-tube reactor (Phong-Anant, et al. 1985)	in argon, subbit. and lignite
	fluidized bed (Nelson, et al. 1992)	inert atmosphere; 3 coals
	pyroprobe in an air-staged entrained flow furnace (Kambara, et al. 1995)	inert atmosphere, bit. and subbit. coals
	radiant flow reactor (Niksa,1996)	slightly oxidizing atmosphere, bit. and subbit. coals
	fluidized bed (Ledesma, et al. 1998)	inert atmosphere, bit. coal
more NH_3 is formed than HCN	electrically heated furnace (Kremer,1986)	oxidizing atmosphere; mv bit. coal
	flat-flame burner (Peck, et al. 1984)	Ar/O_2 flame, subbit. coal
	fixed bed (Leppalahti, 1995)	inert atmosphere; slow heating rate; Russian coal
	TG-FTIR (Bassilakis, et al. 1993)	inert atmosphere; Argonne Premium coals
more HCN is found in high rank coals, while the distribution of NH_3 increases towards lower rank coals, and can become larger than HCN	laboratory-scale combustor (Chen, et al. 1988)	$Ar/O_2/CO_2$; 48 coals; various stoichiometry
	fixed bed (Friebel, 1999)	inert atmosphere, low rank coals

reported HCN and NH_3 yields at various conditions shows that more understanding is needed. A simple correlation between the nitrogen functionalities in coal and the final nitrogen distributions in gas does not yet exist. Therefore, additional dedicated research is necessary on the release of HCN and NH_3 in industrially-relevant systems.

Summary

Thorough understanding of the mechanisms of nitrogen evolution and transformation during the different stages of devolatilization is essential to the comprehension and prediction of the ultimate fate of coal nitrogen during coal combustion. As a result of this literature review, the following needs for the information of coal nitrogen release are identified in order to develop a generalized coal-dependent nitrogen release model:

1) Nitrogen partitioning among the gas, tar/soot and residual char during primary and secondary coal pyrolysis
2) Nitrogen evolution rates from tar, soot and char
3) Interactions of nitrogen species in the gas, tar/soot and char

Unfortunately, after several decades of dedicated studies on NO_x control, a satisfactory and complete solution for the above issues has not yet been obtained. Data on nitrogen release during secondary pyrolysis, which process predominates in novel air-staged coal furnaces, are insufficient. Disagreement still exists regarding which species are the primary NO_x precursors during pyrolysis and combustion. Soot formation mechanisms in coal systems and the effects of soot on nitrogen transformation are not fully understood. And finally, the gas phase reactions involving nitrogen transformation still need improvement. Enhanced knowledge on the above topics is required in order to

develop realistic models of nitrogen evolution in coal combustion, which are essential for further optimization of burner design and pollutant suppression.

3. Objective and Approach

The general objective of this research is to further investigate the secondary reactions of coal volatiles under conditions relevant to commercial pulverized coal furnaces, with emphasis on nitrogen transformations and soot formation. As the research proceeded, an opportunity arose to study a few pure hydrocarbon compounds that are found in coal tar and other fuels (such as jet fuel and diesel). Therefore, a secondary objective of this study was added: to study the solids produced in the early stages of soot formation from representative model compounds.

More specifically, the effects of temperature, residence time, and coal rank on the nitrogen partitioning in the gas, tar/soot and char at high temperature (1150 K-1850 K), high heating rate entrained flow system are examined. Since a complete reaction mechanism for the conversion of stable NO_x precursors (mainly HCN and NH_3) in the gas phase to NO_x is already available (Miller, 1989), special emphasis is placed on the studies of the release rate of these nitrogen precursors during secondary pyrolysis. Soot formation mechanisms are investigated using elemental analysis and ^{13}C NMR analysis on the tar and soot generated from both coal and model compounds. The effects of tar-soot transition on nitrogen transformations are also addressed, since soot retards the conversion of NO_x to N_2 by limiting the nitrogen in the gas phase.

Four coals ranging from lignite to hva bituminous were pyrolyzed in a post-flame environment in a flat-flame reactor. Eighty pyrolysis tests were performed at seven

temperature settings and four residence times, which provide important data for deriving kinetic parameters for secondary reactions of coal volatiles. The condensed products (tar, soot and char) were collected and analyzed separately using various modern analytical techniques including elemental analysis, Inductively Coupled Plasma (ICP) and ^{13}C NMR spectroscopy. The gas phase compositions were analyzed using Fourier Transform Infrared (FTIR) Spectroscopy. The nitrogen evolution were examined both in the condensed phase and in the gas phase.

The main tasks in this project can be summarized as:

1) Determination of the tar/soot yields and mass release in coal pyrolysis under a broad range of conditions.
2) Development of PPB-level gas analysis capability for N-containing and other relevant species using an FTIR system.
3) Examination of the soot formation process from coal and from model compounds. The mechanism of nitrogen evolution during tar-soot transition is proposed based on the analysis of tar and soot from these experiments.
4) Postulation of reaction mechanisms and derivation of kinetic parameters to explain tar reduction, soot formation and nitrogen evolution.

The results obtained from this study are presented in this dissertation. Chapter 4 presents the description of how the experiments were performed. Chapter 5 presents the results of experiments regarding the secondary reactions of coal volatiles, focusing on the hydrocarbon structures. This chapter also presents results of a modeling effort to describe the experimental observations. Chapter 6 presents results of the solid-state ^{13}C

NMR analyses of tars and soots from coal and model compounds, showing changes in the chemical structures in the solid phase products during pyrolysis. Chapter 7 presents the nitrogen release and transformation data. Finally, in Chapter 8, a summary and lists of conclusions drawn from this study are presented, followed by limitations and recommendations for future work.

4. Description of Experiments

Flat Flame Burner

The flat flame burner (FFB) used in this study was described thoroughly by Ma (1996). An FTIR gas analysis system was added and used in connection with the suction probe in the FFB system to allow on-line gas measurement. Figure 4.1 shows the revised FFB system. A syringe-type particle feeder was used to provide a steady feed rate (~1 g/hr) and to allow an accurate measurement of the total amount of sample fed in each experiment. This flow rate ensured single particle behavior in the reactor. The particles from the feeder were entrained in N_2 and injected about 1 mm above the burner surface through a metal centerline tube. The temperature in the FFB can be adjusted by changing fuel type, the amount of dilution N_2, and the equivalence ratio. The calculated heating rate for pulverized coal particles can reach 10^5 K/s (Ma, 1996), which is close to particle heating rates in industrial furnaces. The entire reactor can be raised and lowered relative to the level of the sampling probe to accommodate desired residence times. All the reaction products were collected by a water-cooled probe with nitrogen quench jets at the probe tip. Nitrogen was also transpired though a porous inner wall of the probe in order to minimize soot deposition on the probe walls. A virtual impactor at the end of the suction probe was used to separate the large, dense char particles from the small and low-density soot particles. A cyclone connected behind the virtual impactor was used for char collection. The soot particles were collected on polycarbonate filters with a 1 μm pore

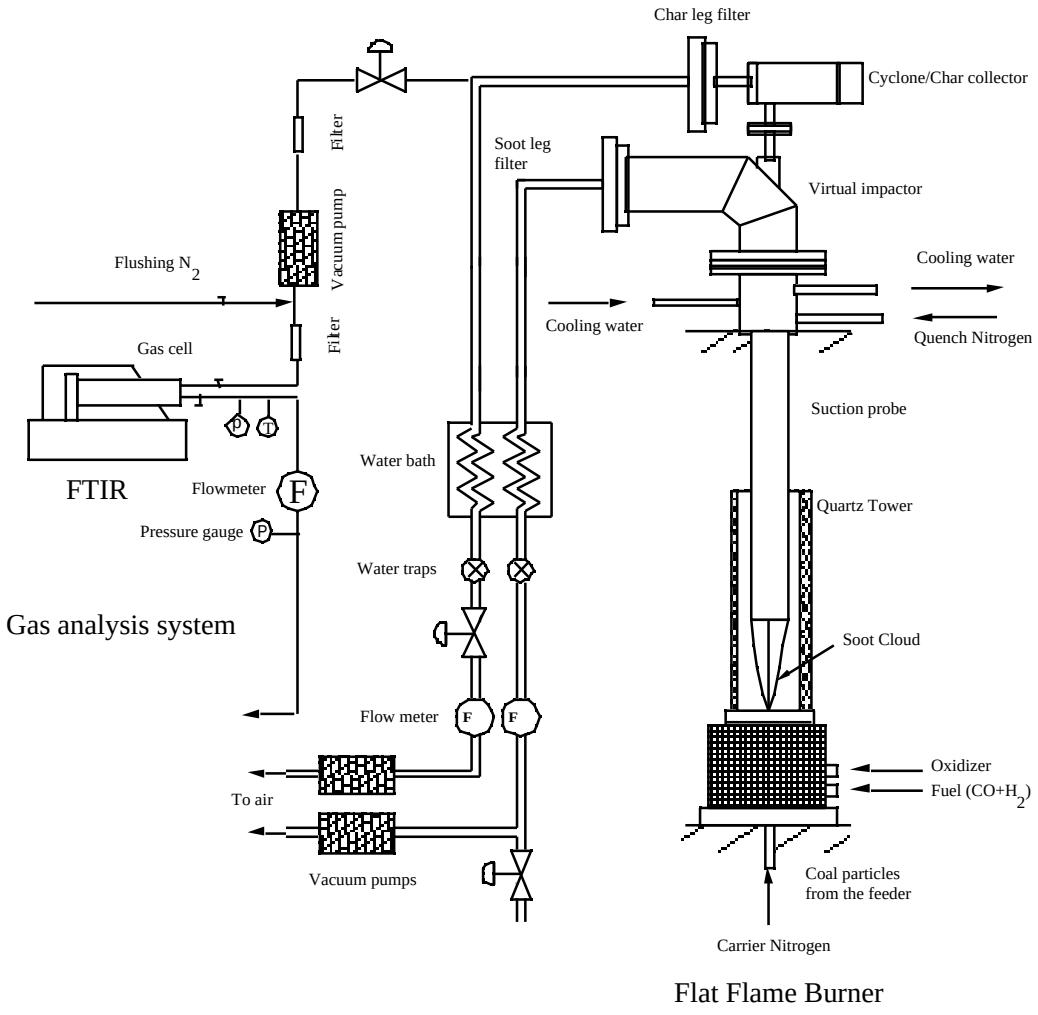

Figure 4.1. Schematic of the Flat Flame Burner (FFB) with the gas analysis system.

size, supported by a separate glass filter. Soot samples were carefully scraped from the filters to avoid the use of solvents. The reaction gas stream was collected after passing the filters and was analyzed by the FTIR to get the gas compositions. A detailed discussion on the gas phase FTIR measurement is presented in a later section.

Gas Temperature Control

Temperature is a critical parameter in coal pyrolysis. For many years, methane was used as the major fuel in the FFB to perform high temperature, high heating-rate experiments. Since the flammability limit of methane is very narrow (from 5% to 15%, volume in air), the lowest operating temperature of a fuel-rich methane flame is about 1600 K. However, significant secondary reactions usually start at a temperature as low as 1100 K for a coal system. A method was devised to lower the temperature to about 1100 K for the study of secondary pyrolysis. As a result of this study, it was found that carbon monoxide (CO) is an ideal fuel for low temperature experiments in the FFB. It has several advantages over other fuels (such as methane). First, because CO has much broader flammability limits (12.5%-75%, volume in air) than most of the common hydrocarbon fuels (2%-15%, volume in air for methane, ethane, propane etc.), the temperature of a stable CO flame can theoretically be maintained at about 1000 K even at very fuel-rich conditions. Such low temperatures can not be achieved using other hydrocarbon fuels. In practice, a small amount of hydrogen was also added to the fuel stream to enhance stability. Second, CO flames also minimize the steam production, which can greatly interfere with FTIR measurement of other weakly absorbed species. Using a CO flame, the temperature can be easily adjusted from 1100 K to 2000 K in the FFB to facilitate the pyrolysis experiments, with steam production less than 1% in the

post-flame gases. A CO monitor was used in the lab for safety reasons when the CO flame was in operation. The experiment was also performed under a safety hood to prevent CO poisoning.

Coal Selection

Coal rank is an indicator of the coalification (maturation) of a coal from a variety of plant precursors. It is well established that coal rank is one of the most important factors that determine the behavior of coal devolatilization. Temperature sensitivity of tar evolution, the tar yields and compositions are strongly correlated with coal rank (Freihaut, et al. 1993). Since secondary reactions and the involved nitrogen chemistry are directly related to tar evolution, the secondary nitrogen release is also influenced by coal rank. For example, it has been demonstrated by most researchers that ammonia formation is usually associated with lower rank coals. Consequently, four coals covering a broad range of coal ranks were employed in this study. These coals, namely Illinois #6 (Bituminous), Utah (Bituminous), Black Thunder (Subbituminous) and Knife River (Lignite), were obtained from the DOE/UCR program at the University of Utah and Brigham Young University. Figure 4.2 displays the sample positions on a coalification band plot. The O/C ratio varies from about 0.1 to 0.27, while the H/C ratio falls in a relative narrow range from 0.86 to 0.9.

Sample Preparation

All the coals were pulverized and sieved to 45-75 μm in an inert environment. Each coal sample was dried in an inert environment at 105°C for two hours prior to the experiment. Drying the samples helps to reduce the unpredictable effects of moisture on pyrolysis, and assists in achieving a steady and reproducible feed rate while avoiding

agglomeration. The coal or char samples were separately evenly using a specifically designed rotating splitter to reduce the heterogeneity, a practice suggested by Perry (1999).

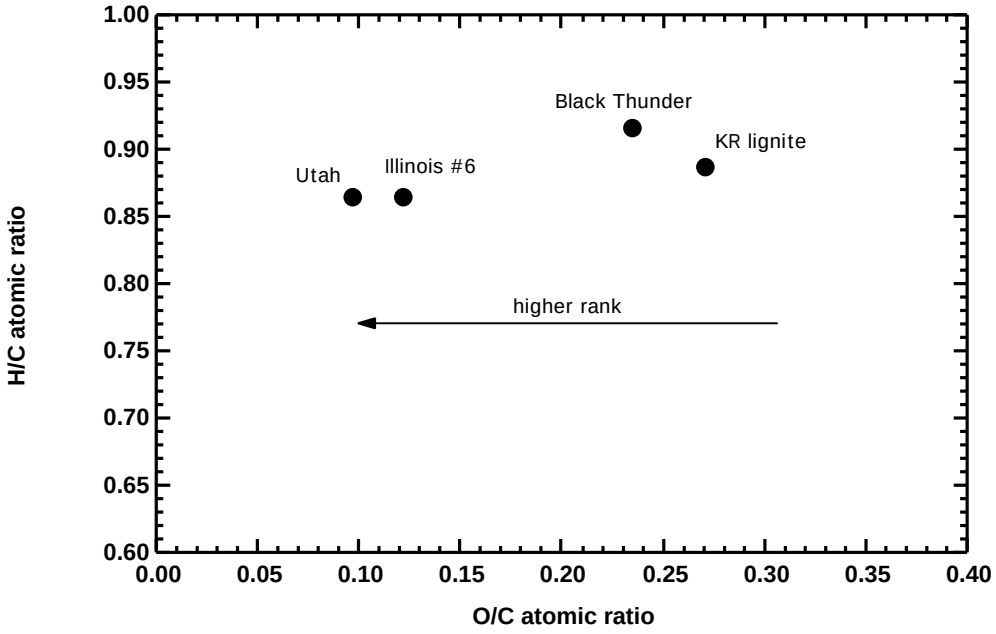

Figure 4.2. Coalification band plot of coal samples investigated.

Particle Feeder

The particle feeding system is the same one used by Ma (1996). Coal particles were contained in a 2.5 ml open-ended syringe. A syringe pump pushed the particles into a funnel, and then the entrained nitrogen flow carried the coal particles to the burner through a thin polyethylene tube (1mm I. D.). The feed rate was adjusted by changing the frequency or period of the pulse signal used for driving the step motor that operates the syringe pump. The stepping rate for all the experiments was set at 2 steps per second,

which corresponded to a particle feed rate of about 1.2 gram/hour for coals. The feed rate was then calibrated by recording the weight of the coal fed during a certain period of time. Figure 4.3 shows the cumulative coal feed versus time for Knife River coal. The profiles for other coals are similar, indicating that an excellent feed rate can be maintained at a given step frequency. The slope of the line gives the actual particle feed rate. At this feed rate, single particle behavior was obtained in the reactor, as evidenced by measurements using a high speed camera (see Chapter 5).

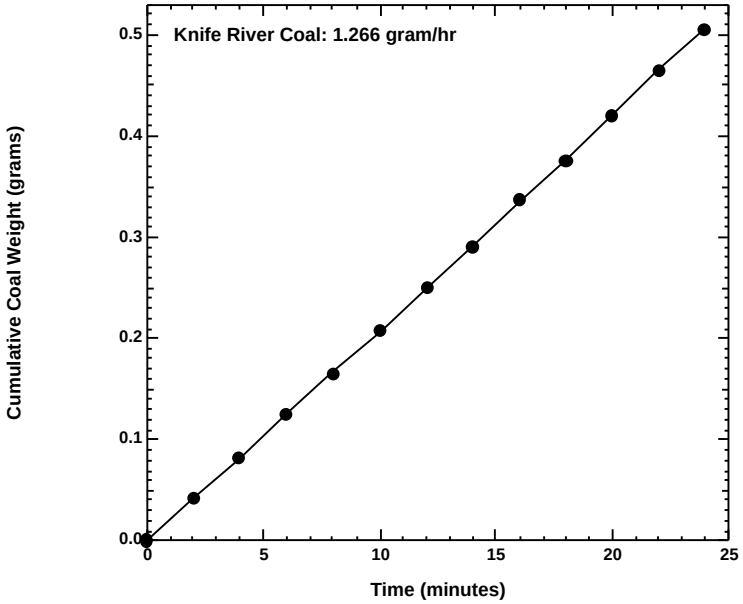

Figure 4.3. Cumulative feed of the Knife River coal.

Temperature Settings and the Corresponding Flow Rate

By shifting the fuel from methane to carbon monoxide, a much broader range of temperature settings can be achieved in the FFB simply through the manipulation of the equivalence ratio and the dilution nitrogen. Seven temperature conditions were devised in this study beginning from about 1100 K, where significant secondary reactions are

believed to start, up to about 1900 K, where previous studies have shown that the mass release from coal will complete. The corresponding flow rates of carbon monoxide, air, hydrogen (enhancing the burning of CO), dilution nitrogen, carrier nitrogen and quench nitrogen are listed in Table 4.1, along with the peak temperature and equivalence ratio.

Table 4.1. Flow Rates in the Seven Temperature Settings.

Peak gas temperature (K)	Air (slpm)	CO (slpm)	H_2 (slpm)	Dilution N_2 (slpm)	Carrier N_2 (slpm)	Quench N_2 (slpm)	Equivalence ratio
1159	9.25	9.75	0.3	6.5	0.0367	60	1.45
1281	11.25	9.75	0.3	6.5	0.0367	60	1.37
1411	13.5	9.75	0.3	6.5	0.0367	60	1.28
1534	19.5	12	0.35	10.2	0.0367	60	1.21
1618	24.5	12	0.4	8	0.0367	60	1.20
1752	23	12	0.32	6	0.0367	60	1.12
1858	24.25	12	0.32	3.5	0.0367	60	1.10

slpm: standard liters per minutes (at 1 atmosphere and 298 K)

Since nitrogen release during pyrolysis, not combustion, is studied, the equivalence ratio for each condition was maintained at a value greater than unity to ensure an oxygen-free environment. The post-flame centerline temperatures were measured in the absence of particles using a thermocouple (OMEGA® type-B) with a small bead (about 0.9 mm in diameter) as a function of height above the flat flame burner surface. The thermocouple readings were then corrected for radiative heat loss using energy balance calculations. The detailed correction procedure is presented in the Appendix C. Because the actual coal loading is so light, the measured temperature profile is believed to sufficiently describe the temperature field the coal particles were subjected to during the experiments. In this dissertation, each condition is referred to by

its peak gas temperature for the sake of convenience. The centerline temperature profiles for the seven conditions used in this investigation are presented in Figure 4.4.

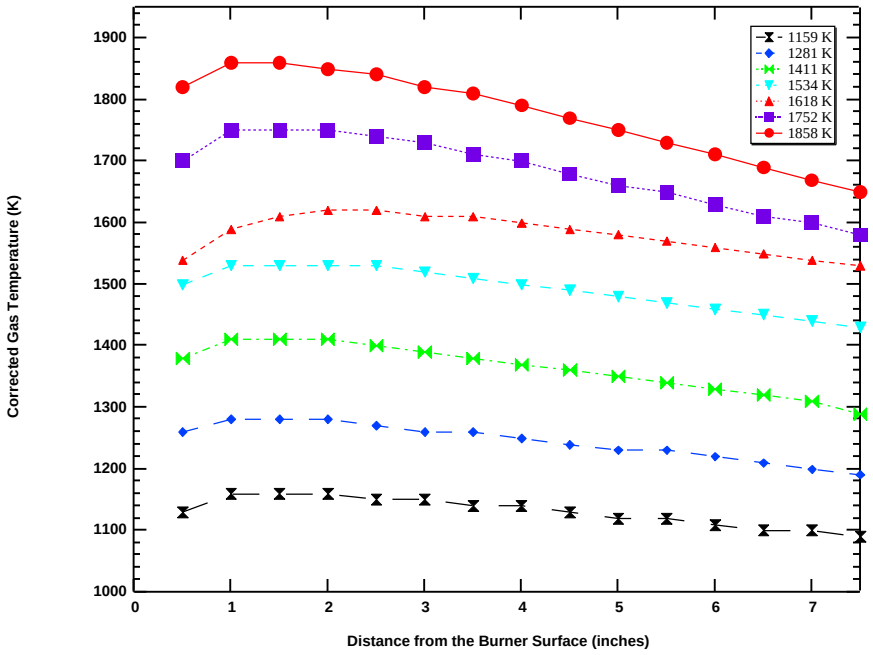

Figure 4.4. Centerline gas temperature profiles (after radiation correction).

Particle Residence Time Measurement

Product yields and compositions collected at different residence times are used to provide kinetic rates of nitrogen transformations during secondary pyrolysis. Accurate measurement of the residence time is critical in modeling the nitrogen release rate from the coal particles. For the bulk collection of the pyrolysis samples, residence time was varied by changing the position of the reactor relative to the stationary collection probe. For each temperature condition, reaction products were collected by the suction probe at four different elevations above the burner, namely 1, 3, 5 and 7 inches. However, even at

the same elevation, the residence times vary for different temperature conditions, since the total mass flow rate and temperatures were changed. A high-speed video camera (Kodak EktaPro Imager) was used to record the trajectory of single coal particles at different temperature conditions. Three recording speeds were used in the measurement: 1000 frames per second; 500 frames per second and 250 frames per second. There is a trade-off when choosing the appropriate recording speed. Higher recording speeds will give a more precise time measurement (due to a smaller time increment for each frame), however, it also requires a much stronger light source. The video images of coal particles were first stored into a memory device (Kodak EktaPro EM Processor). These images were then played back on a TV monitor. Usually three distinct particles were identified and chosen for the measurement, and the three measured values were averaged. The video images can also be transferred to a regular VHS tape for further examination. The major limitation of the residence time measurement was that the resolution of the high-speed camera was not very high (256 pixels). Therefore, only coal particles with sufficient luminance could be identified and measured on the TV screen. At the two lowest temperature conditions of 1159 K and 1281 K, no trajectories of burning particles could be seen, regardless of the recording speed. Actually, the temperatures at these conditions were so low that the coal particles could not be recognized even with the naked eye. Consequently, the residence times at these two conditions were estimated through theoretical calculations. Even at higher temperature conditions, there was still a certain distance between the tip of the coal injection tube and the first luminescent point where the residence time could not be measured directly. The residence time for this distance was also estimated by theoretical calculations (see Chapter 5). The Illinois #6

coal was chosen as the representative sample to perform the residence time measurement. The measured residence times for this coal were applied to all the other coals since it was demonstrated that the profiles of height versus residence time were similar for a broad range of coals (Ma, 1996), as long as the particle size was similar.

Experimental Test Matrix

Nitrogen evolution during the secondary coal pyrolysis is a very complicated process. Coal parameters, burner configurations and operation conditions can greatly affect the nitrogen release during coal combustion. In this study, temperature, residence time and coal rank were chosen as the test variables, since these factors exert most of the influence on the nitrogen transformation.

Temperature is one of the most important parameters that affect the nitrogen chemistry during pyrolysis, since kinetics are strongly dependent on local temperature. Previous study also showed that residence time has a significant influence on coal pyrolysis (Chen and Niksa, 1992a).

Coal rank is another important parameter to be addressed in this study. Tar evolution, its reactivity and the nitrogen release are strongly dependent on coal type (Freihaut, et al. 1989; Solomon, et al. 1990; Chen and Niksa, 1992b). The four coals used in this study have been well characterized previously and have been used extensively in industry. Therefore, the data obtained in this study can easily be compared with relevant data from the literature.

In this study, eighty pyrolysis experiments were performed in the FFB as outlined in Table 4.2. The four coals were pyrolyzed in seven different temperature conditions. Each condition is represented by its peak gas temperature after radiation correction. For

Table 4.2. Testing Matrix for FFB Experiments.

Illinois #6	1 inch	3 inch	5 inch	7 inch
1858 K		▲ (NMR)		
1752 K	▲			▲
1618 K	Δ	Δ	Δ	Δ
1534 K	Δ	▲ (NMR)	Δ	Δ
1411 K	▲	▲ (NMR)		▲
1281 K	▲	▲ (NMR)	▲	▲
1159 K	▲ (NMR)			▲

Utah	1 inch	3 inch	5 inch	7 inch
1858 K		▲		
1752 K	▲			▲
1618 K	Δ	Δ	Δ	Δ
1534 K	Δ	Δ	Δ	Δ
1411 K	▲	▲		▲
1281 K	▲	▲	▲	▲
1159 K	▲			▲

Black Thunder	1 inch	3 inch	5 inch	7 inch
1858 K	▲	▲		▲
1752 K	▲	▲		▲
1618 K	▲	▲		▲
1534 K	▲	▲	▲	▲
1411 K	▲	▲		▲
1281 K	▲	▲	▲	▲
1159 K	▲			▲

Knife River	1 inch	3 inch	5 inch	7 inch
1858 K		▲		
1752 K	▲			▲
1618 K				
1534 K	▲	▲	▲	▲
1411 K	▲	▲		▲
1281 K	▲	▲	▲	▲
1159 K	▲			▲

▲: normal test with on-line gas measurement at the same time
Δ: pyrolysis experiments were performed, and tar/char were collected and analyzed in 1998, gas measurement were performed a year later after adopting a reliable procedure.
NMR: tar and soot samples were analyzed by ^{13}C NMR at the University of Utah

the Illinois #6 and Utah coals in the 1534 K and 1618 K conditions, pyrolysis experiments were performed before the FTIR analysis was available (these experiments are represented by the symbol Δ in the table). The gas analyses for the two temperature conditions were performed a year later. Although special efforts were made to duplicate the experimental conditions, the data obtained in these two conditions are not so accurate as those obtained at other conditions where the pyrolysis experiments and gas analysis were performed at the same time.

Solid-state ^{13}C NMR analysis of the tar and char collected at different reaction severity has previously been performed to provide critical information regarding the chemical structure changes at various stages of devolatilization (Fletcher, et al. 1990; Hambly, 1998: Perry, 1999). It has been shown that nitrogen release during primary pyrolysis is directly associated with the chemical structures of the char (Perry, et al. 2000). Consequently, one would expect that the changes of chemical structures of the tar should also help us to better understand the mechanism governing the nitrogen liberation from tar during secondary pyrolysis. The tar and soot samples collected at five conditions using Illinois #6 coal were therefore analyzed by ^{13}C NMR at the University of Utah. A discussion of the NMR analysis will be presented in Chapter 6.

Because of the time required to perform experiments, sample collection was only repeated for the Illinois #6 coal at the 1 inch height for the 1159 K case and at the 3 inch height for the 1534 K case. However, repeat elemental analyses were performed on all the solid products. ICP analysis on the chars and FTIR analysis on the gas phase were also repeated to evaluate the variations of the results in this study. A detailed discussion

of the repeatability of the current study is presented in the section of error analysis in Appendix E.

Pyrolysis of Model Compounds

Two aromatic model compounds, biphenyl and pyrene, were pyrolyzed in the FFB to generate tar and soot samples for subsequent ^{13}C NMR analysis. Of major importance in this study is the transformation of aromatic hydrocarbons to PAH to soot, and at what temperature this occurs for different soot precursors. The starting model compounds were obtained from the Aldrich Chemical Company.

During the experiment, it was found that the particle feed system, originally designed for feeding coal particles, could not handle the model compounds. The organic compounds, when ground to the approximate size of the coal particles (~50 μm), were almost impossible to inject directly into the reactor because the particles adhered to the wall of the funnel and to the polyethylene transport tubing connecting the funnel and the reactor. Coal particles can be transported smoothly into the reactor because of the mineral matter in the coal. The mineral matter helps to reduce the surface tension or electrostatic forces between the particles and the wall. Pyrene and biphenyl particles become very sticky due to electrostatic forces when ground to small sizes. In this study, an inorganic compound was mixed with the model compounds and then ground to fine powders ranging from 45-75 μm to produce a mixture to be used in the existing particle feeding system. Several inorganic compounds were tested, and silica gel was found to work well. Silica gel (SiO_2, a major component in coal mineral matter) will not be pyrolyzed or vaporized under the desired temperature conditions (1160 K to 1470 K). The SiO_2 shows no color when injected into the hot flame, so there is no interference with

the luminescent yellow cloud produced by soot particles. The luminosity caused by radiation from soot particles is the easiest way to identify the formation of soot in a combustion system. Other inorganic salts do exhibit colors because they contain certain glowing metals. The model compounds, when mixed with silica gel, were easily transported into the reactor through the connection line. In addition, silica gel has a much higher density than soot particles, therefore, it can be separated in a similar fashion as coal char by the virtual impactor and the cyclone.

However, some problems were also identified during the model compound experiments. It was found that the fraction of silica gel deposited with soot on the soot filters could be significant at certain conditions. A detailed discussion on this problem is presented in a later section. The elemental analyses of the soot samples from model compounds were performed at BYU, and a correction was made to account for ash contamination in the soot. The Illinois #6 coal and coal soots were also analyzed by Galbraith Laboratories in Knoxville, Tennessee, as a means of independent verification of the BYU analysis.

Sample Characterization

Separation of Soot from Char

In experiments conducted at the highest temperatures (>1752 K) and the longest residence times, significant amounts of black and low-density powders were found mixed with the char in the cyclone of the collection system. By shaking the vial containing the samples in the cyclone, a totally dark layer was found sitting on top of a gray layer. The top layer was mainly soot particles, as evidenced by the elemental analysis (85-98% carbon) and certain physical characteristics such as density and strong electrostatic property. The bottom layer was mainly char particles, although sometimes nearly white

ash-rich particles were also identified. The existence of soot particles in the cyclone was also reported by Ma (1996). The virtual impactor used for the char/soot separation in the FFB was designed based on the assumption that the soot particles should be smaller than 5 μm. Since the soot agglomerates generated in this system at high temperatures can be as large as 20 μm, it is not surprising that the virtual impactor failed to separate soot from char efficiently. A complete separation of soot from char is essential in order to get an accurate soot yield and elemental analysis of the final soot and char.

A gravity separation of soot from char simply by shaking the mixture in a vial was described by Ma. However, the soot particles near the interface of the two layers were very hard to remove, and a complete separation was almost impossible. A quantitative soot and char separation was also conducted on a fly ash sample containing certain amount of soot and char (Veranth, et al. 1998). The sample was dispersed in ethyl alcohol by ultrasonic agitation. Through a series process of settling and decanting with fresh ethyl alcohol, the carbon found in the final supernatant fraction was assumed to be soot and the carbon in the bottom fraction of the separation was assumed to be char. Since both soot and char are organic in nature, the use of organic solvents in the separation will inevitably introduce errors. The solvent can also change the physical and chemical properties of soot and char, so the subsequent analysis will not be accurate in reflecting the characteristics of the original samples.

A mini-cyclone was designed to accomplish the soot/char separation in the current experiments (Figure 4.5). First, the soot/char mixture was placed into the cyclone, which is closed on one end and open on the other end. Then the mixture was stratified by gravity using a vibrator. The upper part of the soot layer, which was usually pure soot

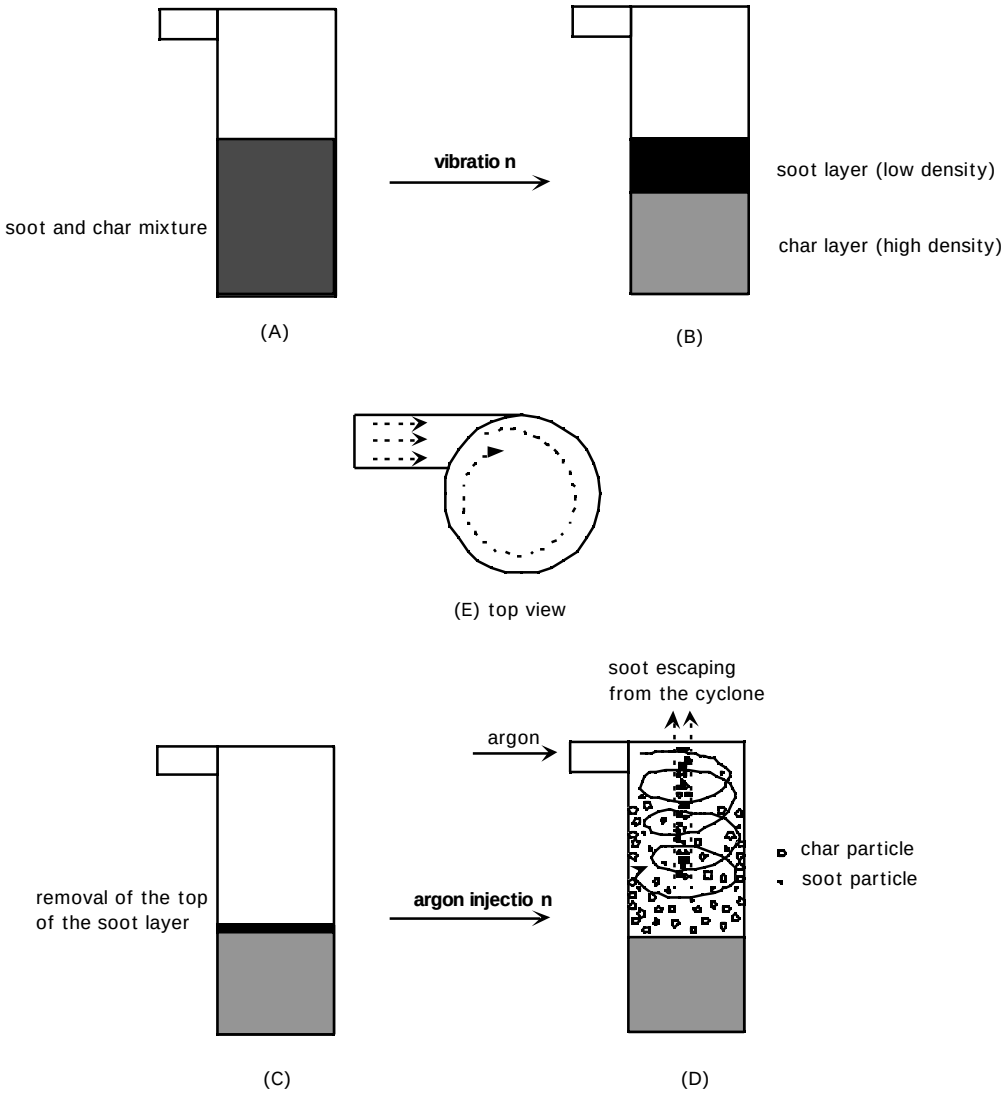

Figure 4.5. Soot/char separation using an aerodynamic method.

particles, was carefully removed by a spatula. When there was little soot left on top of the char layer, tangential argon injection was introduced at the top of the cyclone. As expected in a cyclone, the low density soot particles were first entrained with the swirl flow created by the tangential argon flow. The soot particles were then easily removed by the outgoing argon flow, while the high density char particles remained in the cyclone.

After a visual check, the remaining char was then weighted and used for further analysis. The mass fraction of soot in the mixture was estimated from a mass balance. Comparison of the elemental analysis on the separated soot and those collected on the filters showed similar results, within experimental error. The carbon content of the separated char was never higher than 80%, indicating that soot contamination was negligible.

Tar and Soot Analysis

As explained in the first chapter, the heavy, aromatic volatiles released from the coal particles that condense at room temperature are collectively termed tar. The major components of tar are large polycyclic aromatic hydrocarbons and oils (Nelson, et al. 1986). Under conditions of high temperature and long residence time, the tar has a strong propensity to form soot (black, carbon-rich solids) (Chen and Niksa, 1992b; Ma, 1996). Although any further reactions of the tar are defined as secondary reactions, the study of the transition from tar to soot (which usually occurs at 1350-1450 K) is emphasized in this study.

During the experiments, the tar-soot transition can be qualitatively illustrated by examining the condensable solids collected on the filters from the gaseous pyrolysis products. At low temperatures (under 1200 K), the coal particles in the reactor were not luminescent. The solids collected were very sticky and light yellow in color. This is a characteristic of coal tar. As the temperature increased, the color of the solids became darker and darker (from yellow to brown, then to dark brown) but less and less sticky. Finally the solids turned into jet-black powder and were highly electrostatic in nature. These solids are usually considered to be soot.

Another interesting phenomenon observed during the experiments also clearly demonstrated the difference in the size of the tar and soot (see Figure 4.6). In this study, two filters were packed together in the filter holder to collect any condensable volatiles. A polycarbonate filter (Osmonics, Inc.) with a pore size of 1 μm was placed on top of a glass microfibre filter (Whatman International, Ltd.). The tar/soot samples were easily removed from the polycarbonate filters without the use of solvents, which must be used to obtain samples from the glass fiber filters. The polycarbonate filter is a thin film with a smooth surface, so the deposits were easily scraped off using a blade. The glass filter was used as both a support for the polycarbonate filter and as a second filter to trap escaping aerosols from the first filter.

By examining the deposits on the filters, it was found that at low temperatures (below 1411 K), the particles significantly penetrated through the polycarbonate filter, leaving some deposits even on the glass filter. The lower the temperature, the more deposits were found on the glass filter. This means that some of the tar or young soot molecules were much smaller than 1 μm, as expected. However, at high temperatures (above 1752 K), the amount of soot particles that penetrated through the polycarbonate filter became negligible. The glass filter was absolutely clean at 1858 K, indicating that all the soot particles were larger than 1 μm in diameter. Scanning Electron Microscopy (SEM) analysis showed that soot agglomerates can grow as large as 20 μm in the FFB (Ma, 1996). Since large particles caused less clogging in the polycarbonate filters, longer run times were possible at high temperatures. The tar or soot yields were determined by weighing the two filters together before and after each experiment.

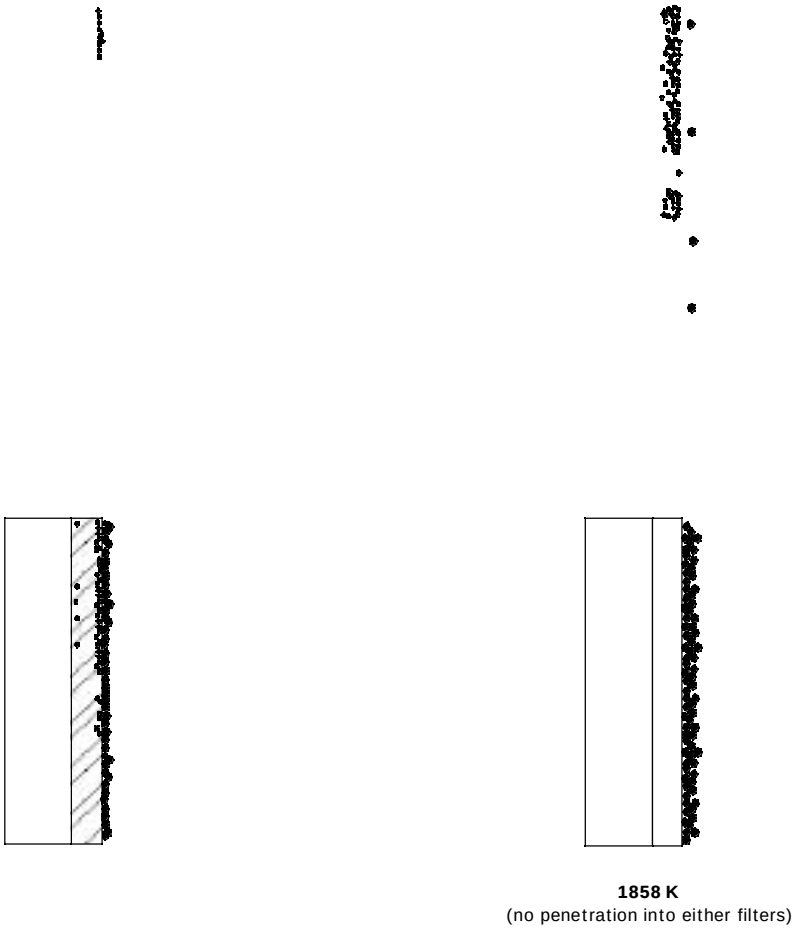

Figure 4.6. Tar/soot deposition on the filters at different temperatures.

The density of the tar is also much higher than that of the soot. Because the transition from tar to soot is a gradual process, it is extremely hard to quantitatively determine the percentage of soot existing in the solids collected on the filters. Chen and coworkers defined soot as the residue remaining after the condensed volatiles were extracted with tetrahydrofuran (THF) in an ultrasonic bath (Chen and Niksa, 1992b).

Pugmire suggested using methylene chloride to extract tar from the collected volatiles in order to determine the soot yield (Pugmire, 1999). However, both methods need large quantities of samples and are subject to errors in many aspects (temperature, extraction time, and polarity will all affect the results). In this study, the collected condensable volatiles are treated as mixtures to avoid using solvents. The volatiles deposited on the filters in this study are therefore collectively termed as tar/soot, and are analyzed together without separation. It is recommended separate examination of extracts and residues from soot/aerosol samples be included in future studies.

Ash Contamination in Tar and Soot

During the coal pyrolysis experiments, it was found that small amounts of char and ash particles were deposited with the tar and soot on the soot filters. The char particles were found on the soot filters when these particles were sufficiently small and could not be separated by the virtual impactor. The small char particles could have been formed from particle fragmentation. The ash in the tar and soot was likely caused by the recondensation of some volatile inorganics and ash, which vaporized from the char during pyrolysis (Nenniger, 1986). From the experiments of the model compounds, a significant amount of silica gel was found mixed with the tar or soot, making a reliable measurement of elemental analysis hard to achieve. The ash contents of the tar or soot samples were therefore determined in the same way as that for the chars and the parent coals as presented in the “Sample Analysis” section.

The measured ash contents of the collected deposits on soot filters during pyrolysis of the coals and model compounds are presented in Appendix E. Table E.1 in Appendix E presents the measured ash content in the tars and soots obtained from coal and model compounds. As seen from the table, ash contamination for the coal tars or

soots is only significant for the Knife River lignite, where about 10% ash was mixed with the tar or soot. A correction was therefore made to account for the ash contamination in the elemental analysis. For the other three coals, ash contamination was negligible. However, the impurities in the tars or soots of the model compounds were much more significant. For biphenyl, the ash content was as high as 77%. For pyrene, the ash content ranged from 7% to 35%. The small particle size (32-63 μm) of the silica gel used in this study is thought to be the major reason for the inefficiency of the virtual impactor in separating silica gel and soot. In addition, silica gel absorbs water (steam) very easily, and does not release the water until about 800°C. Consequently, the absorbed water can interfere with the elemental analysis of the soot samples, especially the hydrogen content.

Sample Analysis

A number of modern analysis techniques were used to characterize the parent coal, char, tar, soot and gaseous samples produced in this study. A detailed discussion on each technique is given in the following sections.

Proximate Analysis

Proximate analysis refers to the determination of the moisture, volatile matter and ash content in a coal or char. Proximate analysis was performed following the standard practice for proximate analysis for coal and coke set by the American Society for Testing Materials (ASTM). Minor changes have been made to accommodate the analysis in our lab. An electrically-heated, programmable oven was used for the proximate analysis.

Moisture

About 0.4 gram of char or 1 gram of coal was weighed and added into a platinum crucible. Then the sample was dried at 105°C in a hood for two hours. The difference in weight before and after the drying procedure gives the moisture content of the sample.

Ash

When the sample was dried, the crucible was placed back into the oven. The oven temperature was ramped up to 500°C in one hour. The sample was flooded with air every 30 minutes by opening the oven door. This ensured the sample was burning well. The temperature was then ramped up to 750°C in another hour. Finally, the sample was soaked at 750°C for at least 12 hours before the sample was cooled down and weighed again. The weight loss was used to calculate the ash content of the sample.

Volatile Matter

Volatile matter of the parent coal was determined in a manner similar to the ASTM test method D3175. About 1 gram of coal was placed into a small ceramic crucible sitting inside of a larger ceramic crucible. The larger crucible was used because it is much easier to handle and it helps to preserve all of the carbon deposit even for sparking samples. The small crucible was covered with a loose fitting lid and put into the oven. The whole set was soaked in 950°C for exactly seven minutes before it was cooled down and weighed. The percentage loss of weight minus the percentage moisture gives the volatile matter content.

Ultimate Analysis

A Leco CHNS-932 elemental analyzer was used to obtain the mass fraction of carbon, hydrogen, nitrogen and sulfur of the coal, char and tar/soot samples. Nitrogen and hydrogen content of samples are the most important data in elemental analysis because it is believed that the nitrogen release is directly associated with these two elements. Elemental analysis is also necessary to close the elemental mass balances in this study.

Each sample was weighed into a tared silver crucible before being totally burned by pure oxygen in the oxidation furnace in the analyzer. The combustion gas was then swept through the non-dispersive infrared absorption detection system. H_2O, SO_2 and CO_2 were measured in sequence, and the signals were converted into weight-percent hydrogen, carbon and sulfur. These infrared sensitive gases were then removed by special reagents, leaving only N_2. The remaining N_2 was measured by thermal conductivity and was converted to the weight percent of nitrogen in the sample. Oxygen content was calculated by difference. Five replicates of each sample were analyzed in succession and the results were averaged.

For coals and chars with high ash content, the samples were first ground to fine powders to reduce heterogeneity using a wig-l-bug device. Several coal standards, one coke standard, and a pitch standard, all with known compositions, were used to calibrate the coal, char and tar samples. An appropriate standard was used between every four samples to account for the possible machine drift. It was observed that the measurements for carbon and hydrogen were very accurate, usually within 1% (relative). Nitrogen and sulfur analyses were also sufficiently accurate. A detailed discussion on the variations in elemental analysis is presented in Appendix E.

Determination of Dry, Ash-free Mass Release by the ICP Technique

Inductively Coupled Plasma (ICP) atomic emission spectroscopy was used to determine the total mass release of the parent coal using a tracer technique described by Fletcher (Fletcher and Hardesty, 1992). It is based on the assumption that the tracer is preserved during the pyrolysis.

A balance on the tracer balance results in the following equations:

$$m_{coal}\ y_{t,coal} = m_{char}\ y_{t,char} \tag{4.1}$$

$$\frac{m_{char}}{m_{coal}} = \frac{y_{t,coal}}{y_{t,char}} \qquad \text{dry basis} \tag{4.2}$$

Then

$$\frac{m_{char,daf}}{m_{coal,daf}} = \frac{m_{char,dry}\ (1-x_{ash,char,dry})}{m_{coal,dry}\ (1-x_{ash,coal,dry})} \tag{4.3}$$

$$\frac{m_{char,daf}}{m_{coal,daf}} = \frac{y_{t,coal}}{y_{t,char}}\ \frac{(1-x_{ash,char,dry})}{(1-x_{ash,coal,dry})} \tag{4.4}$$

By mathematical manipulation, the mass release on a dry, ash-free basis is obtained:

$$MR = 1-\frac{m_{char,daf}}{m_{coal,daf}} = 1-\frac{y_{t,coal}}{y_{t,char}}\ \frac{(1-x_{ash,char,dry})}{(1-x_{ash,coal,dry})} \tag{4.5}$$

Several tracers including silicon, titanium, aluminum, barium and zinc were tried, with Ti and Al giving the most reliable results. The difference of the mass release data obtained from these two tracers is usually less than 5% (relative). The mass release determined by the Ti or Al tracer technique was also compared with that obtained using the ash as a tracer and with the overall mass balance (the mass of char collected, divided by the mass of coal fed into the reactor). The final mass release reported is the averaged value of the two measurements using the Ti tracer and the Al tracer.

Chemical Structure Analysis by ^{13}C NMR Spectroscopy

The average chemical features of the Illinois #6 coal and the tars or soots from both the coal and model compounds were characterized by solid-state ^{13}C NMR spectroscopic techniques at the University of Utah. Three different NMR experiments

were used to determine the carbon skeletal structure of a sample, including a standard cross-polarization and magic angle spinning (CP/MAS) experiment, a variable contact time experiment, and a dipolar dephasing experiment (Solum, et al. 1989). Fourteen structure parameters can be directly derived from the NMR spectra, giving the aromaticity and the relative amount of different types of functional groups of a sample. These structure parameters can be used to calculate the lattice parameters which are used in the CPD model (Fletcher, et al. 1992). The lattice parameters include the aromatic cluster size, attachments per cluster, cluster molecular weight, and bridge mass. For an estimation of the cluster mass and bridge mass, the dry, ash-free carbon content in the sample obtained from elemental analysis is also required.

Quantitative Analysis of the Pyrolytic Gas using the Fourier Transform Infrared Spectroscopy (FTIR)

Analysis of the pyrolysis gases is critical for following the nitrogen species after they are released from the coal. It is also essential for the closure of the mass balance and tracking the effects of other gas species on the nitrogen transformations.

Accurate measurement of the nitrogen species in the product gas stream from the FFB was the biggest challenge in this study. A large amount of CO and H_2 are burned in order to maintain the high temperature, high heating rate environment in the FFB that is necessary for the study of secondary nitrogen release. On the other hand, the coal loading has to be kept very low (about 1 gram/hour) to facilitate single particle reactions (which provide easily interpretable data for computer simulation). In addition, large quantities of nitrogen used to quench the reaction stream further dilute the concentrations of the gas species. Consequently, the concentrations of the nitrogen species in the collection system fall in the range of parts per billions (PPB).

Quantification of the nitrogen precursors (HCN and NH_3) during pyrolysis was previously attempted using an industrial toxic gas monitor (Hambly, 1998; Perry, 1999; Zhang, 1999). However, it was shown that the monitor was not capable of accurately measuring HCN and NH_3 in the FFB because of a large drift in the measurement, sometimes resulting in a standard deviation as high as 500% (Zhang, 1998). This is probably due to the interference of steam. A high resolution gas chromatograph (HP 6890) was also tested, however, the detection limit of the GC is only up to high parts per million (PPM) level. In addition, since the pyrolyzed gases are a complicated mixture, different types of detectors would be needed for the complete gas analysis (Flame Ionization Detector for hydrocarbons; Thermal Conductivity Detector for N_2; .Electron Capture Detector for electronegative species such as HCN).

Application of FTIR on trace-gas analysis in combustion systems has been reported by several researchers (Kallonen, 1990; Breton, 1992; Kassman, 1995; Ledesma, 1998). The techniques in IR spectroscopy can be used for most common combustion gas measurements (except for diatomic gases such as N_2, H_2, etc.), and at the same time eliminate the complexity and reliability problems experienced with systems employing multiple individual gas analyzers, each with their own detectors. By choosing a proper resolution and a suitable gas cell, FTIR spectroscopy replaces the following traditional analyzers:

- Chemiluminescence for NO and NO_2
- U. V. absorption for ozone
- Non-dispersive infrared for CO
- Gas Chromatography for hydrocarbons

· Flame photometry for sulfur-containing species

However, since the reported trace gas concentrations were usually in the range of PPM (from 5 PPM to several hundred PPM), accurate measurement of trace gases was difficult. In addition, the measurement was also complicated by the harsh environment, which contained about 15% CO_2, 25% CO and small amounts of H_2O experienced in this study. All of these gases are extremely strong infrared absorbers, which can greatly interfere with the measurement of other low-concentration and weakly-absorbing species (such as HCN, C_2H_4 and C_6H_6).

FTIR Analysis Procedure

A BOMEM® MB-155 FTIR coupled with a 10 m multi-reflection gas cell (Infrared Analysis, Inc.) was successfully used to perform the on-line measurements of the PPB-level HCN, NH_3, hydrocarbons and other significant species in the FFB. The schematic of the sampling system is shown in Figure 4.7. The IR beam produced from a Globar IR source was introduced into the gas cell by several reflecting mirrors. The beam was reflected between the two sets of gold-plated mirrors installed at the two ends of the gas cell. After passing through the specified path length, the IR beam was directed out of the gas cell and was received by a liquid N_2-cooled MCT detector (EG&G, Inc.) with a detectivity (D*) of 10^{10}. The detailed description of the gas cell can be found in the next section.

The procedure for the gas cell purging and spectra collection can be summarized in the following steps. First, the gas cell was purged with pure nitrogen for 15 minutes to remove any possible contaminants. Next, the combustion gas without coal particles was pumped into the gas cell after passing several glass filters. The glass filters were used to

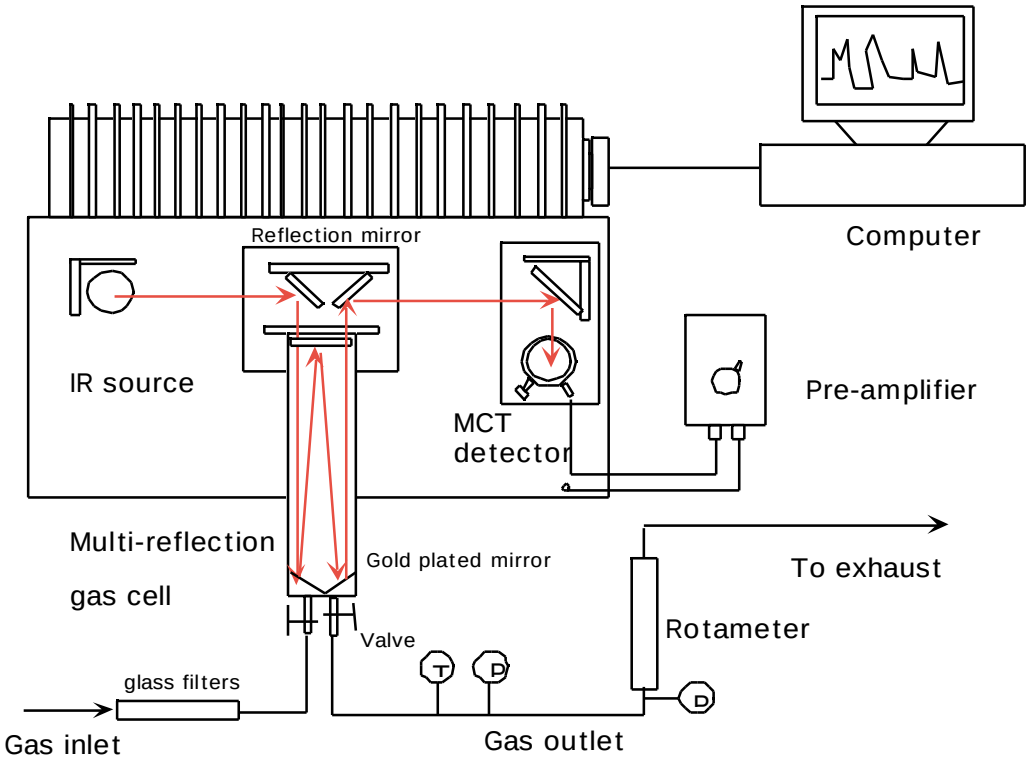

Figure 4.7. On-line FTIR gas analysis system.

remove any possible aerosols that might deposit on the gold-plated reflection mirrors. The reflection mirrors have to be kept extremely clean to ensure best results. After the gas cell was purged for 5 minutes (preliminary tests showed that 5 minutes was enough to totally purge the gas cell at the flow rates used in the gas sampling line), the single-beam background spectrum was collected by the spectrometer. The gas cell was then purged again with pure nitrogen and refilled with the pyrolysis gas with coal particles flowing in the reactor. The sample was allowed to achieve thermal equilibrium for several seconds. Because the pyrolysis gas was quenched and water-cooled, the equilibrium was quickly reached in a few seconds within the gas cell as evidenced by the stability of the measured concentrations. A spectrum of the gas sample was collected, using the previously

collected single-beam spectrum as the background for ratioing. The cell was then flushed with nitrogen to be made ready for the next sample. All the spectra were acquired with a resolution of 1 cm^{-1} and a spectral range of 500-4000 cm^{-1}. By using a liquid N_2-cooled MCT detector, the detection limit of the FTIR can be as low as 50 PPB for certain types of gases (including NH_3, C_2H_4 and C_2H_2). The detection limits for other gases are generally about 100 PPB. Figure 4.8 shows the existence of HCN and NH_3 in the coal pyrolysis spectra and a comparison with the corresponding reference spectra.

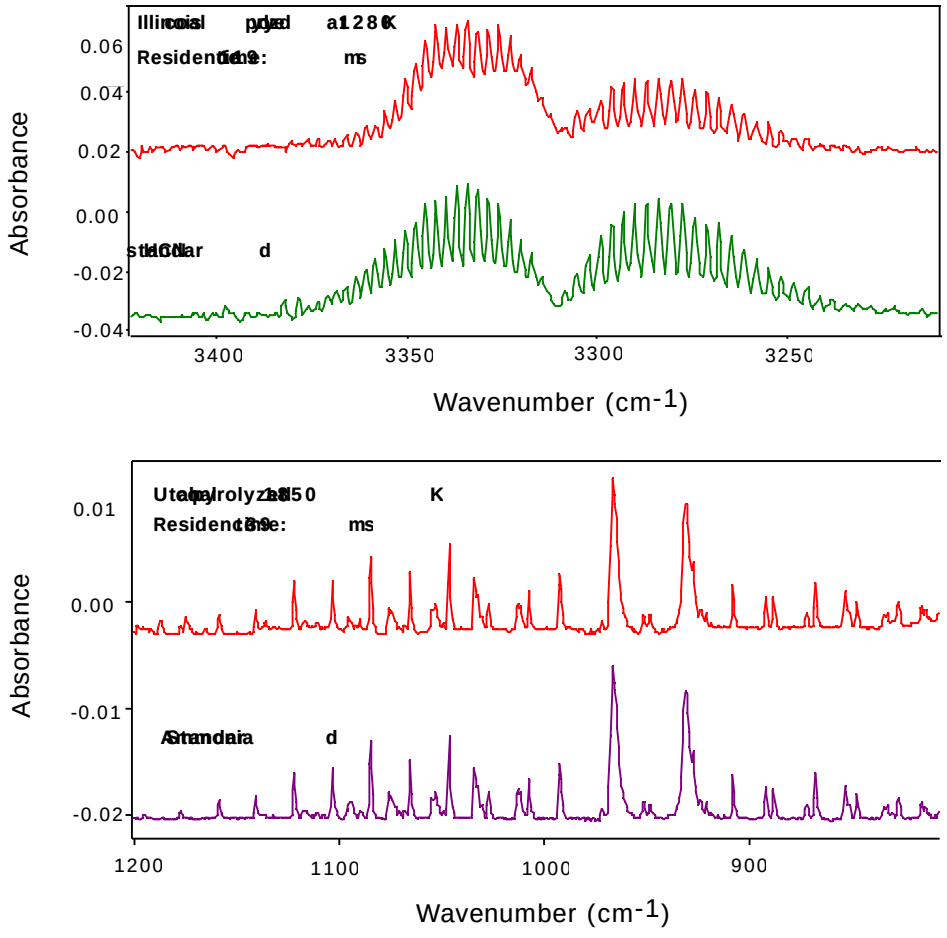

Figure 4.8. Identification of HCN and NH_3 in the coal spectra by comparison with the reference spectra.

Gas Cell Operation

The gas cell is a very important component in the FTIR measurement of the trace-gases in this study. It is impossible to measure low-ppb level trace gases without using a proper gas cell. The long-path heatable gas cell (type G-3-8-H-Ba-Au, Infrared Analysis, Inc.) used in this study was made of borosilicate glass, and therefore was resistant to most corrosive and reactive gases common in combustion systems.

The gas cell was constructed based on the original "White" cell design in which the basic three-mirror system is used to direct the IR beam within the gas cell (Hanst, 1999a). The basic set of four passes of the "White" cell is described as follows. The light from the source is directed into the gas cell. Initially, it is focused on to a real image in the entrance aperture of the cell. The beam then diverges and is collected by one of the two objective mirrors placed on one end of the gas cell. The objective mirror is a spherical mirror situated two focal lengths from the image so that it re-focuses the image, inverted, on the lower part of the opposite field mirror, which has the same focal length as the objective mirror. The field mirror is designed so that the reflected diverging beam falls entirely on the second objective mirror. When the beam is re-focused and redirected out of the cell, there are four passes of the IR beam (see Fig. 4.9).

By manipulating the position of the field mirror, different path lengths in multiples of four passes can be achieved. In the cases where more than four passes are achieved, there are two rows of images on the field mirror. The number of images on the lower part of the field mirror determines the path length. The number of images allowed in the row depends on the placement of the first image in the lower part of the field mirror. If it falls exactly on the centerline, no more than four passes are possible. The further to the right the first image falls, the greater the number of passes allowed. In

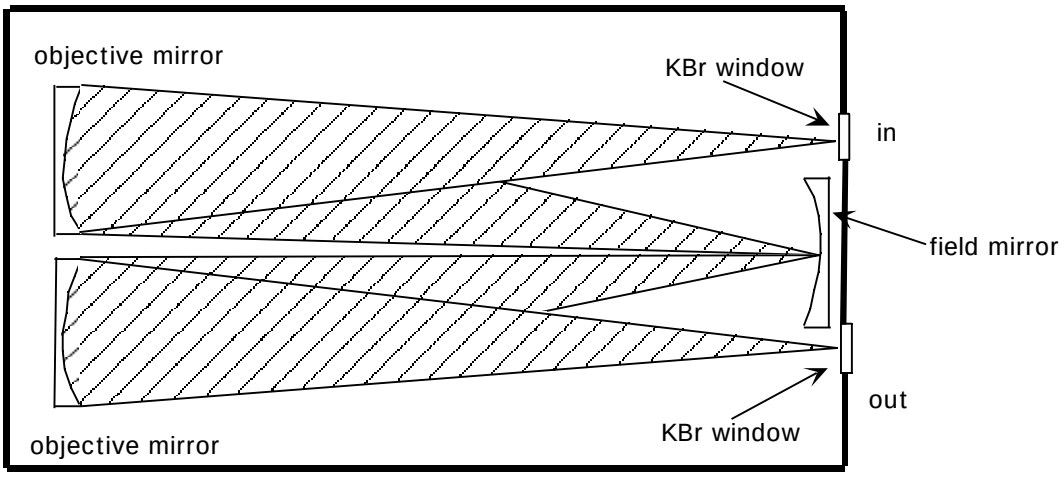

Figure 4.9. Three mirror optical system with a basic set of four passes (White, 1942).

practice, the number of passes is determined by counting the number of images in the bottom row of the field mirror and multiplying by four. In this study, 48 passes were used with 12 images in the bottom row (see Fig. 4.10). The total path length was calculated to be approximately 9.75 m.

The determination of a proper path length is critical in accurate measurement of trace gases in a harsh environment encountered in the FFB. According to Beer's law, the absorbance of an IR beam is proportional to the concentration of the absorbing media and the path length it travels:

$$-\log\left(\frac{I}{I_0}\right) = A = a \; c \; L \tag{4.6}$$

I: intensity I_o: incident intensity a: absorption coefficient
c: concentration of the absorber L: path length A: absorbance

The concentrations of the absorbing species at a certain experimental condition were fixed. Variation of the path length will result in a change of the absorbance. Increasing the path length will raise the absorbance of a certain species, whose peak will

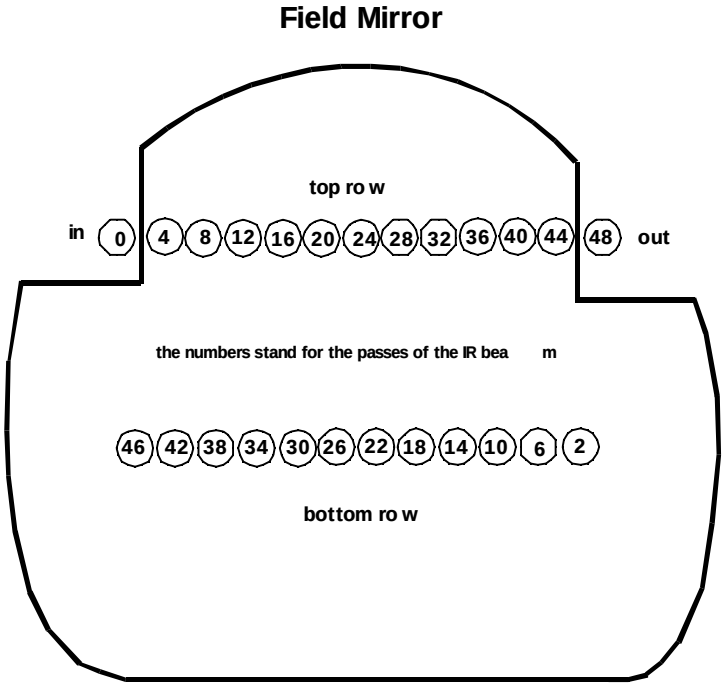

Figure 4.10. Placement of images on the field mirror in this study.

be higher and much easier to identify. Since the concentrations of HCN and NH_3 are extremely low (low-ppb), increasing the path length will facilitate the accurate measurement of these species. However, because there are also large quantities of CO and CO_2 in the system, the increase of path length will simultaneously boost the absorbance of these strong IR absorbers, which results in serious interference with the measurement of other weakly-absorbed or low-concentration species. For example, the strongest absorption peak for HCN is at 712 cm^{-1}, but this peak cannot be used in the analysis, since a strong CO_2 peak absorbed at 680 cm^{-1} significantly overlaps with the HCN peak, making the measurement extremely difficult. Finally, it was found that a path length of 9.75 m would give the best results for most of the conditions used in this study.

Verification of the Reliability and Reproducibility

Obtaining reliable and repeatable gas measurement is critical in the FTIR analysis. The gas measurement can be affected by many factors.

Temperature and Pressure Effects

It is extremely important to carefully control both the temperature and pressure when performing any quantitative analysis on gas species. Absorption band intensities, widths, and areas are dependent upon both parameters. In this study, all the spectra (reference, background and sample spectra) were collected at room temperature ($23\pm1^{o}C$) and ambient pressure (12.4 psia, at the altitude of BYU). Therefore, the spectra were easily manipulated without worrying about the possible absorption band broadening and band shift caused by changes of temperature and pressure.

Memory Effects

The results from trace-component analysis in long-path gas cells can be adversely affected due to the selective adsorption or desorption of materials from the cell walls (Compton, 1993). Figure 4.11 shows the measured concentration of the major species in the gas phase when the Black Thunder coal was pyrolyzed at 1858 K. Those concentrations reported were acquired at different residence times after the gas cell was flushed. These data demonstrate that negligible selective absorption occurred for all the gases except ammonia. Ammonia decays roughly linearly with residence time. In order to remove the cell "memory", the flushing of the gas cell by pure nitrogen was extended to 15 minutes and a spectrum was then collected to verify the absence of any species from the subsequent degassing. The spectra showed that the concentration of ammonia left in the gas cell after flushing was negligible. In order to minimize wall adsorption effects, NH_3 was measured immediately after the gas cell was filled, requiring about 40

seconds (10 scans). Other gases were measured using 144 scans to obtain a better signal to noise ratio, since the signal to noise ratio is proportional to the square root of the number of scans (Ingle, 1988).

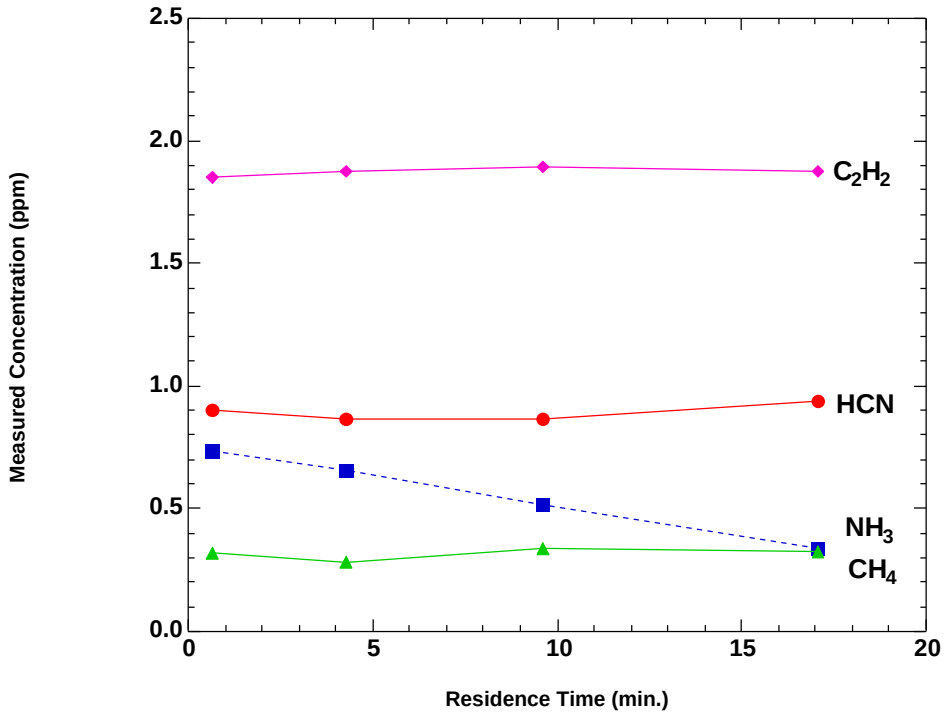

Figure 4.11. Measured concentration of major species at different residence times in the gas cell.

Coal Heterogeneity and Feed Rate

As indicated earlier, the coal samples were dried and split off evenly in order to reduce the heterogeneity. However, particle-to-particle variations in particle size, ash content and elemental composition cannot be totally eliminated. In addition, although the measured coal feed rate was fairly stable over a relative long time (several minutes), the amount of coal fed into the burner was not essentially constant at each instant. Therefore,

the gas concentration also changed during the experiments. Since the coal feed rate was much more steady over a long period of time, the gas cell was allowed to be purged continuously for five minutes before a spectrum was collected. Repetitive measurements showed that the fluctuations in gas concentrations were not serious, as demonstrated in Figure 4.12. All of the concentration data for various species are tabulated in Appendix A.

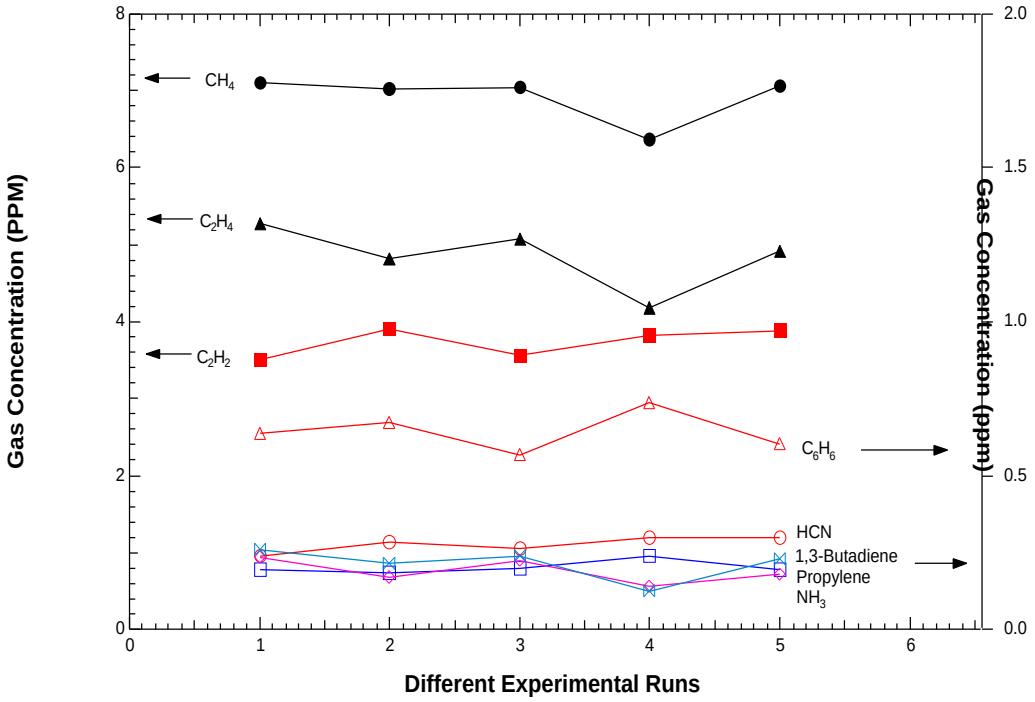

Figure 4.12. Duplicate FTIR measurements of major pyrolysis gas species (The Illinois #6 coal pyrolyzed at the 1 inch location at 1411 K).

Quantification of the Gas Species

Prior to the quantitative analysis, calibration gases of the major species found in the pyrolysis gas were purchased from different sources after being certified to the desired concentration (see Table 4.3).

Table 4.3. Reference Gas Concentrations and Their Origin.

Reference gas	Concentration	Origin
Acetylene	99.8 ppm	SUPELCO
Ethylene	105 ppm	SUPELCO
Methane	97.8 ppm	SUPELCO
Hydrogen Cyanide	9.8 ppm	AGA Specialty Gas
Ammonia	44.5 ppm	AIRGAS
Propyne	98%	SIGMA ADRICH

These reference gases were then diluted to the appropriate range using nitrogen as diluent. The calibration curves were determined from each calibration gas at three different concentrations (roughly 1ppm, 5 ppm and 15 ppm) at the same temperature and pressure as the pyrolysis gas. These calibration curves were only used to check the extent of the linearity of the absorbance versus concentration for each reference gas. Special care was taken to ensure that the concentration range of each gas was within the dynamic range over which the analytical curve was linear. A linear calibration curve for each gas was used in this study in order to facilitate the detection of abnormalities and because of mathematical ease of use (easy subtraction, accurate ratioing). The exact concentrations of a reference gas were determined by a quantitative FTIR program called QASoft developed at Infrared Analysis, Inc (Hanst, 1999b). The corresponding standard gas spectrum (with known concentration) from a quantitative database was used to calibrate the reference gas. This practice ensures that a reference gas is always calibrated by the

same standard gas spectrum, which is digitized in the database. Signal drift caused by the modification of the optical path and detector is unavoidable. Using a single, digitized standard spectrum introduces less error than the traditional calibration method which relies on the calibration curve established by dilution of a certified standard. One of the drawbacks of the traditional method is that the certified standard may decay in the container, resulting in additional uncertainties.

The reference gas was calibrated using a novel analytical technique called RIAS (Region Integration and Subtraction) developed by Philip Hanst. RIAS was originally developed to take advantage of fine structures (very small integration regions) in the spectra. However, in the reference gas calibration, the spectral range over which the integration was made was intentionally chosen to be broad. Because the standard spectra in the database were recorded by a different spectrometer and a different detector, differences of the fine structures in the standard spectra and the reference spectra are expected. A broad integration region covering many peaks helps to reduce such errors. For other species of less importance to this project, i.e., COS, SO_2 and CS_2, the corresponding standard gas spectra in the database were used directly to make the measurements.

After the reference gas was calibrated, the concentrations of the target compound were determined using GRAMS/32® (Galactic Industries Corporation) on the basis of the integrated area of a sample and a reference gas over the same spectral region (Figure 4.13). The integration region and the baseline in the spectra were determined beforehand for the integration using the characteristic absorption peak of each gas. Spectral regions used for quantitative analysis of each gas are given in Table 4.4.

The experimental data showed that the nitrogen is balanced within 10% for most cases. FTIR has proven to be a very effective way to measure the PPB-level gas species simultaneously and accurately in this study.

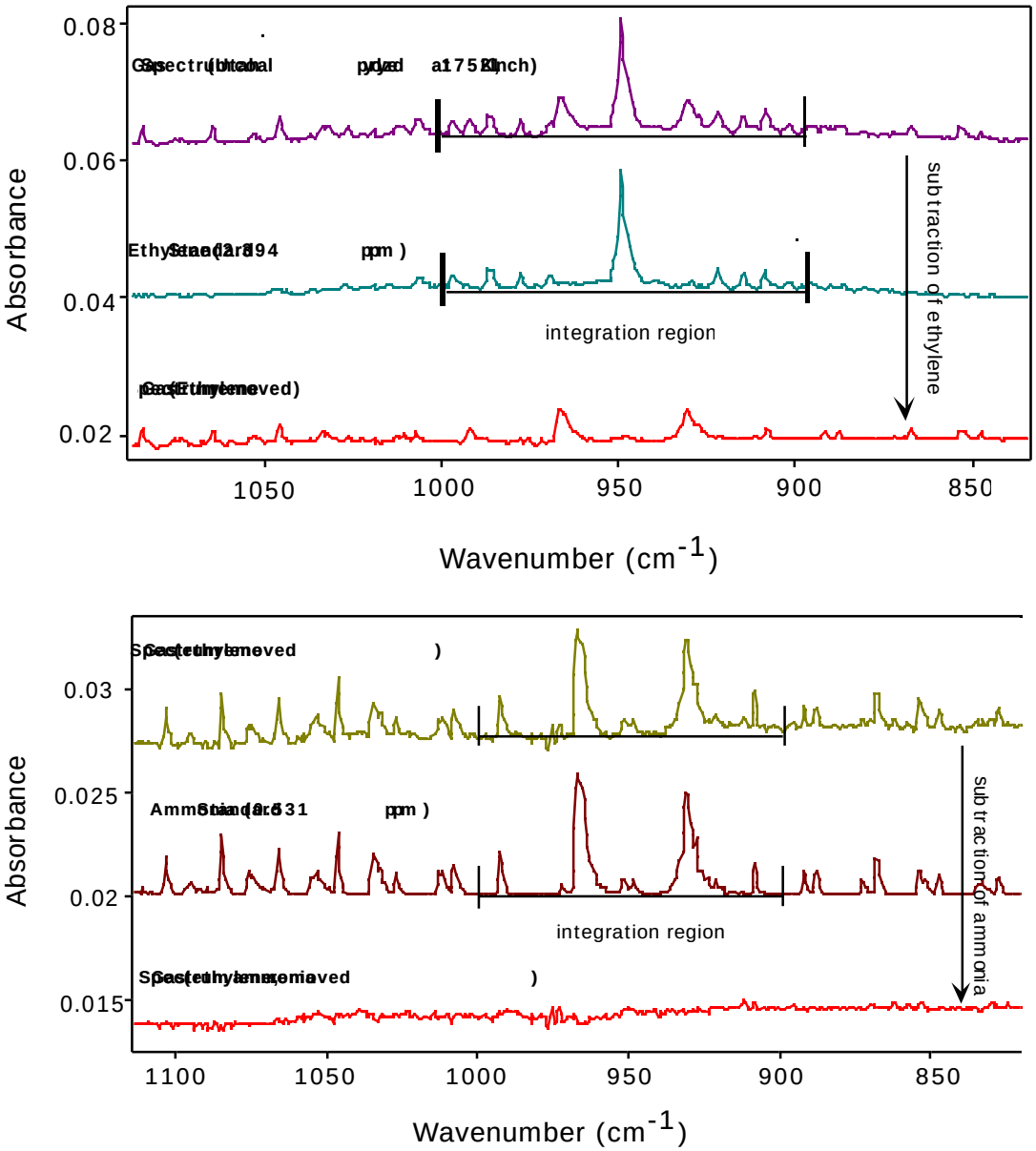

Figure 4.13. Demonstration showing the determination and subtraction of ethylene and ammonia peaks from the coal spectra.

Table 4.4. Spectral Regions used in the Quantitative Analysis.

Compound	Spectral Region, cm^{-1}
HCN	3250-3400
NH_3	900-1000
C_2H_2	3200-3400
C_2H_4	900-1000
CH_4	2855-3185
C_6H_6	1000-1080
Propylene	800-1100
1,3-butadiene	800-1000
NO	1750-1970
SO_2	1300-1400
COS	2000-2100
CS_2	1480-1560

5. Secondary Reactions of Coal Volatiles

Coal Characterization

The proximate and ultimate analyses of the four coals, ranging from lignite to high-volatile bituminous, are summarized in Table 5.1. The experimental methods used to obtain these measurements are explained in Chapter 4. In the ultimate analysis, oxygen content was determined by subtracting out the summation of carbon, hydrogen, nitrogen and sulfur. Because the sulfur values as determined by the elemental analyzer include both organic and inorganic sulfur, the oxygen values are somewhat under-estimated.

Table 5.1. Proximate and Ultimate Analyses of the Coals Used.

Coal	Rank	Proximate Analysis (wt%)		Ultimate Analysis (wt%, daf)				
		Ash	Volatile Matter (daf)	C	H	N	O†	S
Illinois #6‡	hvCb	12.3	48.8	75.7	5.2	1.5	12.8	4.6
Utah	hvBb	9.8	49.3	81.4	5.9	1.6	10.5	0.5
Black Thunder	subC	6.8	52.3	76.6	5.0	1.1	16.9	0.5
Knife River#	lignite	11.2	74.7	70.8	4.8	1.0	21.9	1.5

†: O=100-(C+H+N+S)

‡: Ultimate analyses were obtained from Dr. Mark Solum of the University of Utah
: Ultimate analyses were obtained from the Commercial Testing and Engineering Company
#: Proximate and ultimate analysis for Knife River lignite were obtained from Dr. Eric Eddings of the University of Utah

Residence Time Determination

As described in Chapter 4, the residence times of a coal particle at certain collection locations were measured using a high-speed camera. However, the low-resolution camera can only track those particles with sufficient luminance reaching a certain height in the FFB. The residence time, used for a particle traveling from the tip of the injection tube to the first luminescent point where it can be recognized, has to be accurately estimated in order to obtain the total residence time. The final residence time reported is actually the summation of the time calculated during the non-luminous zone and the time measured after the first luminescent point.

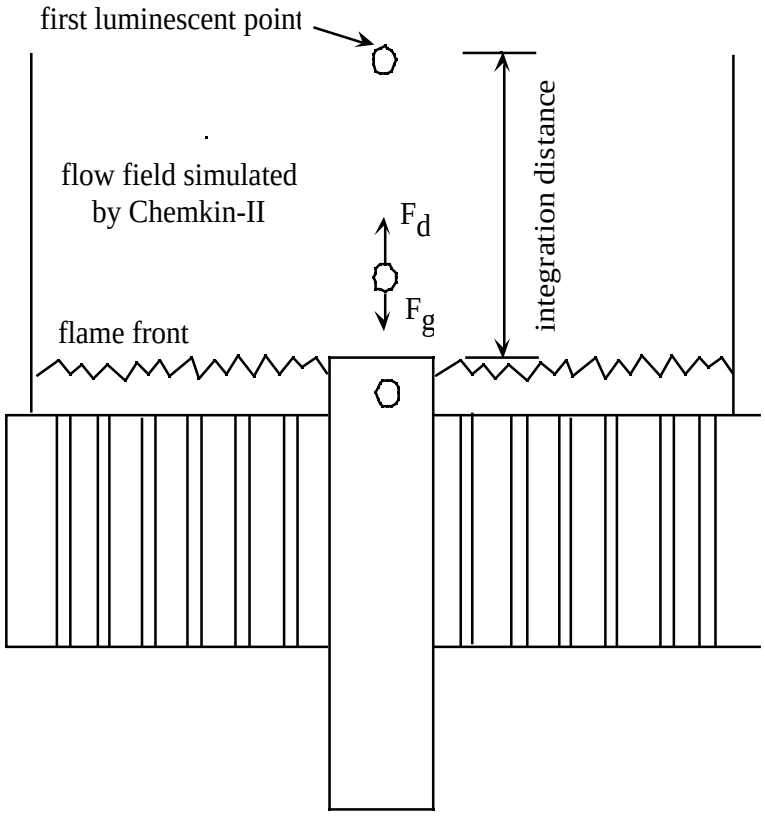

Figure 5.1. Illustration of the non-luminous zone in the Flat Flame Burner for the coal particle residence time calculations.

The residence time over the non-luminous zone was calculated based on a particle momentum balance. The coal particles were carried upward by the carrier N_2 in the injection tube. Since the injection tube is about 300 mm long, the coal particle should reach its terminal velocity at the tip of the tube. This terminal velocity also served as the initial velocity in the calculations of the residence time. The two forces acting on a coal particle, namely the drag force and the force of gravity, can be modeled assuming the coal particle is a sphere with a diameter of D_p and density of ρ_p.

Since the particle size is on the order of microns, *Stoke's law* can be applied for the estimation of the drag force:

$$F_d = 3\pi\mu_g v_\infty \tag{5.1}$$

$$v_\infty = v_p - v_g \tag{5.2}$$

v_∞: slip velocity between the particle and the entraining gas
μ_g: gas viscosity

The gravitational force acting on the particle is

$$F_g = \frac{\pi}{6} D_p{}^3 (\rho_p - \rho_g) g \tag{5.3}$$

Then, the acceleration of the particle can be expressed as

$$a = \frac{F_d - F_g}{m_p}$$

$$= \frac{3\pi\mu_g D_p v_\infty - \frac{\pi}{6} D_p{}^3 (\rho_p - \rho_g) g}{\frac{\pi}{6} D_p{}^3 \rho_p} \tag{5.4}$$

$$= \frac{18\mu_g v_\infty}{D_p{}^2 \rho_p} - (1 - \frac{\rho_g}{\rho_p}) g$$

The terminal velocity of a coal particle can be calculated by setting the acceleration to zero.

$$v_{p,terminal} = \frac{(\rho_p - \rho_g) g D_p^{\,2}}{18 \mu_g} \tag{5.5}$$

For the Illinois #6 coal with a density of 1210 kg/m^3 and an average diameter of 60 μm, the terminal velocity is about 0.133 m/s. This particle velocity was used as the initial velocity for all of the coals. The residence time was obtained by integrating over the height z of the following differential equation set:

$$\begin{cases} \dfrac{dz}{dt} = v_p \\ \dfrac{dv_p}{dt} = \left(\dfrac{18 \mu_g \left(v_g - v_p \right)}{D_p^{\,2} \rho_p} \right) - \left(1 - \dfrac{\rho_g}{\rho_p} \right) g \\ v_{p,o} = 0.133 \end{cases} \tag{5.6}$$

In equation 5.6, the only unknowns are the density, viscosity and velocity of the gas. These values were estimated by simulations using the Chemkin-II premixed code (Kee, et al. 1985). The flame in the FFB was assumed as a premixed flame, although in reality it consists of dozens of tiny diffusion flames. This should be a valid assumption due to the rapid mixing of the fuel and oxidizer. Another assumption was that the flow is one-dimensional, since the premixed code can only handle one-dimensional flow. Although there are some boundary layer effects near the wall of the FFB, previous measurements had shown that the temperatures were almost uniform radially around the centerline (Ma, 1996). The total mass flow rate and measured centerline temperature profiles were used as input in the Chemkin simulation. A comprehensive $CO/H_2/O_2$

combustion mechanism was adapted from a published source (Yetter, et al. 1991). The mechanism was modified later into the Chemkin format (Austin, 1999) and was used throughout all the calculations. The final version of the mechanism can be found in Appendix B.

During the measurement, it was also found that the length of the non-luminous zone is dependent on the total flow rate and the temperature condition. The integration of the residence time was only made over that length. The calculated residence times, the total mass flow rates, and the peak temperatures for all the temperature settings are tabulated in Table 5.2.

Table 5.2. Calculated Residence Times in the Non-Luminous Zone.

Conditions	1858 K	1752 K	1618 K	1534 K	1411 K
total flow rate (g/cm^2-sec)	0.033	0.034	0.039	0.034	0.024
measured integration length (mm)	12.7	16.5	13.3	12.7	33.6
calculated residence time (ms)	11.9	15.2	12.1	14.7	42.2

The residence time after the first luminescent point, as measured by the high-speed camera, was then added to the calculated residence time in the non-luminous zone to obtain the total residence time for a given height. For the two lowest temperature conditions in this investigation, the residence times were calculated using a bulk gas

velocity, since no visual particle velocity measurement could be made at these conditions. The 1411 K condition was used as a reference for the calculation.

$$\dot{m} = \rho v A \tag{5.7}$$

$$\frac{v_2}{v_1} = \frac{T_2}{T_1}\ \frac{\dot{m}_2}{\dot{m}_1}\ \frac{M_1}{M_2} \tag{5.8}$$

$$\Delta t = \frac{\Delta z}{v} \tag{5.9}$$

Where T, M, $\dot{m}$ and v stand for temperature, molecular weight, mass flow rate and gas velocity, respectively.

The mean molecular weight of the gas was estimated from an equilibrium calculation using the NASA-Lewis code. Equation 5.8 was used to calculate the velocity of a particle in a new condition, and the residence time over a small step of height can be obtained from equation 5.9. The total residence time was obtained by adding all the small time steps together. The residence times for any given height at all the conditions are presented in Table 5.3. These values are also shown in Figure 5.2 with a residence time measurement at Sandia National Laboratories as a reference. The Sandia measurements were made at 1700 K in a similar reactor.

Table 5.3. Residence Time versus Height at All Conditions.

Height (in.)	1159 K (ms)	1281 K (ms)	1411 K (ms)	1534 K (ms)	1618 K (ms)	1752 K (ms)	1858 K (ms)
1	46	38	33	19	18	19	17
3	105	88	74	44	38	43	39
5	143	119	102	66	58	63	58
7	182	153	130	88	76	84	78

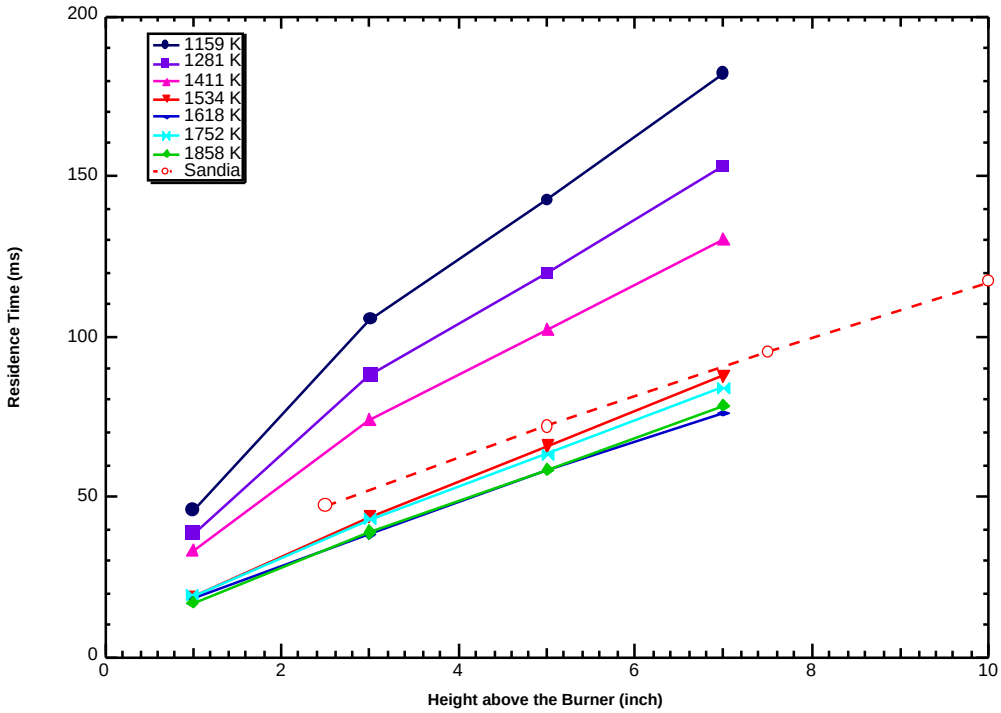

Figure 5.2. A plot of residence time versus height for all conditions (the dashed line represents residence times measured at the Sandia National Lab using a similar reactor at about 1700 K).

Mass Release

Results

The mass release data measured at selected collection elevations for all the coal types are shown in Figures 5.3 through 5.6. The mass release approached an asymptote at the most severe pyrolysis condition (highest temperature and longest residence time) for all cases in this study. That means the ultimate value of the mass release at the current heating rate was reached and the devolatilization reaction was essentially completed at the most severe condition. Since the nitrogen released during the devolatilization is the focus of this study, the ultimate mass release will help to better understand the relationship between the nitrogen release and the total volatile yield.

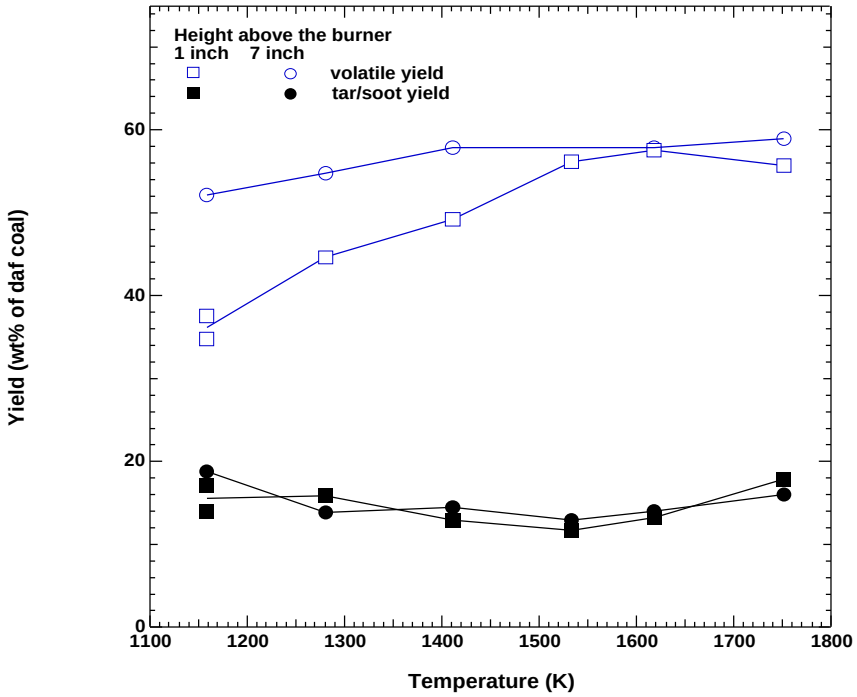

Figure 5.3. Volatile and tar/soot yields of the Illinois #6 coal at selected collection heights.

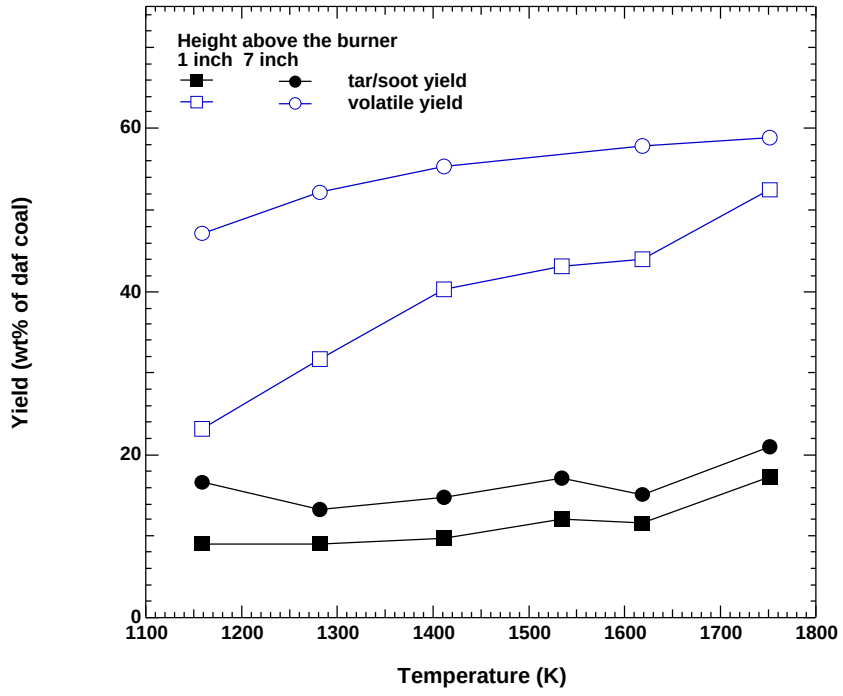

Figure 5.4. Volatile and tar/soot yields of the Utah coal at selected collection heights.

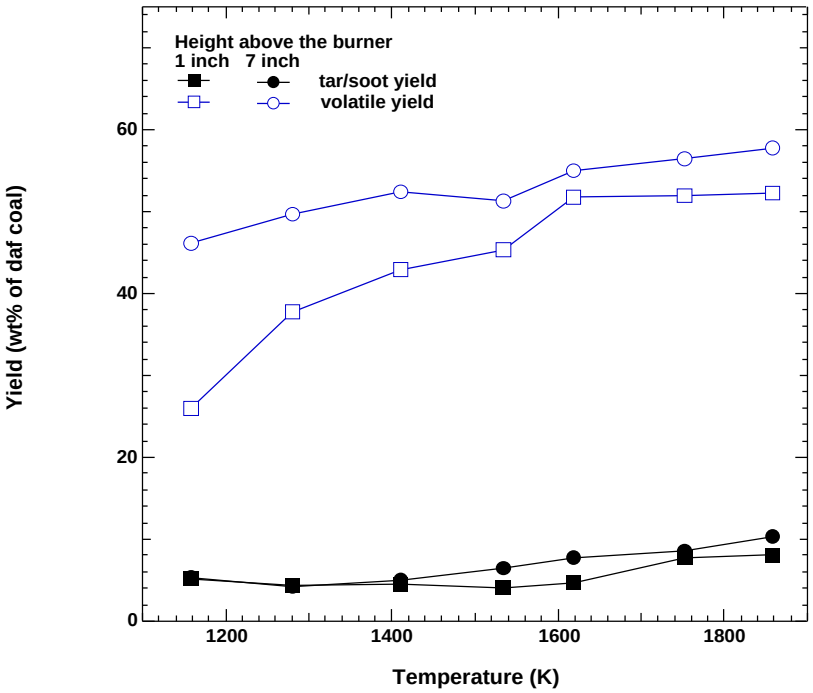

Figure 5.5. Volatile and tar/soot yields of the Black Thunder coal at selected collection heights.

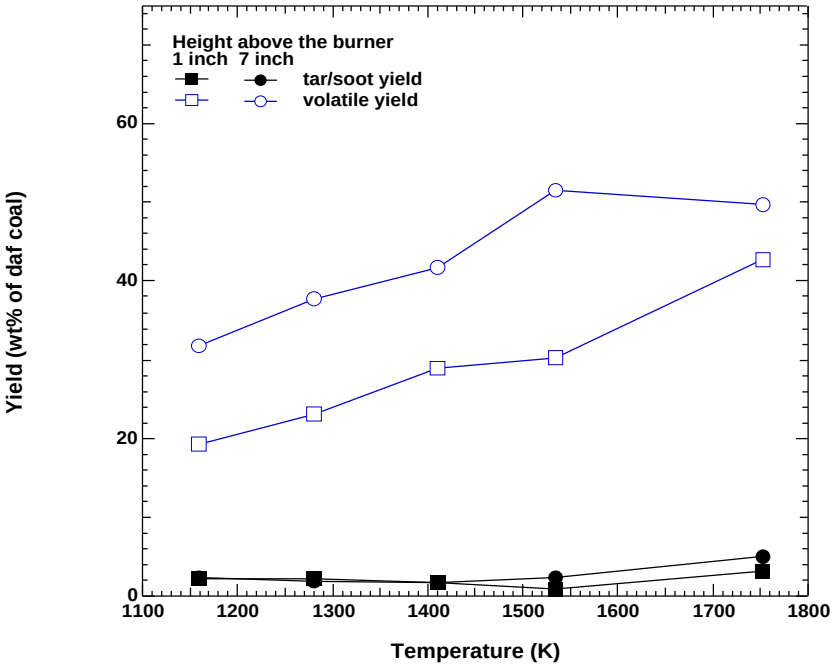

Figure 5.6. Volatile and tar/soot yields of the Knife River lignite at selected collection heights.

As seen in these figures, a large difference in the total mass release was observed between the 1 inch and 7 inch data. It is interesting that the total mass release observed at 7 inches in the 1159 K condition is very close to that obtained at 1 inch in the 1858 K condition for all coals except lignite. This indicates that temperature and residence time both influence the total mass release. Such an effect was noticed in a previous study on primary tar yields (Chen, 1991). The data obtained in the current study indicate that secondary reactions are also strongly influenced by temperature *and* residence time.

Rank Dependence of Ultimate Mass Release

The ultimate mass release for the four coals used in this study are compared with the data reported by other researchers, as shown in Figure 5.7. The ultimate mass release refers to the asymptotic value achieved at the most severe condition for each coal in this study. The ultimate mass release for these experiments are remarkably consistent with

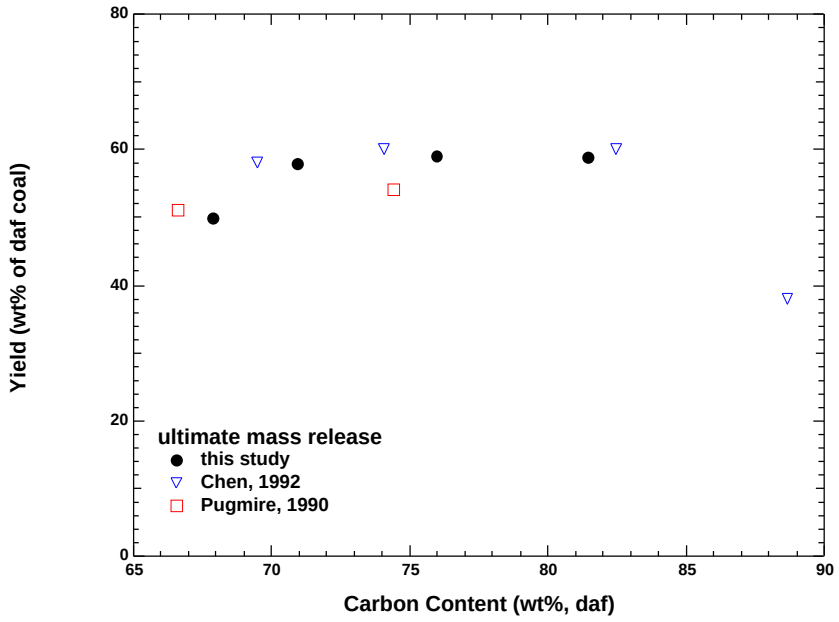

Figure 5.7. Rank dependence of the ultimate mass release.

Chen's data, showing that the ultimate mass release is approximately constant from high-volatile bituminous to subbituminous. However, the ultimate mass release decreases for lignites and low-volatile coals. The ultimate mass release data reported by Pugmire and coworkers are also comparable with the results in this study, showing that the ultimate mass release for a lignite is lower than that for a bituminous coal (Pugmire, et al. 1990).

Secondary Reactions of Coal Volatiles

This section of experimental results and discussion is grouped into three sub-sections. First, the results of measured tar and soot yields and the distributions of light hydrocarbons from the coal pyrolysis are presented. Second, a modeling effort to describe the secondary reactions of coal volatiles under high temperature, rapid-heating conditions is presented. Finally, a comparison and discussion of the results in this study with those reported in the literature is presented.

Results

Tar and Soot Yields

Temperature Effects

A graphical summary of the measured tar/soot yields at all conditions is plotted in Figure 5.8, so the trends can be clearly examined. Despite the scatter in the data, it is found that the "tar plus soot" yields first decrease with temperature, then increase at higher temperatures. This observation is different from the findings of Chen (1991) and Nenniger (1986) which showed that the sum of the tar and soot yield is constant during secondary pyrolysis.

The trend of the decrease of "tar plus soot" yield at low temperatures followed by an increase at high temperatures is especially true for the low rank coals. The tar/soot yields collected at the 7 inch location in the 1752 K condition for the Knife River and

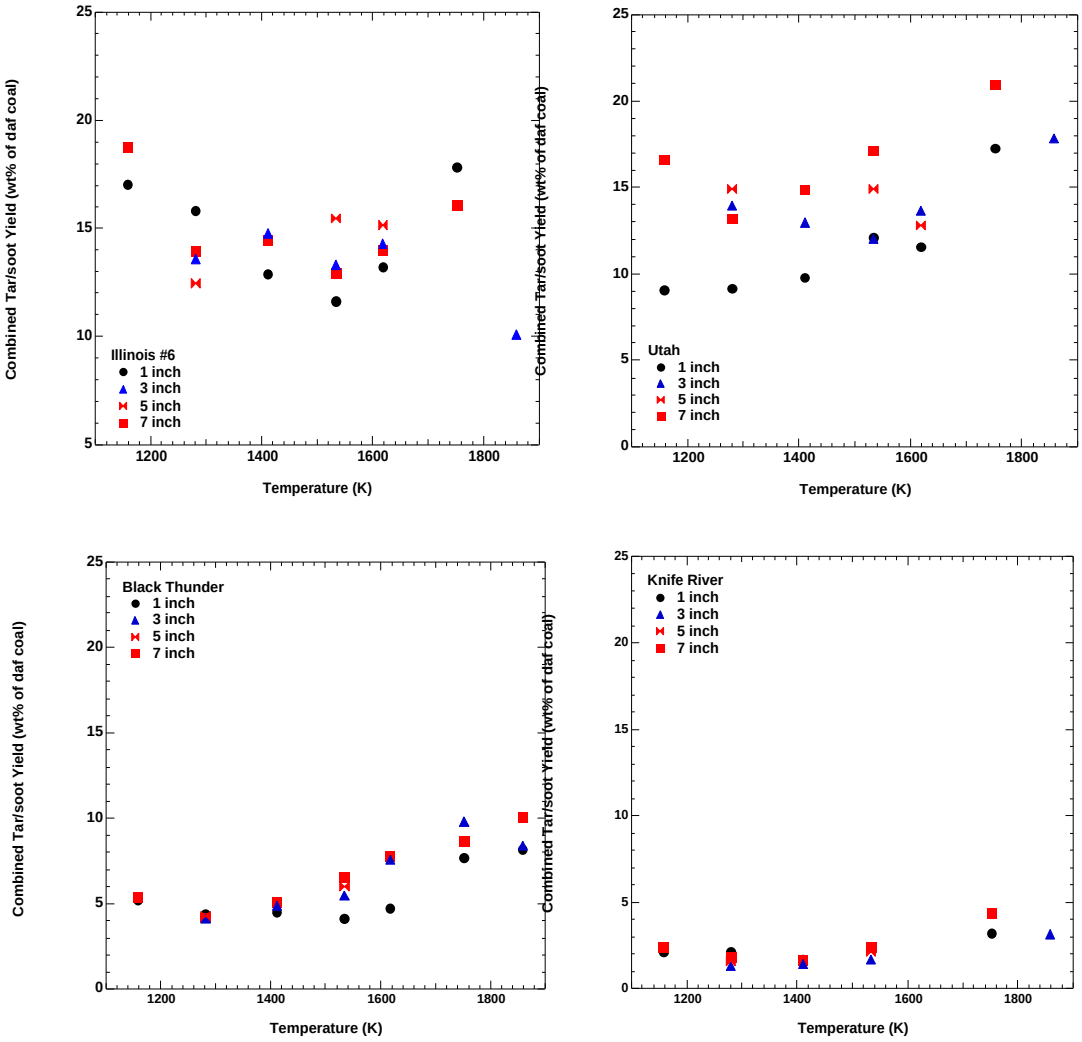

Figure 5.8. Measured tar/soot yields with temperature for the coals in this investigation.

Black Thunder coals are 4.36% and 10.32%, respectively. At the 1281 K condition, these values are 1.79% and 4.17% respectively. The measured yields are more than doubled when the temperature was changed from 1281 K to 1752 K, which cannot be explained by experimental error. During the experiments, it was found that the color of the deposits collected on the filters started to become darker at 1281 K, which implies that soot began

to form at that temperature. This is consistent with the soot inception temperature from the pyrolysis of the model compounds in this study and other research (Glassman, 2000). The primary tar usually starts to decline after reaching the ultimate yield at about 1000 K (Fletcher, et al. 1992). At low temperatures (1000-1300 K), the decline of the tar yield is due to thermal cracking reactions, which lead to the release of secondary gases (light hydrocarbons, CO and CO_2) (Doolan, et al. 1986). At these temperatures, soot formation is still insignificant, causing the measured tar and soot yield to decrease with temperature. The high soot yield at high temperatures (>1800 K) cannot be explained by direct tar conversion alone; the light gas released from char seems to participate in the soot formation. It should be noted that the temperature at which the tar and soot yield starts to increase is different for different coal ranks. This means that the tar/soot yield not only depends on the secondary reactions of the tar but also strongly depends on the tar structure and reactivity.

Residence Time Effects

The tar and soot yields measured at different residence times can be used to understand the detailed secondary reaction kinetics of the tar. Since there is a certain portion of nitrogen trapped in the tar and soot, elemental analysis of the tar also reveals the nitrogen release during secondary reactions. Figures 5.9 and 5.10 show the variation of the measured tar and soot yields with residence time at different temperature conditions for the Illinois #6 and Black Thunder coals, respectively. At the 1281 K condition, the tar cracking reaction predominated, resulting in a net decline of the combined tar/soot yield. Significant soot formation from tar was observed at 1534 K, as seen by the rapid growth of the tar/soot yield in the figures. At the 1858 K condition, the

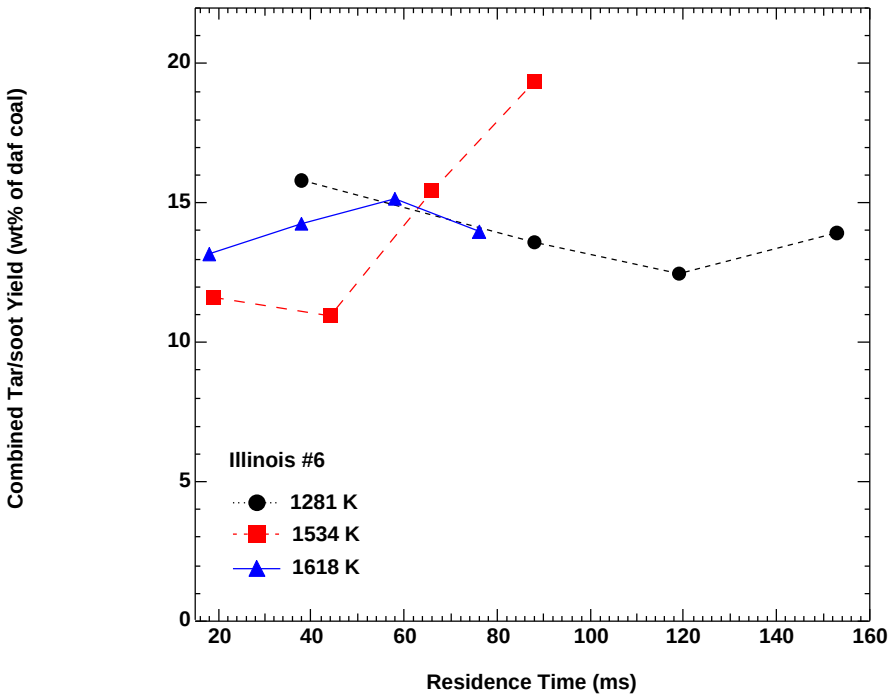

Figure 5.9. Tar/soot yield versus residence time for Illinois #6 at various temperatures.

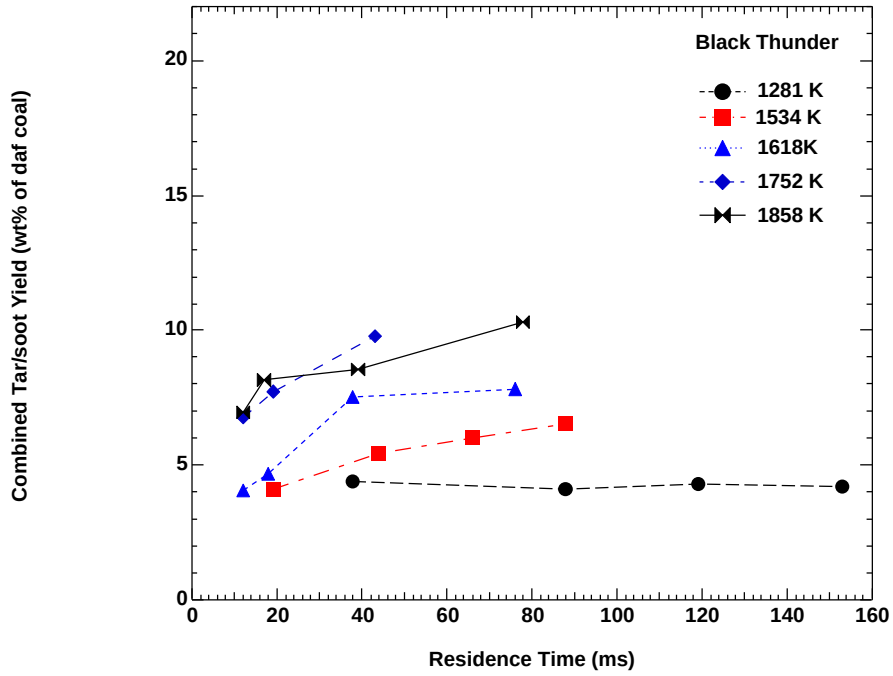

Figure 5.10. Tar/soot yield versus residence time for Black Thunder at various temperatures.

soot growth was observed to occur at a slower rate. Such trends can be viewed more clearly by examining the slopes of the soot yield versus residence time curves at different temperatures as shown in Figure 5.10. These data indicate that the rate of soot growth was highest in the temperature range from 1500 K to 1700 K.

Gas-Phase Product Distributions

CO, CO_2 and H_2O are products of CO combustion in the FFB. Because the coal loading is very low (about 1 g/hr), the incremental amount of these gases released from the coal could not be measured accurately. The hydrocarbons released from the coal during pyrolysis were carefully measured and are presented here.

Previous studies have shown that homogeneous secondary reactions have a strong effect on the distributions of hydrocarbon gases. The hydrocarbon gases play an important role in soot chemistry at high temperatures. Also, the nitrogen transformations during secondary reactions can be greatly influenced by hydrocarbon gases, as suggested by the reburning mechanism (Smoot, 1993). In the practice of reburning, nitrogen oxides are converted to N_2 by injecting methane or natural gas into the coal flame. Some researchers have proposed detailed reaction mechanisms for the interaction of hydrocarbon radicals (CH, CH_2, etc.) with both NO_x and NO_x precursors such as HCN and NH_3 (Miller,1989; Glarborg, 1994; Miller, 1996). Therefore, the yields of individual hydrocarbons during secondary reactions must be examined in order to fully understand the nitrogen reaction pathways.

The yields of hydrocarbon gases reported here were calculated from the FTIR measurements. There are two types of hydrocarbons that cannot be accurately quantified by the FTIR, so they are not reported here. One type is the alkynes in the spectral region

3300-3360 cm^{-1}. Careful examination revealed that this should be a mixture of propyne, 1-butyne, 1-pentyne and phenylacetylene. The large amount of overlap of these peaks made the identification and quantitative measurement of each individual species impossible. The total area (which is proportional to their concentrations) underneath these alkyne spectral peaks exhibited a temperature dependence similar to that of methane or benzene. By comparing the spectral area, it was found that these alkynes only accounted for less than 5% of the total hydrocarbons. Therefore their effects should be quite small. The other type of unidentified hydrocarbon fraction is the non-condensable light oils (gaseous hydrocarbons having more than six carbons) whose spectra overlap with the methane peak. Although FTIR spectroscopy offers far more accuracy and much lower detection limits for light hydrocarbons (less than six carbons) than the conventional analyzing instruments such as gas chromatography, it is not an ideal analyzer for differentiating hydrocarbons having more than six carbons. In this study, the individual species in these light oils were not measured. However, the measurement of the total spectral area of these light oils showed that their combined fraction never exceeded 5% of the total hydrocarbons in the gas phase.

Temperature Effects

Figures 5.11 to 5.14 shows the distribution of the non-condensible hydrocarbons with temperature for the four coals used in this study. These measurements were performed at the longest residence time at each temperature setting. The distributions at other residence times are similar to those presented here (see Appendix A). The hydrocarbon release data exhibited a similar trend with temperature for all coal types. Propylene (C_3H_6) and 1,3-butadiene (C_4H_6), which only constitute a very small fraction of

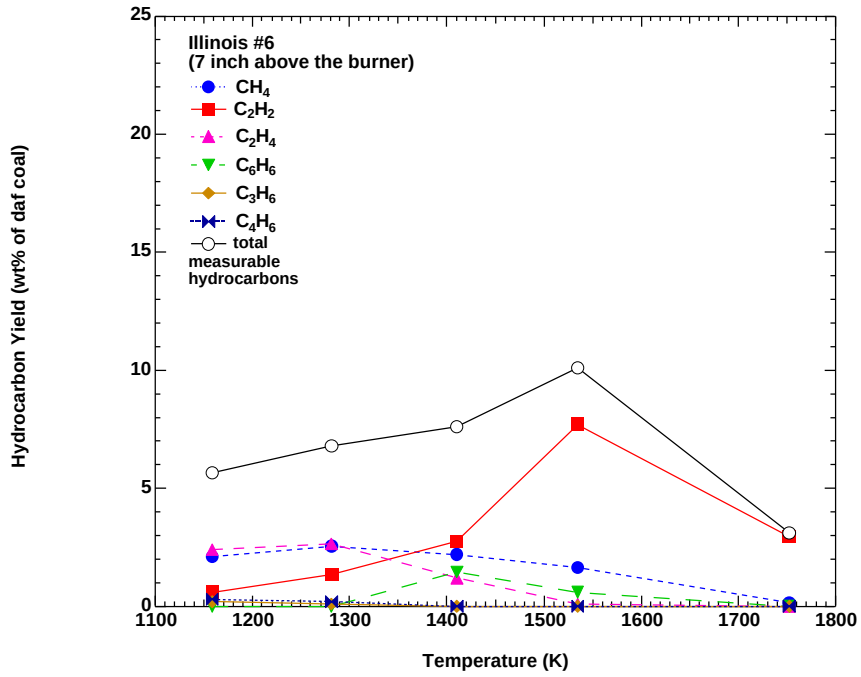

Figure 5.11. Temperature dependence of hydrocarbon yields for the Illinois #6 coal.

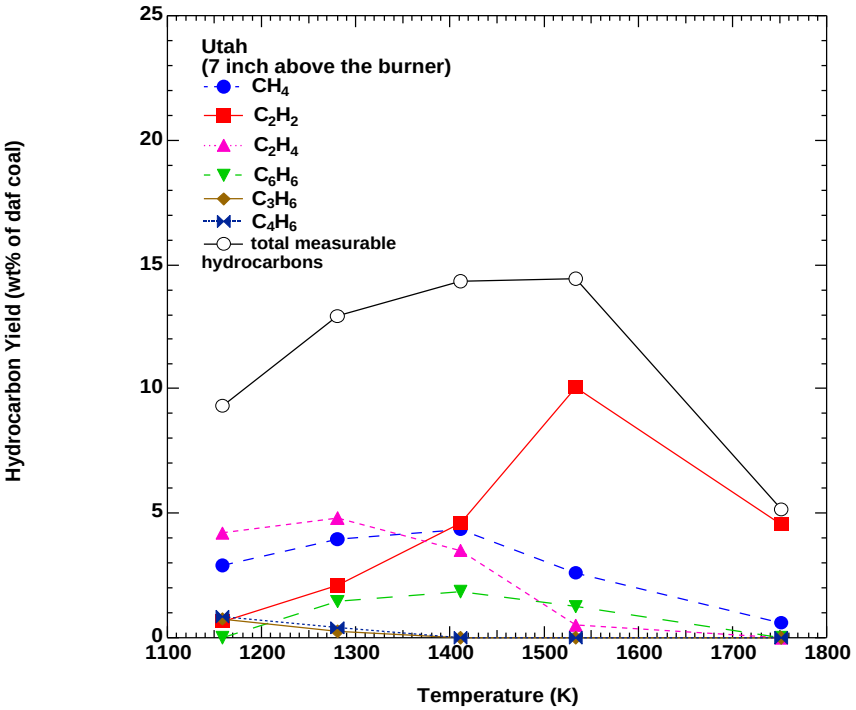

Figure 5.12. Temperature dependence of hydrocarbon yields for the Utah coal.

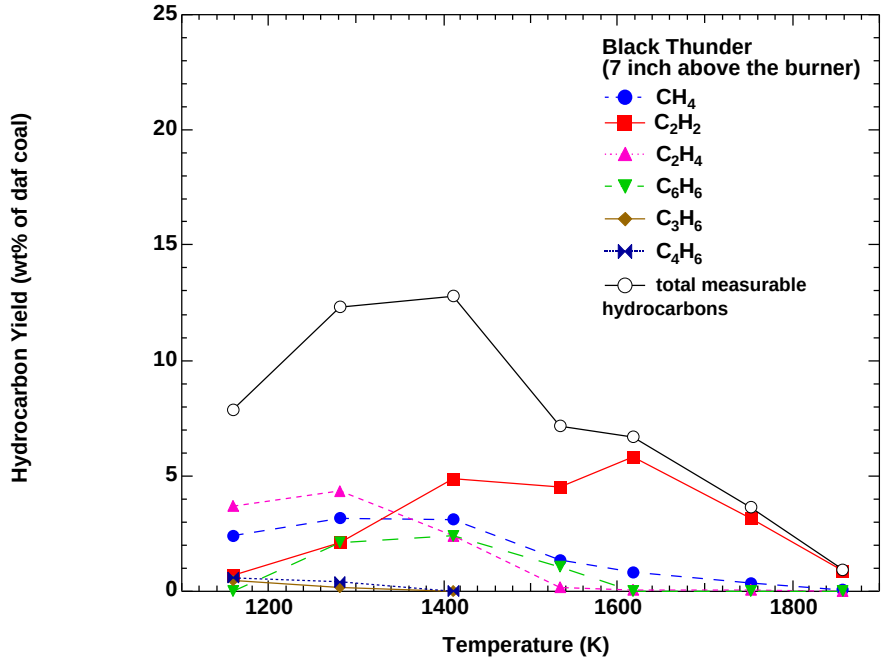

Figure 5.13. Temperature dependence of hydrocarbon yields for the Black Thunder coal.

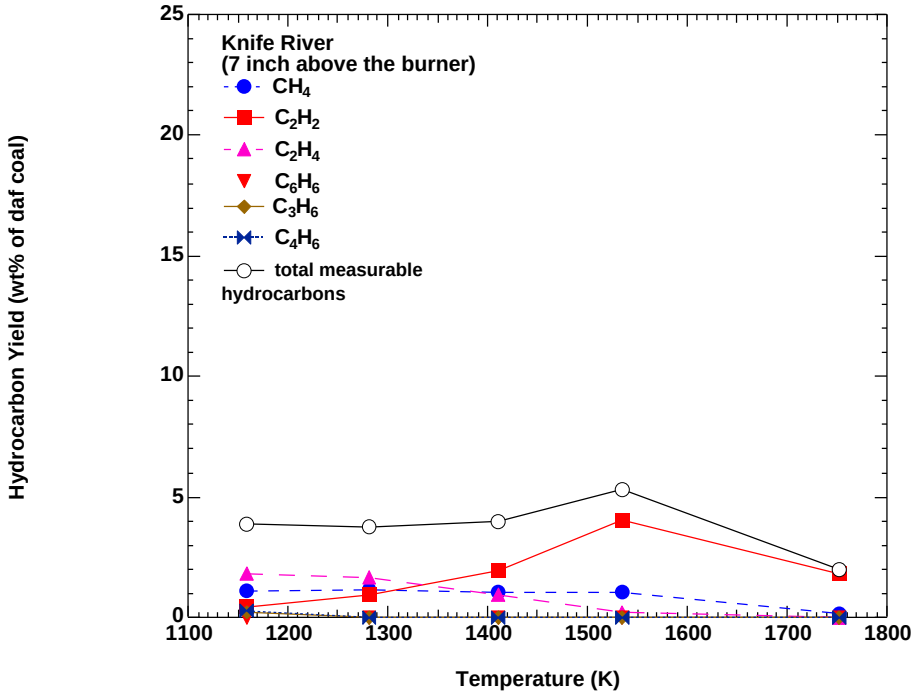

Figure 5.14. Temperature dependence of hydrocarbon yields for the Knife River coal.

the light gases at the lowest temperature, decreased monotonically with temperature and were completely depleted at about 1400 K. Except for the lignite, the yields of all the other gas species increased with temperature, reached a maximum, then declined. Each individual species exhibited a characteristic maximum evolution temperature, which seemed to be independent of coal. However, different species exhibited different maximum evolution temperatures. For instance, methane reached its peak at about 1400 K, ethylene at 1300 K and acetylene at a much higher temperature of 1550-1600 K.

It should be noted that the set of gas species measurements at the 1534 K condition for the Illinois #6, Utah and Knife River coals was performed before a reliable FTIR procedure was adopted. Therefore, the data reported for the 1534 K condition should be viewed with caution. However, reliable measurements on the Black Thunder coal covering the whole temperature spectrum showed a similar trend, indicating that the early measurements were reasonable.

The lignite demonstrated a different pattern of hydrocarbon release at long residence times. All the gases were found to decrease monotonically with temperature, except for C_2H_2. This may suggest an earlier release of light hydrocarbons for lignite than for other higher rank coals. Such observation is consistent with the ^{13}C NMR analysis of the coal, which shows a higher fraction of aliphatic side chains and bridges in lignites. The early release of light gases from low rank coals is also accounted for in the CPD model (Fletcher, et al. 1992).

Another interesting finding is that all the gases were consumed except for C_2H_2 at the most severe condition. The trend in the figures strongly implies that all of the light gases will eventually be depleted at even higher temperatures. Doolan and coworkers

showed that the major carbon-containing species from coal volatiles are CO and soot at temperatures above 1800 K (Doolan, et al. 1986).

Residence Time Effects

The hydrocarbons are believed to form from two different sources during the coal pyrolysis. Some of the hydrocarbons are released during primary pyrolysis by breaking the bonds of the aliphatic attachments or bridges. The others are released through the secondary reactions of the tar and/or light oils. At high temperatures, these species (especially C_2H_2 and C_6H_6) may make significant contributions to the surface growth of the soot particles (Frenklach, et al. 1986). Investigations of these hydrocarbons help to understand the mechanism governing the transition from tar to soot.

Figures 5.15 and 5.16 show the measured hydrocarbon yields for the Utah and Black Thunder coals as a function of residence time. The other two coals showed similar results. At the 1281 K condition, C_2H_4 and CH_4 were the major species. C_2H_2 only accounted for less than 20% of the light gases. The yields of all the gases increased with residence time at this temperature, then declined. The decline of the total hydrocarbon yields is consistent with the increase in soot yield. At the 1618 K condition (Figure 5.16), C_2H_2 became the most prevalent species in the pyrolysis products. The total hydrocarbons also dropped more rapidly with residence time at higher temperatures. Since C_2H_2 can play an important role in the early stage of soot formation (Glassman, 1988), the existence of high concentrations of C_2H_2 may indicate that significant soot formation has begun in the flame. This trend can be seen more clearly in Figure 5.17. Even at 1534 K, the growth of the soot yield seemed to be partially compensated by the decline of the C_2H_2 yield, indicating that C_2H_2 addition may be one of the primary sources

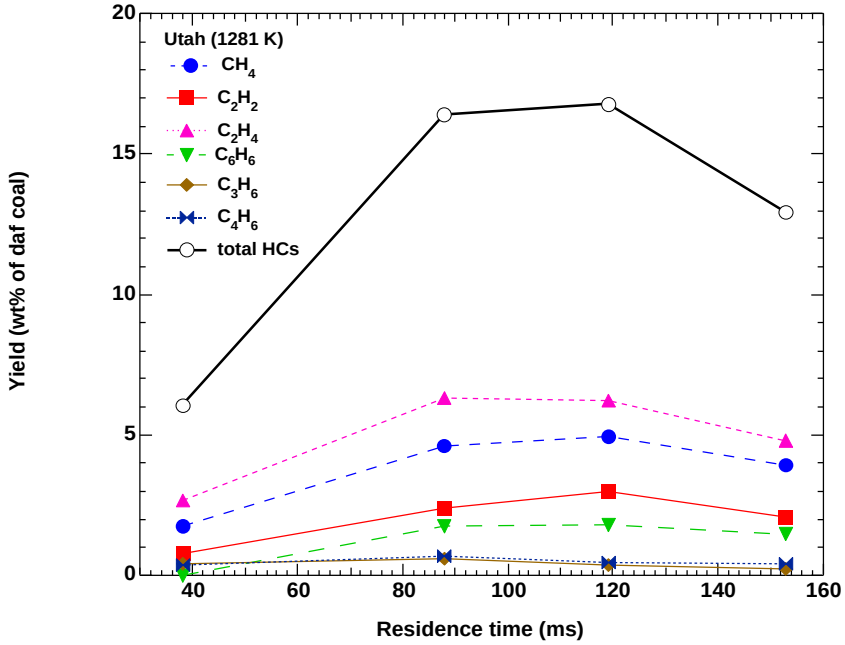

Figure 5.15. Yields of hydrocarbons for the Utah coal during pyrolysis at 1281 K.

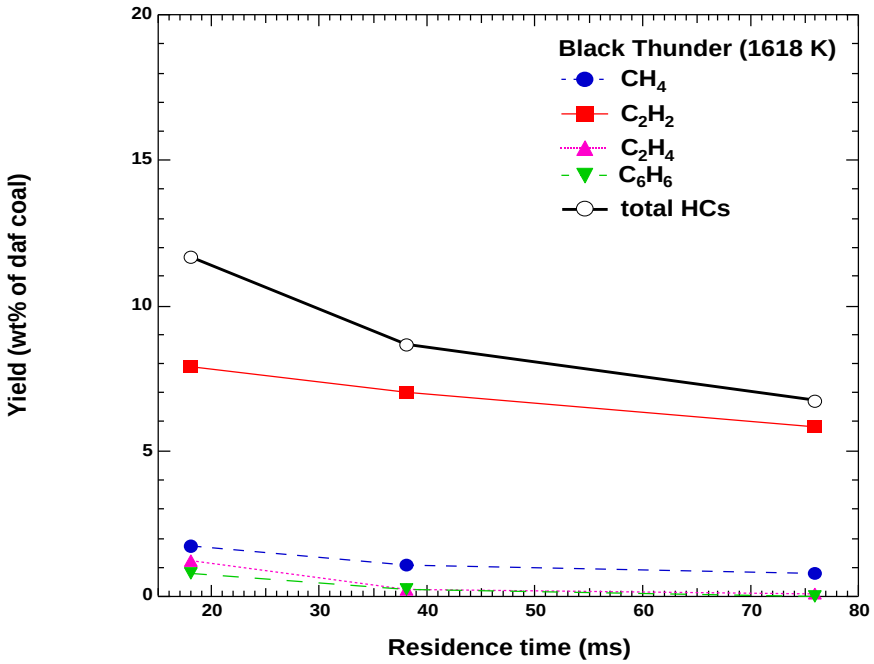

Figure 5.16. Yields of hydrocarbons from the Black Thunder coal during pyrolysis at 1618 K.

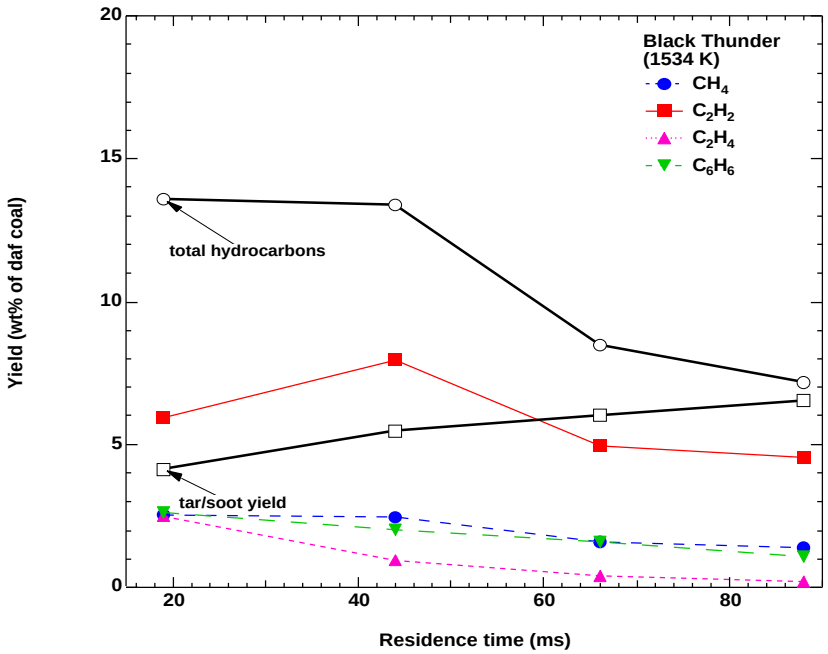

Figure 5.17. Yields of tar/soot and hydrocarbons from Black Thunder coal during pyrolysis at the 1534 K condition.

for soot growth. The proposed mechanism of soot addition from secondary light gases will be discussed in the next section.

Modeling

Simulation of the CO flame

In this study, the coals were pyrolyzed in a post-combustion environment, and the effects of the post-flame gases on secondary coal pyrolysis must be addressed. The flame structure of the CO flame was modeled by the Chemkin/Premix code using the measured centerline gas temperatures as input. The assumptions made in the simulation were given in the previous section. The profiles of the major molecular species in the CO flame at the 1159 K and 1858 K conditions are plotted in Figure 5.18. It can be seen that the steam production never exceeds 1% for either case, as originally designed, to facilitate

the FTIR analysis in the gas phase. At the 1159 K condition, CO is dominant and its mole fraction is much higher than that of CO_2. However, at the 1858 K condition, the reverse trend is observed. Large quantities of CO_2 in the post-flame have the potential to reduce the soot yield, according to the following gasification reaction:

$$CO_2 + C = 2CO \tag{5.10}$$

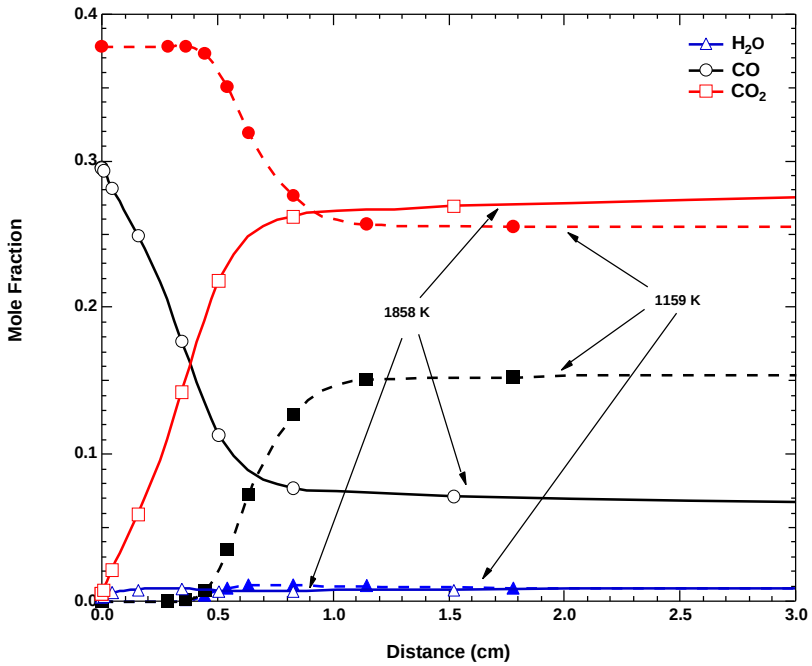

Figure 5.18. Calculated mole fractions of the municipal molecular species versus distance in the FFB with a CO flame.

Oxygen-containing radicals are of special interest, due to their high reactivity in a flame. Calculations have shown that five major species exist in the flame, including O_2, O, OH, HO_2, and H_2O_2. HO_2 and H_2O_2 are not considered in the discussion because their molar fractions never exceed 10^{-5}. The calculated concentrations of the other three species, O_2, O and OH, at 1159 K and 1858 K are shown respectively in Figure 5.19. The

profiles at other temperatures are similar. Several trends are observed from the plot. First, the mole fractions of molecular oxygen at high temperatures are higher than those at low temperatures. This is partly due to the lower equivalence ratio in the high temperature condition (see Table 4.2). Second, the mole fractions of O and OH radicals are only significant at the flame front and decay rapidly thereafter. This suggests that the influence of oxygen-containing radicals on coal pyrolysis is only appreciable at the flame front, which is only about 1 cm thick, as seen from the oxygen concentration profiles. Third, the mole fractions of OH and O radicals at 1858 K are much higher than those at 1159 K. This is not surprising since a high temperature can provide enough energy to initiate bond scission to produce more radicals. Finally, it is interesting that the mole fractions of O radical are much higher than those of OH radical at all cases in the CO flame. However, in a methane flame, the calculations showed more OH than O, as shown in Figure 5.20. The higher OH concentration in the methane flame may have important implications on the trend of the measured soot yields versus temperature in a CO flame versus a methane flame.

Fletcher and coworkers (Fletcher et al., 1997) reported a slight decrease in soot yields with increasing temperature (above 1650 K) when coal was pyrolyzed in a methane flame. However, in contrast, soot yields were found to increase with increasing temperature for all the coals in the current study (see Figure 5.8). These coal pyrolysis experiments were performed in the same reactor; the only difference is the fuel. The slight decrease in soot yields at high temperatures in the methane flame was thought to be due to two major reasons. First, the much higher steam production in a methane flame could reduce the soot yields by steam gasification, as shown in equation 5.11. Second,

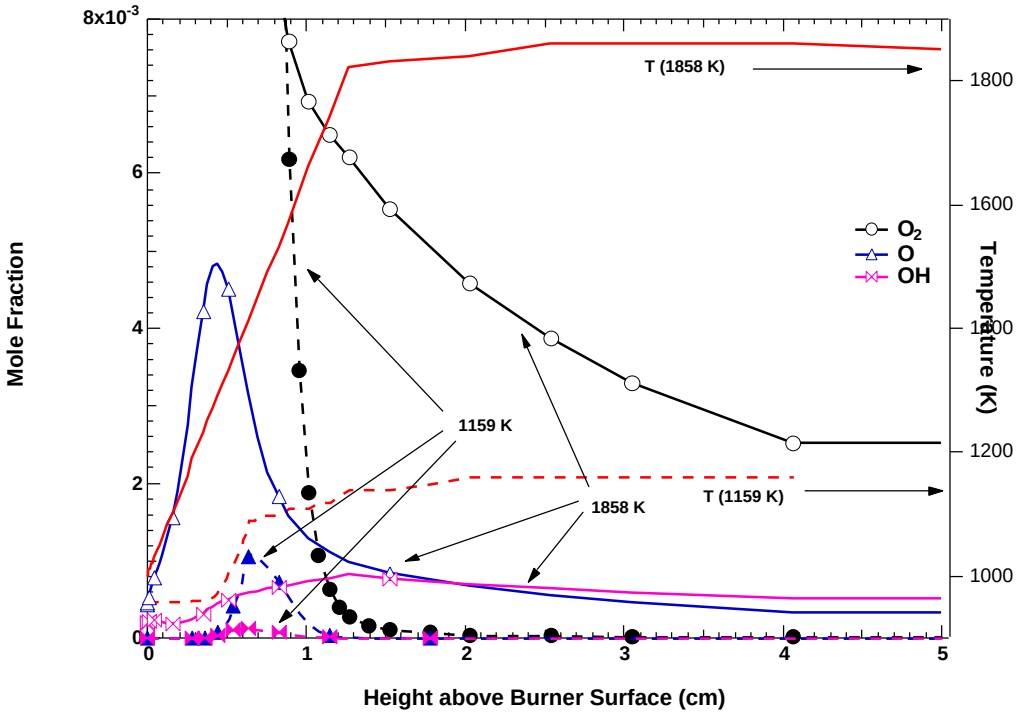

Figure 5.19. Calculated mole fractions of the major oxygen-containing species versus distance in the FFB with a CO flame.

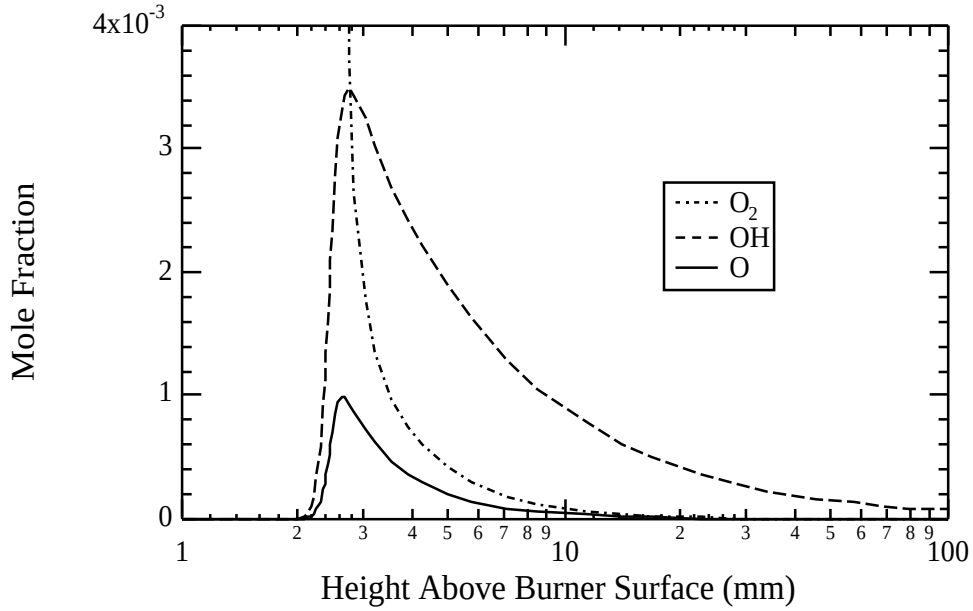

Figure 5.20. Mole fractions of the major oxygen-containing species in the FFB with a methane flame at 1900 K (adapted from Ma, 1996).

the higher fractions of OH in a methane flame could react with soot precursors such as PAH in the tar, resulting in lower soot yields.

$$H_2O + C = CO + H_2 \quad (5.11)$$

Bittner and Howard have suggested that the addition of OH to the ring may be responsible for the destruction of benzene in a sooting flame (Bittner and Howard, 1981). Haynes also pointed out that OH radicals appear to be the chief oxidant of the PAH formed from a coal or liquid fuels (Haynes, 1991). Therefore, it is logical to believe that OH radicals could play a more important role than other radicals in the destruction of tar molecules before soot formation. At 1860 K, the peak mole fraction of OH is about 8×10^{-4} in the CO flame, while the peak mole fraction of OH in the methane is about 3.5×10^{-3}, which is more than four times higher at a similar temperature condition. It is possible that the larger concentration of OH radicals in the methane flame that causes the decline of soot yield with increasing temperature at temperatures above 1600 K.

Since radicals are very reactive, the destruction of soot precursors by radicals is very plausible. The fact that the methane flame has higher mole fractions of OH is therefore consistent with the observed decrease in soot yields in that flame.

Modeling of Tar and Soot Yields

As explained in the first chapter, there are three stages in coal combustion including primary pyrolysis, secondary pyrolysis and char oxidation. Among these three processes, the primary pyrolysis is the most sensitive to the chemical structures of different coal types (Niksa, 1994). Based on the measured chemical structure parameters, the CPD model (Fletcher, et al. 1992) can describe the early stage of devolatilization with adequate accuracy. However, secondary reactions of volatiles from primary pyrolysis are not treated in the CPD model.

A simple mechanism is proposed here based on previous studies to describe the major reaction pathways during secondary coal pyrolysis. Only secondary reactions are modeled here, with three major reaction routes illustrated in Figure 5.21. It is assumed that there are two competitive reactions, cracking (r_c) and polymerization (r_p), for primary tars. At temperatures below 1200 K, the cracking reaction is dominant, causing the release of aliphatic materials and carbon oxides. These secondary gases are mainly formed from the side chains and oxygen-containing functional groups in the tar molecules. At more severe pyrolysis conditions, secondary reactions cause ring opening reactions, preferentially those aromatic structures with heteroatoms such as oxygen and nitrogen, to release HCN (Chen, 1991) and CO (Ledesma, 1998). Beginning at 1400 K, ring structures will undergo polymerization to form soot after stripping off the functional

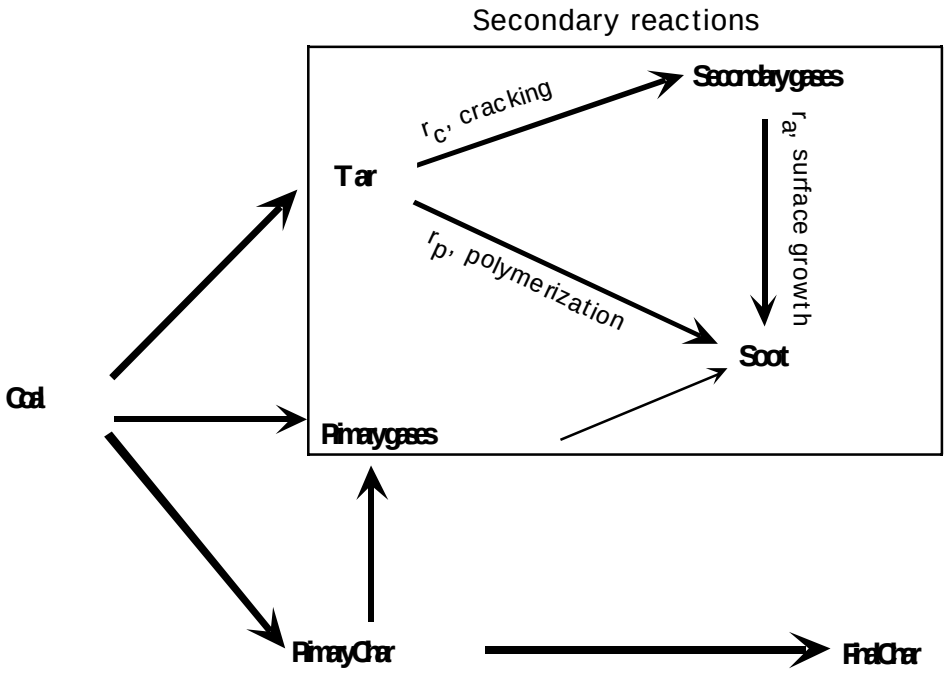

Figure 5.21. Proposed reaction mechanism in modeling the secondary pyrolysis.

groups. It is further assumed that only a certain fraction of primary tar can be directly converted to soot. This assumption is based on the fact that the secondary gas production from primary tar reaches an asymptote at high temperatures. The fraction of primary tar that can be directly transformed to soot is assumed constant for each coal and dependent on coal rank (correlated with coal oxygen content). In order to simplify the problem, another assumption is made that the cracking and polymerization reaction, which are very complicated and involving hundreds of elemental steps, can be lumped into a set of first-order reactions.

During the construction of the model, it was also found necessary to include a secondary soot growth mechanism to best fit the experimental data. The soot addition (r_a) is also modeled as a first-order reaction by the attachment of hydrocarbons in the flame to the primary soot. Previous studies show that the surface of hot soot particles readily accepts hydrocarbons from the gas phase (Homann and Wagner, 1967). Pyrolysis experiments on coals also demonstrated that certain hydrocarbon gases (such as C_2H_2 and C_6H_6) may participate in soot formation at high temperatures (Haussmann and Kruger, 1989; Chen, 1991). Chen suggested that only the light hydrocarbons released from tar cracking (i.e., secondary gases) may participate in the soot addition. However, it seems more reasonable to include the hydrocarbons released during the early stage of devolatilization *and* the additional gases from thermal cracking of char (primary gases) as sources for soot growth. In this simulation, no differentiation was made between soot addition from the primary gases and from the secondary gases.

It should be noted that no chemical structure parameters were used in the simulation. The FTIR and GC analysis showed a distinct similarity in the major

components for primary tars from various coal types (Freihaut, et al. 1989; Nelson, et al. 1990). The cracking reactions of tars from different coals also showed similar kinetic parameters (Doolan, et al. 1986; Serio, et al. 1987). Therefore, secondary reactions may be less influenced by the chemical structure than the local environment, such as temperature and stoichiometry. However, the chemical structure of the nascent tar is still important. It is well established that more aromatic structures exist in the tars of high rank coals, which implies a higher sooting tendency under pyrolysis conditions. However, for simplicity, the chemical structure of tar is omitted in this model development. The description of the rates for tar cracking, polymerization and gas-phase soot addition are as follows.

$$r_c = \frac{df_{tar,c}}{dt} = k_c(f^*_{tar,c} - f_{tar,c}) \tag{5.12}$$

$$r_p = \frac{df_{tar,p}}{dt} = k_p(f^*_{tar,p} - f_{tar,p}) \tag{5.13}$$

$$r_a = \frac{df_{soot,a}}{dt} = k_a(f^*_{soot,a} - f_{soot,a}) \tag{5.14}$$

$$\frac{df_{tar}}{dt} = -(r_c + r_p) \tag{5.15}$$

$$f^*_{tar,c} + f^*_{tar,p} = 1 \tag{5.16}$$

where $f_{tar,c}$ stands for the mass fraction of primary tar that participates in tar cracking; $f_{tar,p}$ stands for the mass fraction of primary tar that participates in tar polymerization, and $f_{soot,a}$ stands for the mass fraction of the total additional soot (as dry, ash free coal) from hydrocarbons in the gas. The asterisk means the asymptotic solution (i.e., ultimate yield) for a specific fraction of primary tar or soot. For example, $f_{tar,c}^*$

stands for the ultimate mass fraction of primary tar that is eventually gasified to secondary gases; $f_{tar,p}^{*}$ stands for the ultimate mass fraction of primary tar that is eventually converted to soot, and $f_{soot,a}^{*}$ stands for the ultimate mass fraction of additional soot from hydrocarbons. It should be pointed out that it is the fraction of primary tar or the fraction of the ultimate soot growth from hydrocarbons that was modeled, not the coal mass fraction. The residual tar and soot yield based on the dry, ash-free coal can be calculated by the following equations:

$$y_{tar}(t) = y_{tar}^{0} \quad f_{tar}(t \quad (5.17)$$

$$y_{soot}(t) = y_{tar}^{0} \quad f_{tar,p}(t) + f_{soot,a}^{*} \quad f_{soot,a}(t) \quad (5.18)$$

where t, f and y are residence time, fraction of the ultimate products (tar or soot) and fraction as dry, ash-free coal, respectively.

Calculation of Kinetic Parameters

The tar cracking reaction was assumed to have an activation energy of 100 kJ/mol, obtained from the vapor-phase secondary cracking of nascent tars from a Pittsburgh #8 coal as reported by Serio et al. (1987). A comparable activation energy was also derived by fitting the tar cracking data for a subbituminous coal (Doolan, et al. 1986) and a bituminous coal respectively (Ledesma, 1998).

For the Illinois #6 coal, the primary tar yield was calculated from the CPD model using the measured ^{13}C NMR data. For the other coals, the primary tar yields were first calculated by the CPD model using a correlation of the structure parameters based on the elemental composition of the parent coal (Genetti, 1999). The first data point of tar yield in the current study is much lower than the "CPD-predicted" tar yield. The kinetic parameters presented here are the best fit for the data measured in the FFB. However, the

tar decay rate using these parameters cannot explain the decay from the "CPD-predicted" tar yield to the first data point measured in this study. The "CPD-predicted" tar yield is too high to allow development of a reasonable tar decay model to fit the data in the current study. The low tar yields measured in the present work were probably due to the post-flame environment in which the coals were pyrolyzed; the short residence times in the FFB may be another reason. Determination of the exact reason for the low tar yields is beyond the scope of the present work.

The activation energy for soot formation from tar (E_p) was assumed to be 230 kJ/mol and the activation energy for soot addition from hydrocarbons (E_a) was assumed to be 320 kJ/mol. E_p is based on the result of previous studies (Ma, 1996) and is modified to better fit the experimental data. E_a is the best-fit parameter for this study. The activation energy for soot formation from tar is lower, because the tar has a higher sooting tendency since it contains PAH. With the activation energy fixed, the experimental data were used to fit the pre-exponential factor for different coals. The ultimate fraction of primary tar that can be converted to soot was also assumed based on the oxygen content of the coal.

A summary of the coal-dependent kinetic parameters by fitting the experimental data is shown in Table 5.4. The values of $f_{tar,c}^*$, $f_{tar,p}^*$ and $f_{soot,a}^*$ are presented in Table 5.5. These numbers have no specific physical meaning, but represent the best values to fit the experimental data. However, this does not mean these values are only random numbers. CO and CO_2 are the major secondary gases from tar cracking. It was found that yields of CO and CO_2 are much higher for low rank coals than for high rank coals (Cliff, et al. 1984; Doolan, et al. 1986; Chen, 1991). The higher yield of secondary gases from tar

implies an accordingly lower soot yield. Therefore, values of the ultimate tar fraction in Table 6.2 that can be directly converted to soot (f_p^*) were adjusted according to the coal rank. It is believed that secondary gas production from tar is somewhat associated with the oxygen content of the parent coal, but the exact nature of this relationship is still unclear. The measured and calculated profiles of the tar plus soot for the four coals are presented in Figures 5.22 to 5.25. It must be emphasized that these kinetic parameters are not expected to extrapolate to temperatures or conditions significantly different from those in the current experiments. The results, however, do provide insight into the rate of homogeneous (cracking) and heterogeneous (soot formation) tar secondary reactions for coals of different ranks.

Table 5.4. Summary of the Best-Fit Kinetic Parameters for Secondary Reactions of Coal Volatiles.

	A_c (sec^{-1})	E_c (kJ/mol)	A_p (sec^{-1})	E_c (kJ/mol)	A_a (sec^{-1})	E_a (kJ/mol)
Illinois #6	2.5E5	100	2.0E9	230	5.0E10	320
Utah	5.0E5	100	2.0E9	230	8.0E10	320
Black Thunder	1.0E6	100	2.0E9	230	3.0E11	320
Knife River	4.0E5	100	2.0E9	230	5.0E11	320

Table 5.5. Values of $f_{tar,p}^*$, $f_{tar,c}^*$ and $f_{soot,a}^*$ Used in the Simulation.

	ultimate tar fraction to soot ($f_{tar,p}^*$)	ultimate tar fraction to secondary gas ($f_{tar,c}^*$)	ultimate additional soot from hydrocarbons ($f_{soot,a}^*$)
Illinois #6	0.7	0.3	0.04
Utah	0.78	0.22	0.04
Black Thunder	0.63	0.37	0.04
Knife River	0.4	0.6	0.02

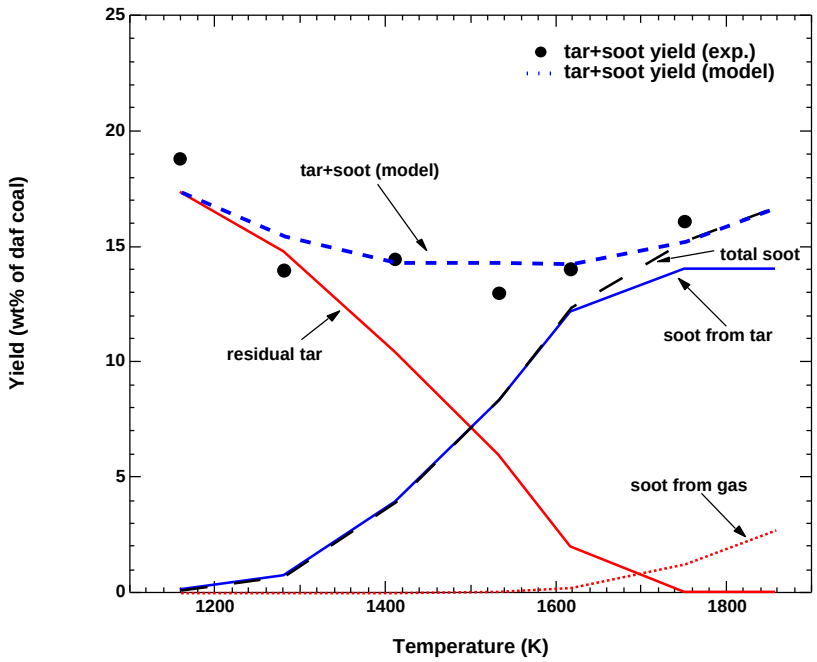

Figure 5.22. Calculated tar and soot yield for the Illinois #6 coal.

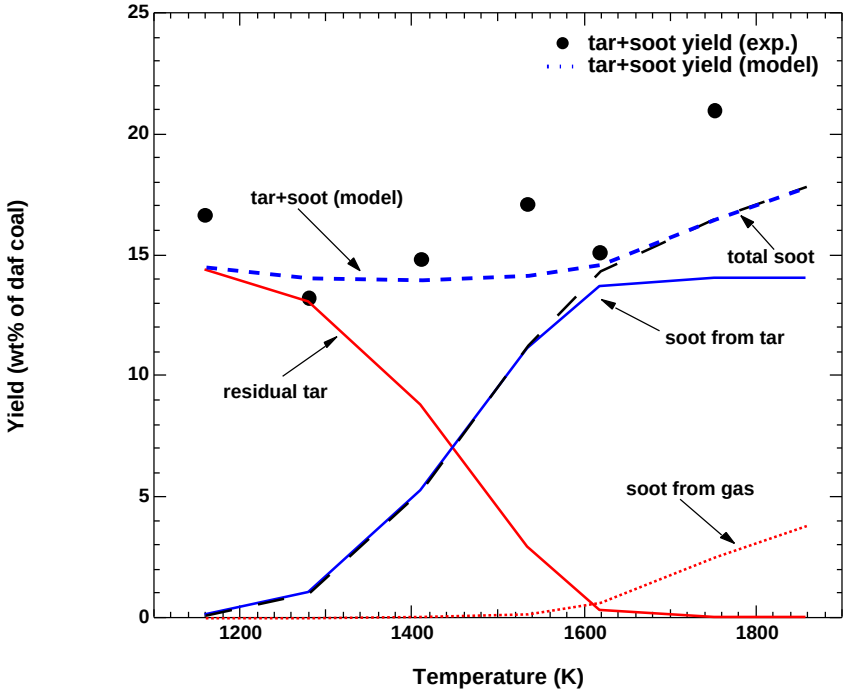

Figure 5.23. Calculated tar and soot yield for the Utah coal.

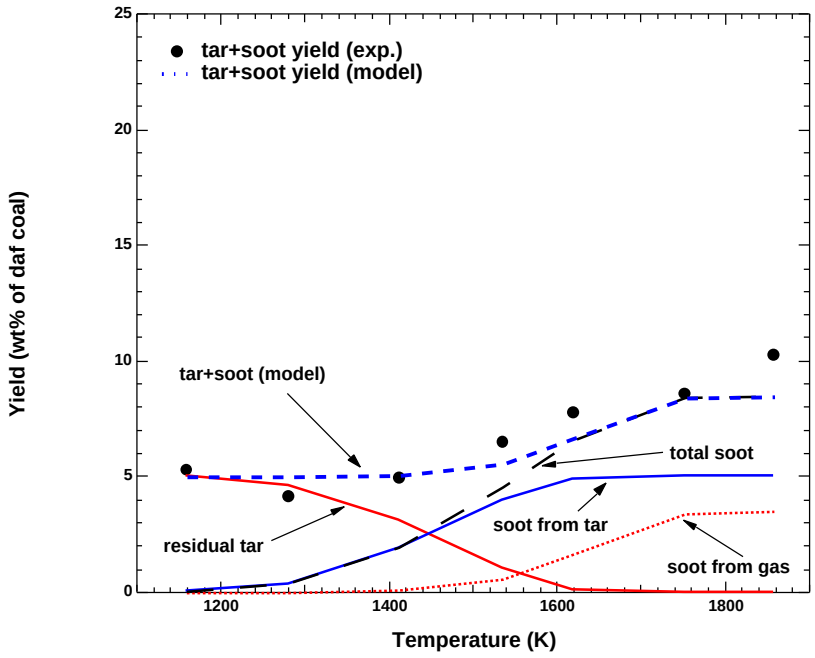

Figure 5.24. Calculated tar and soot yield for the Black Thunder coal.

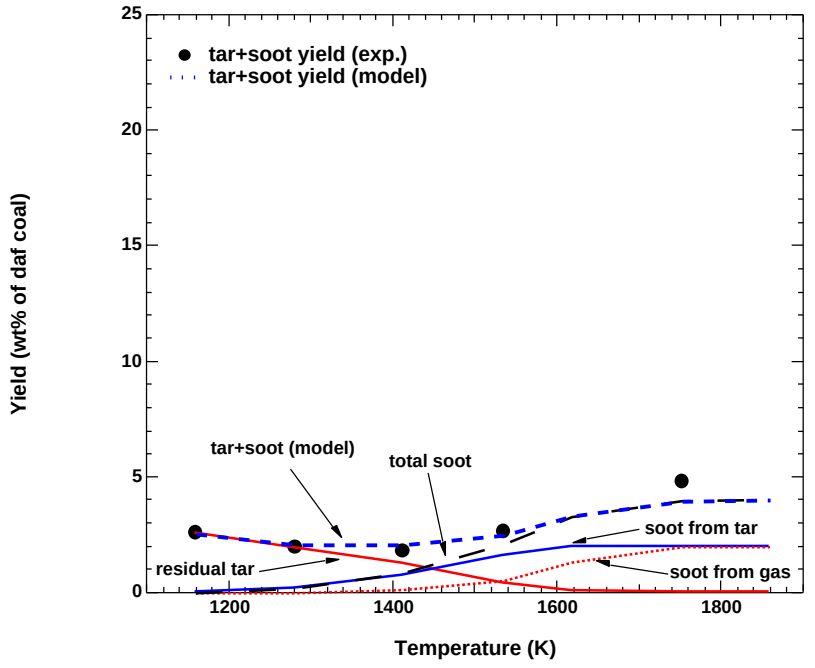

Figure 5.25. Calculated tar and soot yield for the Knife River lignite.

Discussion

Tar and Soot Yields

The Illinois #6 coals have been extensively studied, so a comparison of tar or soot yields with previous work can be made, as shown in Figure 5.26. The tar yields of Hambly (1998) and Watt (1996) were obtained by pyrolyzing the coal in a drop-tube reactor in an inert environment. Their data show a similar trend to that found in this study: the yields of tar plus soot decreased first at temperatures below 1400 K, due to secondary reactions. At high temperatures, the soot yields in this study agree well with Ma's data except the one point at 1650 K. Also shown in the figure is the maximum tar yield from primary pyrolysis reported by Chen (1991). The tar yield is more than 60%

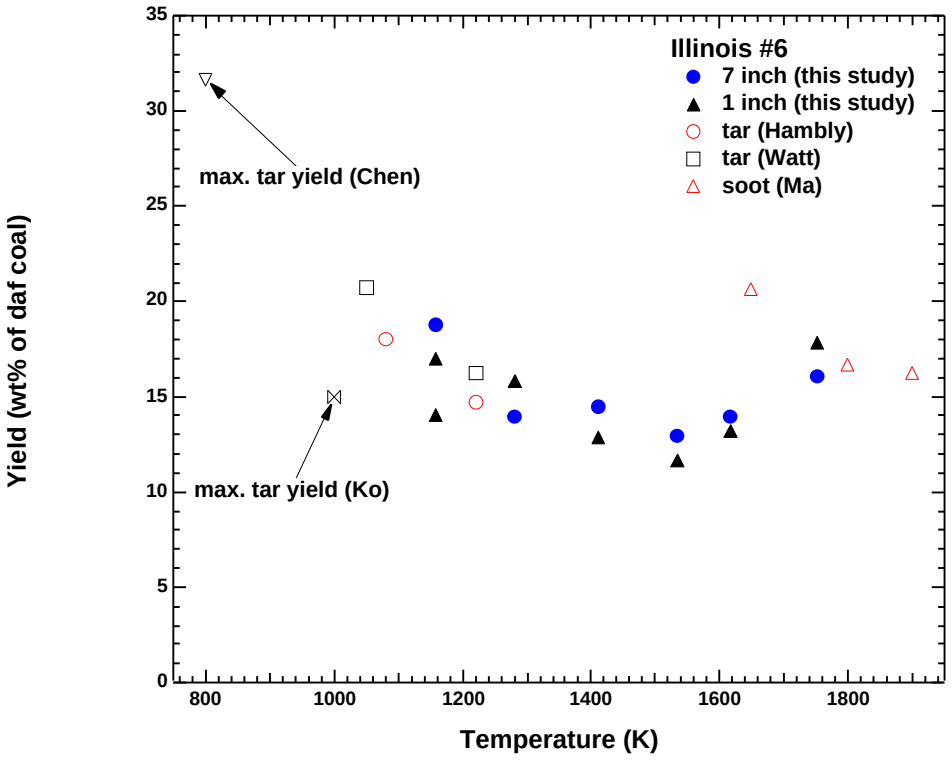

Figure 5.26. Comparison of tar and soot yields for Illinois #6 coal (the temperature is the particle temperature for Chen and peak gas temperature for others).

higher than the highest tar/soot yield obtained in this study. This cannot be solely attributed to secondary reactions. In Chen's experiment, the collected tar was extracted from glass filters by a solvent (THF). The pure tar sample was then weighed after evaporation of the solvent. The tar yield measured this way could be subject to the following errors: incomplete evaporation of the solvent arising from a partial miscibility between the solvent and the tar and possible residues from the solvent itself. Both can result in a higher value than the actual tar yield. The maximum tar yield obtained in a heated grid reactor (Ko, et al. 1988) is lower than that in this study. There are probably two reasons for the difference. First, the low temperature and low heating rate used in the heated grid reactor may result in a lower tar yield. Second, tar collection may be incomplete due to recondensation of tar to the remaining char and deposition of tar on the trap wall, as reported by the author.

A comparison of the tar and soot yields of Utah seam coals is presented in Figure 5.27. It should be noted that the yields reported by Freihaut and coworkers (Freihaut and Seery, 1981) were obtained under vacuum pyrolysis and on a dry coal basis. It is clear that the tar and soot yields collected at the 1 inch location in this study are much lower than those collected at the 7 inch location. By examining the mass release data at 1159 K, it was found that mass release at the 7 inch location is 25% (absolute) higher than that measured at the 1 inch location, while the difference is about 10-15% for other coals. That means the lower tar and soot yields are probably due to the incomplete devolatilization process at short residence times. The tar and soot yields collected at the 7 inch location are comparable with those reported by Friehaut and Ma at temperatures below 1650 K. However, at temperatures higher than 1650 K, a different trend is

observed. In this study, the soot yields continued to increase with increasing temperature, while the tar or soot yields declined with increasing temperature in the case of Freihaut and Ma. In Freihaut's experiment, tar was generated on a heated metal screen. Since the tar quickly escaped the hot screen once it was released, it had no chance to form soot. The systematic decrease of tar yields was totally due to the intra-particle or extra-particle thermal cracking of the tar. In Ma's case, the decrease of the soot yield is thought to be due to the existence of large quantities of OH radicals in the methane flame front that may destroy the soot precursors such as tar and PAH, as explained in the previous section.

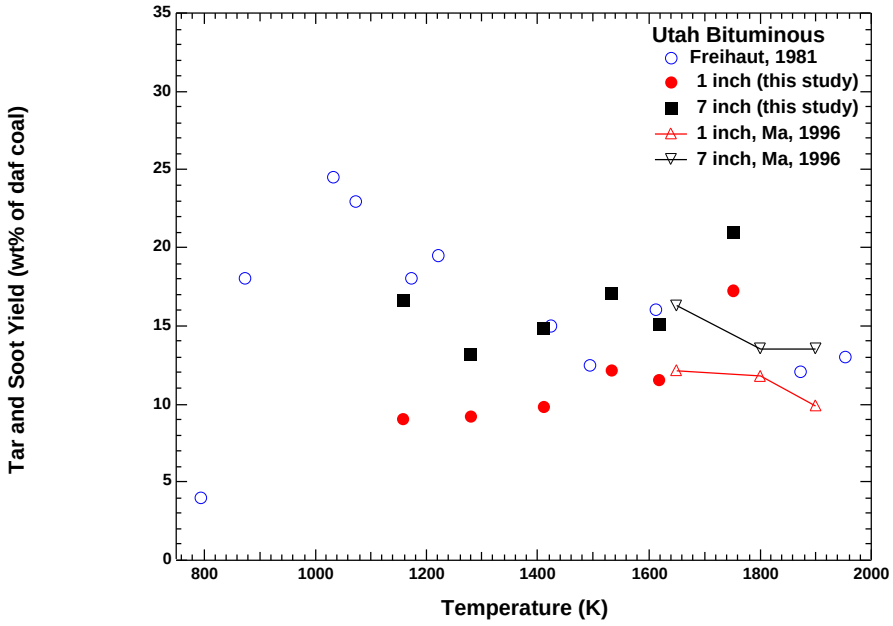

Figure 5.27. Comparison of tar and soot yields for Utah coal (Freihaut's data were on the dry coal basis).

For Black Thunder and Knife River coals, a similar comparison cannot be made due to a scarcity of data. The only tar yield for a Wyodak coal (which comes from the

same seam as Black Thunder) was reported by Ko. Under 0.1 M Pa, the maximum tar yield was 19.3% (daf).

Finally, the rank dependence of tar and soot yields is compared to those from the literature (see Figure 5.28). The maximum tar yield defined in this study is the highest collectable tar at the lowest temperature setting, 1159 K. Xu and Tomita determined the maximum tar yield by pyrolyzing 17 coals at 1037 K in a Curie-point pyrolyzer (Xu and Tomita, 1986). The heating rate was approximately 3000 K/s. Tyler's data are exclusively for Australian bituminous coals pyrolyzed in a fluidized bed reactor (Tyler, 1979). The data reported by Chen (1992 a) are the maximum tar yields during primary pyrolysis. The maximum tar yields obtained in the BYU drop tube reactor are also shown. From the figure, several trends of the dependence of tar/soot yield on coal type

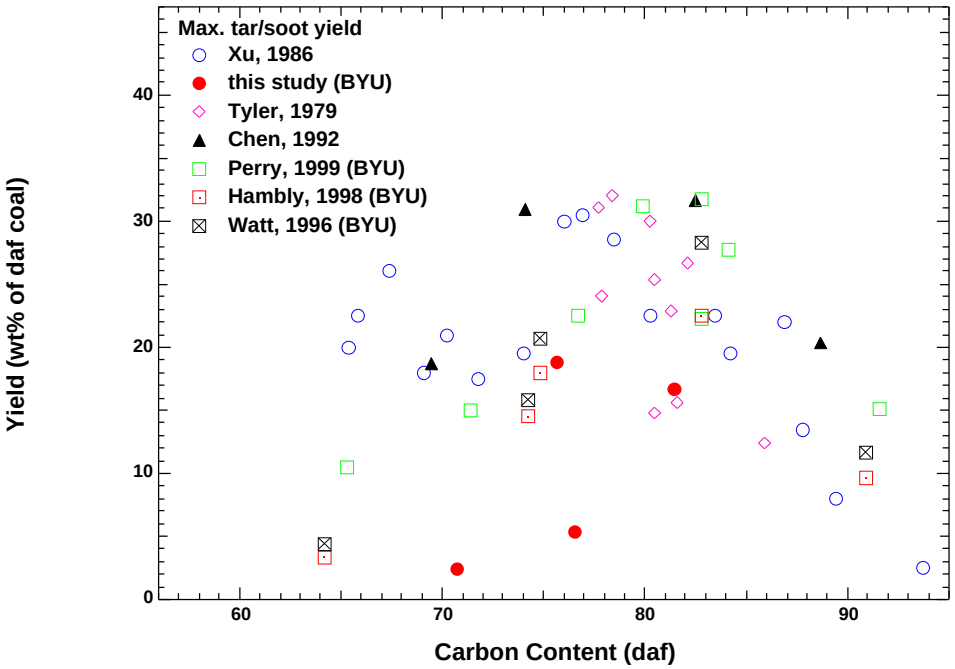

Figure 5.28. Comparison of rank dependence of tar and soot yields.

can be observed. First, there is no distinct relationship between carbon content and the maximum tar yield, as seen by the large scatter in the data. From Tyler's data, even for similar bituminous coals, the tar yield of one coal can be twice as much as another coal. The general rule of thumb is that the tar yield is highest for bituminous coals, but drops for lower rank coals such as subbituminous and lignite and higher rank coals such as anthracite. Second, for low rank coals, the yields reported at BYU are much lower than those of Xu. This is probably because Xu's tar yields were calculated by difference from the gas analysis and the weight loss, making them susceptible to over-estimation (Perry, 1999).

The tar/soot yields obtained in this study are much lower than those by other researchers, especially for low rank coals. Several factors may be responsible for such a difference. First, the data reported in this study are not the actual maximum tar yields. Significant secondary reactions have already occurred before the first sampling location in the FFB, leading to a lower tar yield. The measured tar/soot yields declined monotonically with temperature below 1500 K. Second, it is possible that tar was trapped inside the filters instead of on the surface at low temperatures (Figure 4.6). However, the filters were weighed together to determine the tar yield. A yellowish deposit was found on the glass wool installed downstream before the gas cell. However, this amount was insignificant. Therefore, the low tar yield is not thought to be caused by the tar filters. Third, semivolatile species of molecular weight 100 to 200 amu may be another reason. They do not fit clearly into either the tar or gas categories (Solomon, et al. 1992). These species are too volatile to remain condensed on tar collection surfaces, but are not volatile enough to stay in the gas phase. This sometimes can result in 5-10%

loss in materials. Fourth, the post-combustion environment used in this study may also contribute to the lower tar and soot yield. The combustion products, such as CO, CO_2 and H_2O, readily react with the highly active nascent tar molecules, resulting in a lower tar yield. The influence of the oxygen-containing species in the flame should be insignificant at low temperatures, due to the low concentrations. However, they may have a substantial effect on high temperature soot yields.

It was found that the secondary reactions of the tar before the first collection point in the FFB and the interactions of the post-combustion environment with the tar are likely the reasons for the observed low tar and soot yields in this study.

Secondary Reactions of Nascent Coal Volatiles

When heated, tar and light gases will be released from coal particles during primary pyrolysis. Primary pyrolysis is a fast reaction, usually occurring in a few milliseconds under a typical pulverized coal firing condition. The tar quickly reaches its maximum yield at about 1000 K. Under high temperature and fuel-rich conditions, the primary tar will undergo two competitive reactions: thermal cracking and soot formation.

Gas-phase Thermal Cracking Reactions

The chemical structure analysis by ^{13}C NMR methods clearly demonstrates that thermal cracking is dominant at low temperatures, leading to the release of secondary gases (Solum, et al., 2000). Serio et al. (1987) investigated kinetics of the thermal cracking of fresh coal tars generated from fixed-bed pyrolysis at 500-900^{o}C. Tar conversion was found to be insignificant below 600^{o}C. At higher temperatures, the major products were light gases, oils and some transformed tar. The formation of char from secondary reactions of tar was also identified. There is certainly a possibility that the primary tar will redeposit onto the char surface to participate in the crosslinking reaction.

However, under the high temperature, high heating rate conditions encountered in an industrial furnace, such reactions should be minimal.

Secondary reactions of primary tar were examined more clearly in Doolan's experiment (Doolan, et al. 1986). The primary tar was obtained by pyrolyzing an Australian subbituminous coal in a flash pyrolyzer operated at 870 K. The tar was then cracked in a quartz tube reactor at 870-1370 K and in a shock tube reactor at 1100-2000 K. The yields of various products in the quartz tube reactor are shown in Figure 5.29. Below 1300 K, the major products were various hydrocarbon gases, CO, H_2O and possibly some light oils. It is clear that thermal cracking of tar is a major source of hydrocarbon gases during pyrolysis. The release of light hydrocarbons increased with temperature up to 1300 K, then started to decline slightly after reaching the maximum yield. Soot formation commenced at 1300 K by direct conversion from tar, as evidenced by the sharp decrease of the remaining tar.

It is also interesting to find that the combined yields of light hydrocarbons, CO and H_2O reached an asymptote at 1200-1370 K. That is to say, the ultimate yield of secondary gases from primary tar is somewhat constant at high temperatures. Although the highest temperature used by Doolan in the quartz reactor was 1370 K, it is most likely that this trend will remain valid at even higher temperatures. The dashed line in Figure 5.29 represents the model prediction of the production of secondary gases from tar during secondary reactions using the kinetic parameters in the Tables 5.4 and 5.5. Only the cracking mechanism was included in the model prediction; no soot formation was included. An excellent agreement is reached between the data points and model predictions regarding the remaining tar below 1300 K, before the onset of soot formation.

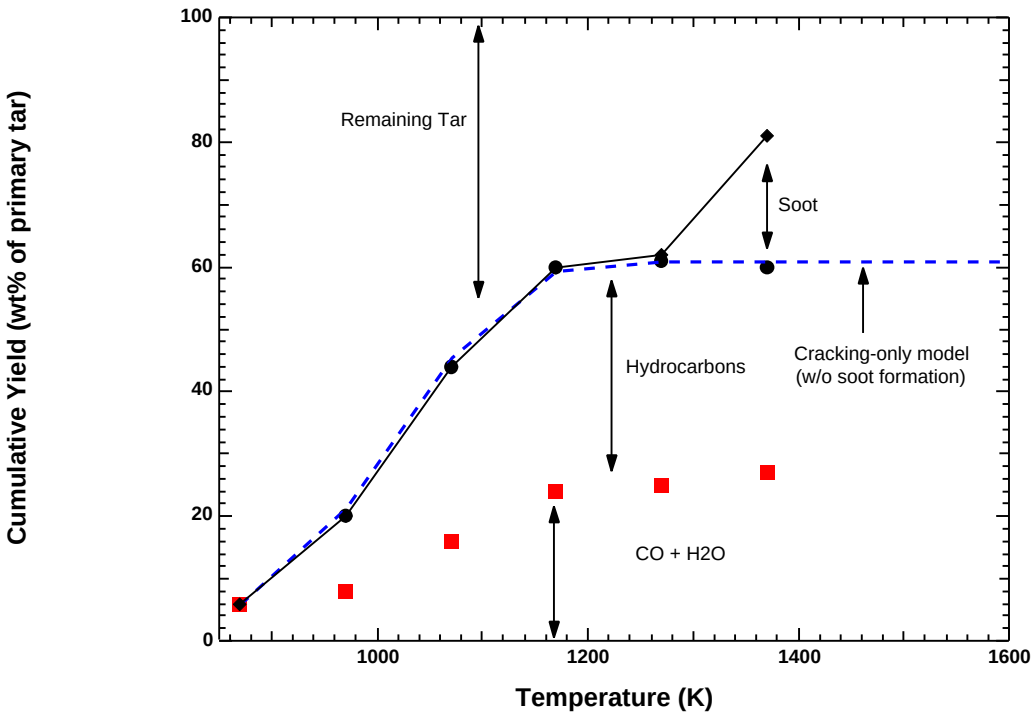

Figure 5.29. Cumulative product yields of the primary tar as a function of reactor temperature (adapted from Doolan, et al. 1986).

The hypothesis of constant gas production from the tar at higher temperatures (>1300 K) is supported by the following observations. First, in Doolan's high temperature shock tube experiment where a temperature as high as 2000 K was achieved, the yield of CO reached an asymptotic value of 18% (wt% of primary tar) at temperatures higher than 1600 K. The amount of oxygen in the CO produced from the tar was equal to the original oxygen in the tar. Second, the tar yields obtained at different final temperatures for various coal types reported by Freihaut (1981) also confirmed a constant ultimate gas release from primary tar at temperatures higher than 1400 K (see Figure 5.30). The tars were generated in a heated grid reactor operated at different temperatures.

Despite the scatter in the data, a general trend can be identified for each coal: the tar yield quickly rises to its maximum during primary pyrolysis then decays slowly to an asymptote which is coal-dependent. The decay of the tar was solely due to thermal cracking reactions, since no soot was present even at 1800 K. Once released from the coal, the tar was quenched immediately by the surrounding cold gas. Therefore, the tar had no chance to transform to soot, which is favored at high temperatures. The constant tar yields at high temperatures in Freihaut's study suggest a constant gas production from primary tar.

It is well established that the fresh tar is comprised of polycyclic aromatic clusters with various attachments. On the other hand, soot is composed of much larger aromatic clusters and/or polymerized PAH's. The fraction of hydrogen and other heteroatoms in

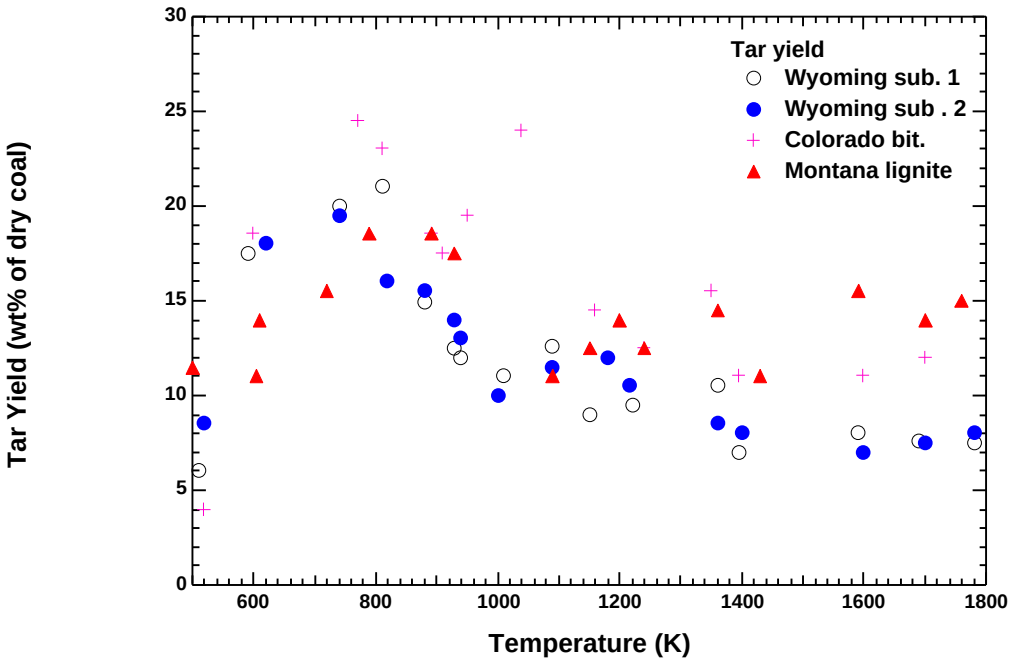

Figure 5.30. Tar yields as a function of final temperature for different coal types (adapted from Freihaut, et al. 1981).

soot is very small. In order to form soot that is relatively free of hydrogen, oxygen and nitrogen, the tar must first shed the attachments or even open the aromatic rings to release those elements. The oxygen will be converted to CO or, to a lesser extent, CO_2. Aliphatic side chains will be converted to light hydrocarbons. The nitrogen will be released mainly in the form of HCN.

In the simulation of the secondary reactions of tar in the modeling section, it was also assumed that the mass fraction of primary tar, which is eventually converted to gas, is also coal dependent, with lower rank coals producing more secondary gases. This hypothesis can be justified by the chemical structure data reported by Perry (1999).

In Table 5.6, the structural parameters derived from ^{13}C NMR for two coals and their corresponding tars and soots are presented. South Banko lignite and Pittsburgh #8 hv bituminous coal represent the two different coal types. Previous measurements have shown that the fresh tar released from coal usually has a similar chemical structure to that of the coal (Pugmire, et al. 1990). Therefore, here the coal parameters are used for the primary tar.

Table 5.6. Structural Parameters Derived from ^{13}C NMR Analysis for Tars (adapted from Perry, 1999)[#].

sample	condition	χ_b	C_{cl}	σ+1	P_0	B. L.	S. C.	M_{cl}	M_δ
South Banko	coal	0.278	13	5.3	0.55	2.9	2.4	410	47
(lignite)	1250 K	0.255	12	2.7	0.95	2.6	0.1	164	5
Pittsburgh #8	coal	0.314	15	4.5	0.62	2.9	1.6	311	28
(hv bituminous)	1250 K	0.341	17	4.2	0.95	4.0	0.2	249	9
	1650 K (soot)	0.429	21	4.8	0.89	4.3	0.5	316	12

[#]see Nomenclature for the definition of the parameters.

There are 30% more side chains per cluster (2.4) in South Banko parent coal than in the Pittsburgh #8 coal (1.6). These side chains are usually aliphatic in nature and are released as light hydrocarbons during pyrolysis (see Figure 2.2). At 1250 K, the side chains for the two coal tars are similar (0.1 and 0.2 respectively), indicating that more side chains are lost for the lignite tar. This can be viewed more clearly by comparing the total attachments per cluster ($\sigma+1$) and the average molecular weight per attachment (M_δ). For the Pittsburgh #8 coal, the number of total attachments per cluster for the primary tar (4.5) and the tar at 1250 K (4.2) are similar. However, $\sigma+1$ drops substantially from 5.3 to 2.7 for the South Banko coal tar over this same temperature range. The corresponding average molecular weight per attachment drops from 28 to 9 for the Pittsburgh #8 coal tar for this temperature range and from 47 to 5 for the South Banko tar. This means that low rank coal tars not only lose more attachments, but also lose more mass per attachment. This is direct evidence that low rank coal tars lose more mass than high rank coal tars during secondary reactions. However, a quantitative correlation of such rank dependence cannot be established from the limited data in this study.

Soot Formation

Soot formation from coal tar usually commences between 1350 and 1400 K, as indicated by the significant change of the tar structure during that temperature range (Solum, et al. 2000). Ring opening may be the first step in soot formation. Pyrolysis experiments on biphenyl (see Chapter 6) showed that ring opening is the first step to soot formation for some model compounds. Ring opening releases the heteroatoms and other aliphatic materials and creates free radicals. These radicals will then undergo a series of

reactions to form larger clusters through such reactions as condensation and polymerization. The coal tar has a higher sooting tendency than aromatic model compounds and light hydrocarbons, since the soot incipient temperature for coal tar is much lower. This can be explained in two aspects. First, the coal tar can produce more radicals and is more reactive because it has more attachments per cluster (σ+1). Second, the larger ring structure in coal tar has a higher stabilizing effect during polymerization (Badger, et al. 1964).

The sooting potential of different coal types was studied in an inert pyrolysis environment in a drop-tube reactor (Nenniger, 1986). It was found that the soot yield increased while the tar and hydrocarbon gas yield decreased as the pyrolysis temperature was raised. The soot yield reached an asymptote at high temperatures, which is dependent on coal rank. Wornat et al. (1988a) investigated changes in the composition of PAH during the tar evolution from the pyrolysis of high-volatile bituminous coal in argon. The compounds with more complex attachments were found to be more reactive than compounds with simple or no attachments. This is consistent with the previous discussion claiming that coal tar has a higher sooting tendency than the model compounds. PAH serves as a soot precursor, since the increase of soot yield was nearly offset by the decrease of PAH. In another pyrolysis experiment, Chen and co-workers (Chen and Niksa, 1992b) reported that the yields of tar/oils plus soot during secondary pyrolysis were constant and were equal to the maximum tar-plus-oil yields obtained during primary pyrolysis.

All of these pyrolysis experiments conducted in inert environments reported that the sum of tar plus soot remained constant during pyrolysis. The soot yields increased

monotonically with temperature or reached an asymptotic value at high temperatures. However, the sum of tar plus soot in this study follows a different pattern: the soot yield first decreased and then increased with temperature. The sum of tar plus soot at 1858 K is almost two times the value at 1159 K for Knife River and Black Thunder coals, although the soot yields are small.

It is possible that the soot yield at high temperatures is susceptible to overestimation by ash contamination. Ash in the parent coal may vaporize during pyrolysis, then recondense with soot on the filters. Analysis of the high temperature soot samples showed about 10% ash in the Knife River soot and minimal amounts in the soots from the other three coals. Therefore, ash contamination of soot was not a major factor in these experiments, and cannot explain the increase in soot yields.

The chemical structure analysis facilitates the investigation of the major changes of tar during secondary pyrolysis, which can, in turn, be used to explain the measured tar and soot yields measured in this study. At 1159-1411 K, the thermal cracking reaction predominated, which is characterized by two distinct processes. First, the tar lost most of the aliphatic side chains and oxygen functional groups. Next, ring opening reactions also commenced to produce more light hydrocarbons and to release heteroatoms. Since soot formation is negligible at this temperature range, a net decline of the yield of tar plus soot was observed. From 1411 K, direct conversion of soot from tar began, as evidenced by the increase of aromatic carbon per cluster. As secondary reactions proceeded, both ring rupture and polymerization became significant. As the cluster size became larger, polymerization of PAH was accelerated. The rate of soot formation surpassed the rate of tar decay, therefore, the sum of tar plus soot increased steadily from 1411-1618 K. The

continuous growth of soot yield after 1618 K can only be explained by the addition of hydrocarbon species released from primary pyrolysis and the subsequent secondary cracking reactions. Eventually, these hydrocarbons were depleted at high temperatures (probably higher than 1900 K), and the soot yield reached an asymptotic value which is dependent on coal type.

Strong evidence has shown that direct addition of certain hydrocarbon species to the soot surface is a major soot growth mechanism at high temperatures. Soot formation from hydrocarbon fuels has been studied extensively. However, the effects of light hydrocarbons during the soot formation in a coal system are still unclear.

The participation of hydrocarbons in the growth of coal-derived soot was first noticed by Chen based on a carbon balance (Chen, 1991). In his experiment, the carbon fraction (total carbon in the coal) incorporated into the sum of tar/oils and soot was found to increase with increasing severity of secondary reactions. Since the carbon fraction released as CO during pyrolysis was negligible (less than 1%), the only source of carbon that contributed to soot growth would be hydrocarbons in the gas phase. Char is another possible carbon donor. However, the carbon in char (solid phase) cannot directly participate in soot growth, since carbons must be released as hydrocarbons first.

In this study, a similar phenomenon was also identified. The carbon fractions in the tars or soots are plotted in Figure 5.31 for the four coals in this study. As seen from the figure, at temperatures higher than 1500 K, the fraction of coal carbon incorporated into tar/soot increased substantially on a relative basis with increasing temperature. During secondary pyrolysis, primary tar will lose carbons due to the release of light hydrocarbons. When heteroatoms (mainly oxygen) in tar are expelled during ring

opening reactions, additional carbons are lost since oxygen is released from tar as CO (Nenniger, 1986) and nitrogen as HCN (Chen, 1991). In Figure 5.31, the fraction of coal carbon in the sum of tar plus soot at 1858 K is much higher than that at 1159 K. That means the carbon loss during tar decomposition was compensated by gains in carbon from other sources. Previous studies showed that the CO yield always increases with increasing temperature during secondary reactions (Doolan, et al. 1986; Ledesma, et al. 1998), CO is therefore not considered to be a carbon source for the soot growth. The decline of measured total hydrocarbon yields at temperatures higher than 1500 K (Figures 5.11 to 5.14) conclusively demonstrates that hydrocarbons in the gas phase contribute significantly to the soot growth in a coal system.

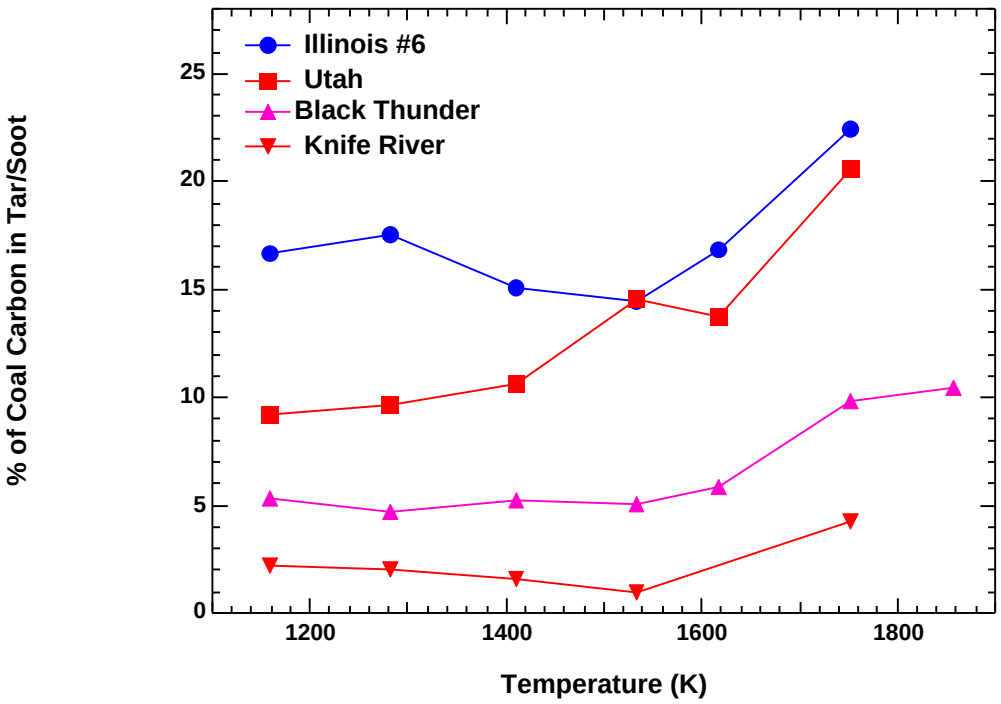

Figure 5.31. Fraction of coal carbon incorporated into tar and soot (collected at 1 inch above the burner surface).

Gas analysis in this study showed that C_2H_2 became the predominant species in hydrocarbons at temperatures higher than 1600 K (see Figure 5.16). Therefore, C_2H_2 should be the main species participating in the soot surface growth at high temperatures. Other researchers also reported that C_2H_2 is the only hydrocarbon that survives at temperatures above 1800 K (Doolan, et al. 1986). Direct C_2H_2 addition to the soot surface was modeled in a premixed hydrocarbon flame (Frenklach and Wang, 1990). It is most likely that this reaction is also important in coal pyrolysis. Benzene, claimed to be another important species in surface growth, seems to make much less contribution than C_2H_2, since benzene was consumed quickly at temperatures higher than 1600 K (Figure 5.16). The addition of hydrocarbons was modeled as a separate route for soot growth at high temperatures. The activation energy obtained for hydrocarbon addition is 320 kJ/mol, which is much higher than the activation energy for the direct tar conversion (230 kJ/mol). In other words, soot formation from tar is rapid compared to soot growth through hydrocarbon addition.

6. Chemical Structure Analysis

Chemical Structure Results

Solid-state ^{13}C NMR analysis gives insight into a variety of average chemical structural features in solid organic samples, such as coal, tar or soot. The NMR analyses were performed at the University of Utah for the tars and soots from the Illinois #6 coal and two model compounds. All the tar and soot samples used in the ^{13}C NMR analysis were collected at the 3 inch location in the FFB, except one tar sample was collected at the 1 inch location in the 1159 K condition from the Illinois #6 coal. A summary of these NMR analyses is given in Tables 6.1 and 6.2 respectively. In each table, the structural parameters derived directly from the NMR spectra are presented, followed by the lattice parameters calculated from the structural parameters. The elemental compositions of each sample are also shown. This is the first set of solid-state ^{13}C NMR analyses on tars from aromatic *model* compounds. These data, together with those previously reported on coal tars and soots (Hambly, 1998; Perry, 1999), give substantial insight into the transition from tar to soot. These data provide the basis for developing reliable soot mechanisms from aromatic compounds.

Analysis of Chemical Structure Data

Figure 6.1 shows the chemical structure of the two starting model compounds: biphenyl and pyrene. Biphenyl is made of two benzene rings connected with a single bond. Pyrene has a structure containing four fused benzene rings. These two compounds

Table 6.1. Structural and Lattice Parameters for Tars/Soots from Illinois #6 Coal. (samples obtained at the 1 inch location at 1160 K, at the 3 inch location at other temperatures)

Structural Parameters[a]														
sample	f_a	f_a^C	f_a^O	f_a^{OO}	$f_{a'}$	f_a^H	f_a^N	f_a^P	f_a^S	f_a^B	f_{al}	f_{al}^H	f_{al}^*	f_{al}^O
coal	0.72	0.05	0.02	0.03	0.67	0.21	0.46	0.08	0.18	0.20	0.28	0.19	0.09	0.05
1160 K	0.85	0.04	0.02	0.02	0.81	0.33	0.48	0.08	0.19	0.21	0.15	0.09	0.06	0.02
1280 K	0.92	0.02	0.005	0.015	0.90	0.42	0.48	0.04	0.19	0.25	0.08	0.05	0.03	0.02
1410 K	0.97	–	–	–	0.97	0.33	0.64	0.00?	0.19	0.45	0.03	0.03	0.00	–
1530 K	1.00	–	–	–	1.00	0.26	0.74			0.74	0.00	0.00	0.00	–

Lattice Parameters[b]								
	χ_b	C_{cl}	$\sigma+1$	P_0	B. L.	S. C.	M. W.	M_δ
coal	0.299	15	5.8	0.65	3.8	2.0	355	30
1160 K	0.259	12	4.0	0.78	3.1	0.9	227	21
1280 K	0.278	13	3.3	0.87	2.9	0.4	203	14
1410 K	0.464	23	4.5	1.00	4.5	0.0	319	9
1530 K	0.74	89		1.00			1186	

Elemental Analysis (daf)[c]				
	C (%)	H (%)	N (%)	O (%)
coal	75.68	5.16	1.50	12.78
1159 K	78.23	5.02	1.75	11.28
1281 K	85.61	4.00	1.89	4.22
1411 K	89.37	3.19	1.36	2.69
1534 K	90.15	1.73	0.6	3.37
1858 K	90.07	1.18	0.56	3.11

[a]Structural parameters:
Percent carbon: f_a-total sp^2-hybridized carbon; f_a^C-carbonyl, d>165 ppm; $f_{a'}$-aromatic carbon; f_a^H-aromatic with proton attachment; f_a^N-nonprotonated aromatic; f_a^P-phenolic or phenolic ether; f_a^S-alkylated aromatic d=135-150 ppm; f_a^B-aromatic bridgehead; f_{al}-aliphatic carbon; f_{al}^H-CH or CH_2; f_{al}^*-CH_3 or nonprotonated; f_{al}^O-bonded to oxygen, d=50-90 ppm

[b]Lattice parameters:
χ_b: fraction of bridgehead carbons; C_{cl}: aromatic carbons per cluster; $\sigma+1$: total attachments per cluster; P_0: fraction of attachments that are bridges; B. L.: bridges and loops per cluster; S. C.: side chains per cluster; M_{cl}: the average molecular weight of an aromatic cluster; M_δ: the average molecular weight of the cluster attachments

[c]Elemental analyses were performed by Galbraith Laboratories in Knoxville, Tennessee

Table 6.2. Structural and Lattice Parameters for Model Compound Soots. (samples obtained at the 3 inch location)

Structural Parameters													
	f_a	f_a^C	f_a^O	f_a^{OO}	$f_{a'}$	f_a^H	f_a^N	f_a^P	f_a^S	f_a^B	f_{al}	f_{al}^H	f_{al}^*
Biphenyl 1365 K	0.91	0.00	0.00	0.00	0.91	0.54	0.37	0.03	0.20	0.14	0.09	0.08	0.01
Biphenyl 1410 K	0.93	0.00	0.00	0.00	0.93	0.50	0.43	0.02	0.19	0.22	0.07	0.07	0.00
Biphenyl 1470 K	0.98				0.98	0.36	0.62	0.04	0.19	0.39	0.02	0.02	0.00
Pyrene 1410 K	0.98	0.02		0.02	0.96	0.47	0.49	0.02	0.12	0.35	0.02	0.02	0.00
Pyrene (1)[d] 1460 K	0.99				0.99	0.36	0.63		0.05	0.58	0.01	0.01	0.00
Pyrene (2)[e] 1460 K	0.99				0.99	0.36	0.63	0.03	0.13	0.47	0.01	0.01	0.00

Lattice Parameters								
	χ_b	C_{cl}	σ+1	P_0	B. L.	S. C.	M. W.	M_δ
Biphenyl 1365 K	0.154	9	2.3	0.96	2.2	0.1	–	–
Biphenyl 1410 K	0.237	11	2.5	1.00	2.5	0.0	–	–
Biphenyl 1470 K	0.398	20	4.7	1.00	4.7	0.0	–	–
Pyrene 1410 K	0.365	18	2.6	1.00	2.6	0.0	–	–
Pyrene (1)[d] 1460 K	0.586	35	1.8	1.00	1.8	0.0	–	–
Pyrene (2)[e] 1460 K	0.475	23	3.7	1.00	3.7	0.0	–	–

[d]Determined by deconvolution of the CP/MAS spectra.
[e]Determined by chemical shift range normally used in data analysis

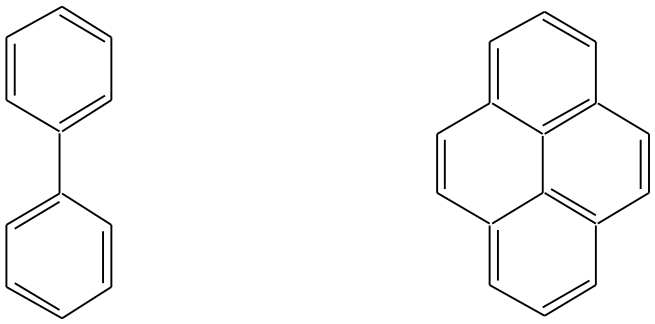

Biphenyl Pyrene

Figure 6.1. Chemical structure of biphenyl and pyrene.

are pure aromatic compounds and found extensively in coal tars. Analysis of the chemical structure data of the tars from model compounds helps to reveal the important reaction pathways during soot formation from hydrocarbons. The tar/soot samples were generated at a temperature range where the transition from tar to soot is highlighted. During the experiment, it was found that no particles were observed in the reactor at temperatures lower than 1300 K. The deposits collected on the filters were yellowish and sticky, which is typical of tar. Only when the pyrolysis temperature was raised sufficiently high was luminosity noticed in the flame. The luminosity is due to the radiation emitted from the solid soot particles formed from tar. The soot incipient temperature varies for different starting compounds. In this study, the temperature was found to vary from 1350 to 1400 K for solid aromatic compounds.

The data in Tables 6.1 and 6.2 compare the chemical structures of the pyrolysis products at various stages of tar-soot transition. The numbers of side chains per aromatic cluster are plotted in Figure 6.2. For the coal tar sample at 1159 K, the number of side chains per cluster has been reduced by over 50% from that in the parent coal. Perry (1999) showed that the number of side chains per cluster in primary tars generated at

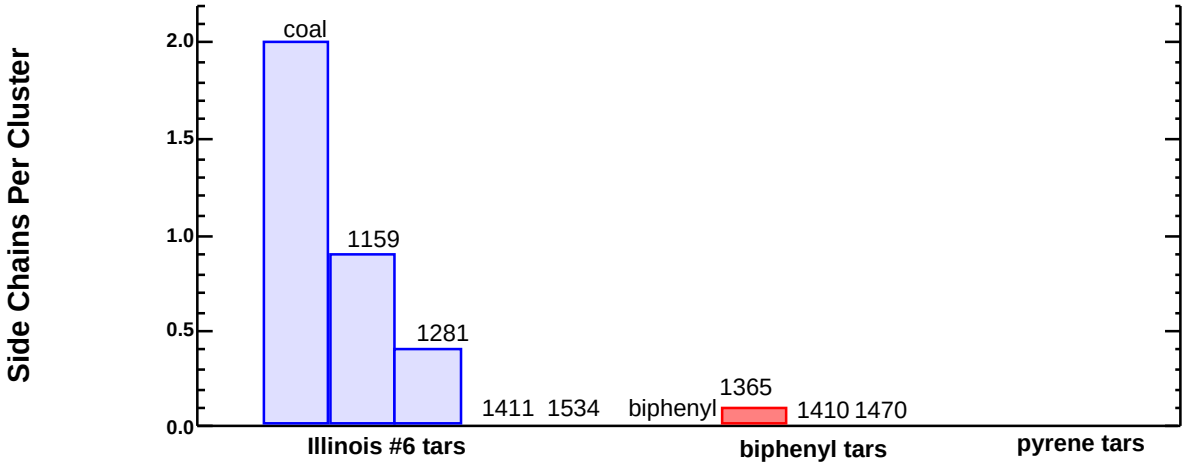

Figure 6.2. Changes of side chains per cluster with temperature for tars from Illinois #6 coal and two model compounds.

900 K in a drop-tube reactor were only 11% less than in the parent coal. This is a strong indication that significant secondary reactions had already occurred for the first tar samples collected in this study, resulting in a substantial loss of side chains. When the reaction severity increases, the tar continues to lose side chains, which are the source of the secondary gases such as light hydrocarbons, CO and H_2O. At 1411 K, no side chains were found in the coal tar. All the clusters were connected together by bridges or loops. In the case of biphenyl, there are no side chains in biphenyl itself. However, a small number of side chains was detected in the biphenyl tar at 1365 K. No side chains were found in pyrene tars, probably due to the high stability of the fused ring structure.

The number of bridges or loops can also be compared throughout the transition from tar to soot (see Figure 6.3). At 1159 K and 1281 K, the coal tar had fewer bridges or loops per cluster than the parent coal. This is consistent with the previous notion that tar is formed from bond-breaking of the large coal network and is small enough to be

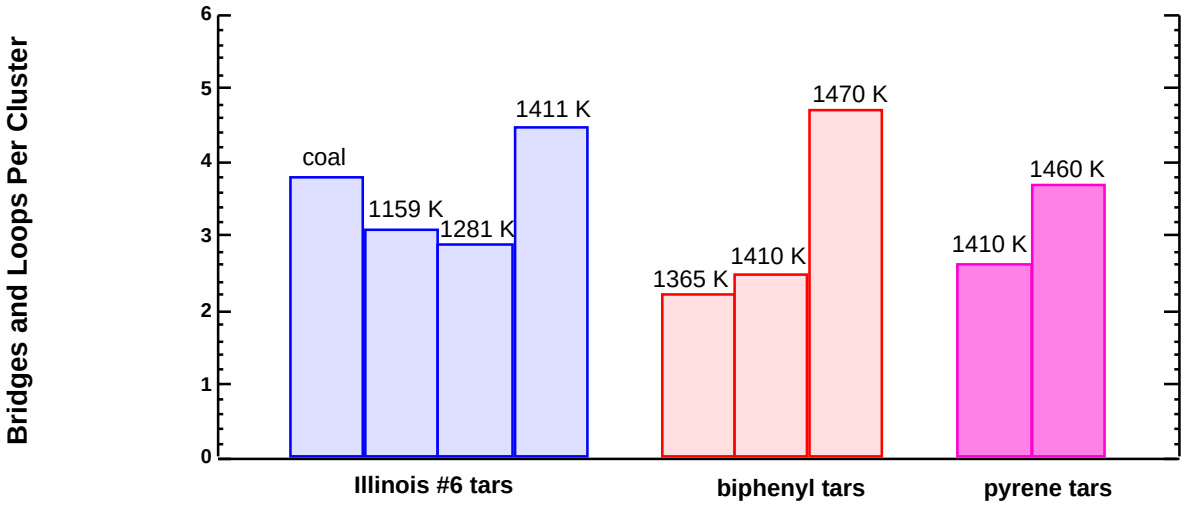

Figure 6.3. Changes of bridges and loops per cluster with temperature for tars from Illinois #6 and two model compounds.

vaporized into the gas phase. At 1411 K, the number of bridges and loops increased and was even higher than that in the parent coal. This means that the clusters in the tar are more interconnected, a sign of soot initiation. A similar finding was also reported by Hambly (1998) and by Perry (1999), but at a much lower temperature, 1080 K for Hambly and 1250 K for Perry.

The residence time at 1411 K in this study is about 74 ms, while the residence time is about 210 ms in Hambly's experiment and 300 ms in Perry's experiment. As explained previously, residence time also has an important effect on secondary reactions. The short residence time in this study may be responsible for the difference in the starting temperature of crosslinking in the tar.

The initiation of soot formation from tar can be best viewed from the number of aromatic carbons per cluster represented in Figure 6.4. The early coal tars have less aromatic carbons per cluster than the parent coal, consistent with the findings of previous

studies (Watt, et al. 1996; Perry, 1999). One explanation is that the clusters have to be sufficiently small in order to escape the coal matrix to form tar. Beginning at 1411 K, the number of aromatic carbons per cluster was higher than that in the parent coal. At the same time, the number of side chains decreased sharply. The only possible explanation is that the tar molecules began to undergo polymerization reactions (like crosslinking reaction in the char) after stripping off the side chains at this temperature. At 1534 K, the number of aromatic carbons per cluster is almost four times higher than that at 1411 K. However, for the tars from model compounds, the change is more gradual, but is comparable at temperatures below 1500 K.

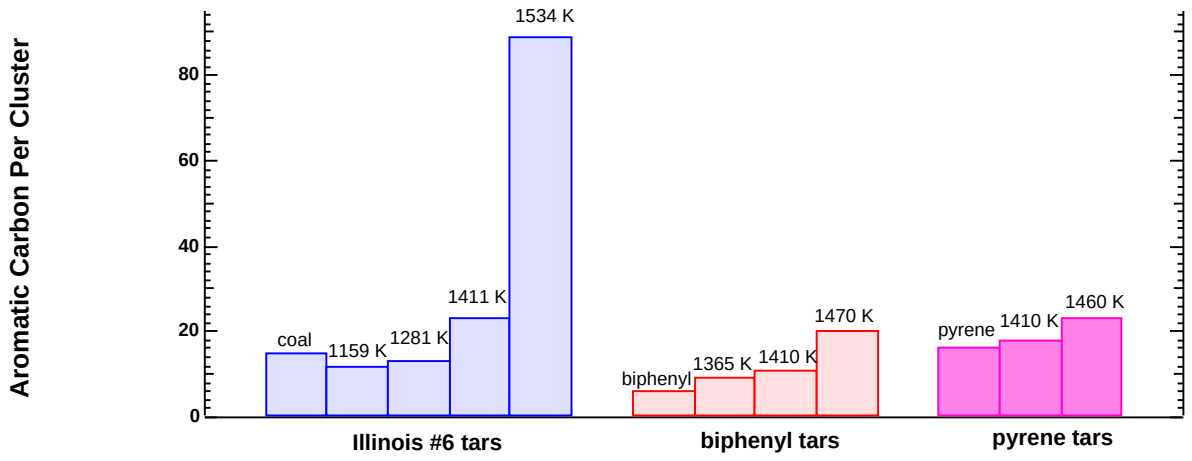

Figure 6.4. Changes of aromatic carbon per cluster with temperature for tars from Illinois #6 and two model compounds.

The average molecular weight of coal tar is shown in Figure 6.5. It is found that during the transition from tar to soot, the size of the aromatic cluster grows substantially, consistent with the increase in the number of aromatic carbons per cluster. The

molecular weight of soot samples from the two model compounds is not available due to the erroneous elemental analysis. However, the calculations showed that the increase (relative) of molecular weight of soots from the model compounds was much smaller than that for the coal tar, which indicates that coal tars have a higher sooting tendency than the model compounds.

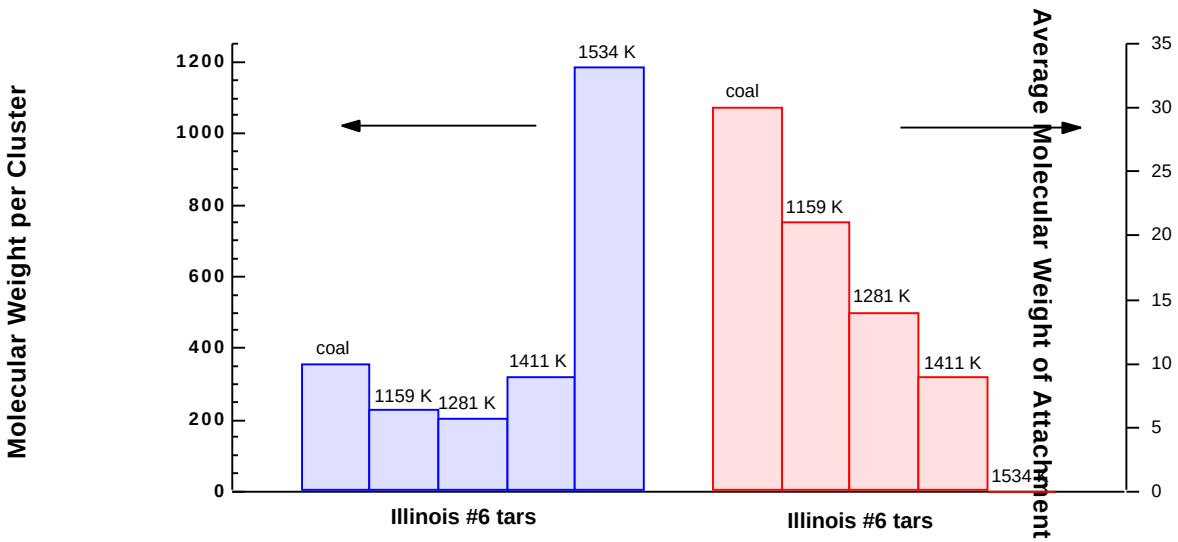

Figure 6.5. Changes of average molecular weight per cluster and average molecular weight per attachment with temperature for tars from Illinois #6 and two model compounds.

There is a striking similarity between the changes in aromatic carbons per cluster and the average molecular weight per cluster in the coal tars (compare Figures 6.4 and 6.5). The increase of the cluster size is almost entirely due to the increase in aromatic carbon. This is confirmed by the carbon aromaticity data (percent of carbon that is aromatic) in Figure 6.6. The portion of the aliphatic carbon (side chains in this case)

continued to decrease with the severity of the secondary reaction. Above 1400 K, almost all the carbons are aromatic, which means that ring growth reactions were dominant over ring opening reactions in the early stage of tar evolution. These aromatic clusters will continue to grow to form a large network of fused rings. A possible reaction pathway for the cluster growth is shown in Figure 6.7.

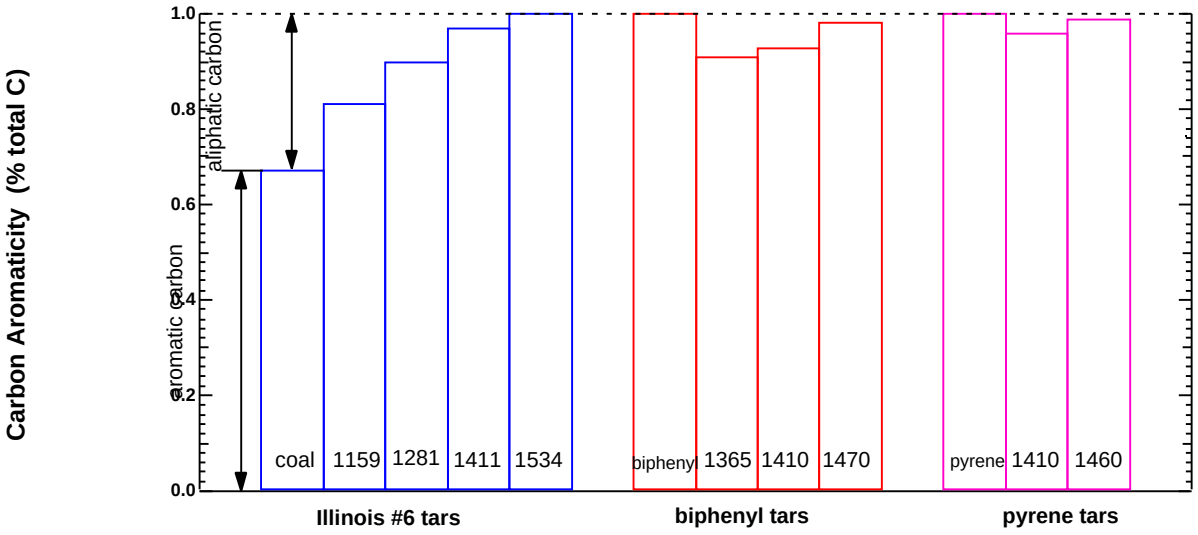

Figure 6.6. Changes of aromaticity with temperature for tars from Illinois #6 and two model compounds.

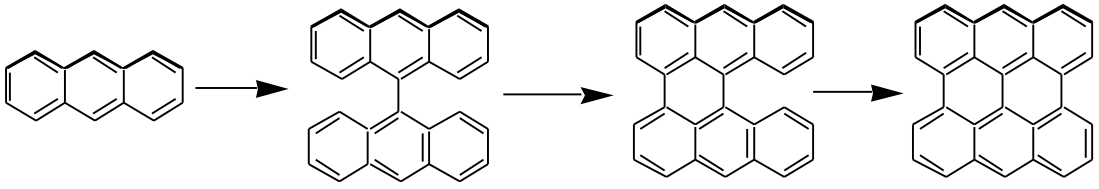

Figure 6.7. Hypothetical ring growth reaction in anthracene pyrolysis (adapted from Badger, et al. 1964).

In the case of coal, the primary tar, released from the coal matrix by breaking the labile bridges connecting the aromatic clusters, will first lose side chains or functional groups attached to the ring structure (see Figure 6.2). This will cause the release of secondary gases, which are seen in low temperature tar cracking studies. The side chain loss is also confirmed by the decrease in average molecular weight per attachment seen in Figure 6.5. From 1159 K, the molecular weight per attachment for the coal tar dropped quickly due to the mass release to the gas phase. At higher temperatures (1300-1500 K), the tar molecules undergo ring opening reactions. PAH with oxygen functional groups seem to have a higher reaction rate than non-polar PAH, as evidenced by the quick decline of f_a^O from 1159 K to 1411 K. Analysis of nitrogen-containing PAH from coal pyrolysis also indicated the preferential reaction of polar PAH in secondary reactions (Wornat, et al. 1988b). At temperatures higher than 1400 K, PAH undergoes polymerization to form larger clusters. This reaction is sensitive to temperature and becomes very fast at elevated temperatures, as evidenced by the marked increase in molecular weight per cluster seen in Figure 6.5, where the molecular weight increased by a factor of three between 1411 K and 1534 K. At this stage, the clusters are getting larger *and* more aromatic. At 1534 K, the aromaticity is very close to unity for the coal tar/soot. The higher number of bridges and loops for this sample also showed that the clusters are more interconnected. At the final stage, the cluster size (number of carbons per cluster) of the soot sample can be quite large (e.g. greater than 200 at 1858 K), suggesting that the polymerization reactions are dominant from 1600-1800 K. This is also consistent with the previous conclusion that soot formation is favored at high temperatures.

The data obtained for the biphenyl samples exhibit a different pathway for pyrolysis and soot growth. First, ring opening reactions have occurred during early pyrolysis, which is clearly evident by the aliphatic carbon present in the samples (see Table 6.2). FTIR analysis of the gas phase during the model compound pyrolysis also showed the existence of small hydrocarbon molecules including CH_4, C_2H_2 and benzene. Therefore, it is believed that a ring opening reaction occurs early in the soot formation process for biphenyl. The decrease of the fraction of aliphatic carbon with increasing temperature (e.g., 0.09, 0.07 and 0.02) indicates that major structural rearrangements are occurring following the initial ring opening reactions. The number of bridges and loops per cluster, which is 1.0 in unreacted biphenyl, doubles to 2.2 and 2.5 at 1365 K and 1410 K and then doubles again to 4.7 at 1470 K. The cluster size, which starts at 6 in the parent molecule, grows to 9, 11 and 20 aromatic carbons respectively. Hence, the ring size not only grows significantly but the number of bridges and loops per cluster also increases from a value of 1 to nearly 5 over the relevant temperature range. This suggests that soot growth in biphenyl soot consists not only of ring size growth but also cluster crosslinking which could result in the formation of large crosslinked structures. Although NMR analyses for model compound samples at higher temperatures are not available, it is most likely that they will follow a trend of soot growth similar to that of the coal tar.

The evolution of pyrene soot follows still another path. First, little evidence is noted for ring opening reactions. Only approximately 1% of the carbon appears as sp^3 hybridized species, indicating that very little ring opening occurs, unless stable alicyclic molecular species are formed following ring opening. The smaller amount of aliphatic

carbon in pyrene tar/soot samples is probably due to the high stability of fused ring structure in pyrene. Second, ring growth of only approximately 10% has occurred at 1410 K compared to nearly 100% in the case of the corresponding biphenyl soot. However, data on this 1410 K soot sample indicate that the relatively small cluster size has been augmented by an average of 2.6 crosslinking sites per cluster. The data obtained from this study are inconclusive regarding the exact mechanism for ring growth in the pyrene soots between 1410 K and 1460 K, since different analysis methods on the broadened aromatic band of pyrene soots generated different results.

7. Nitrogen Release During Coal Pyrolysis

Nitrogen Distribution

Temperature is a critical factor in determining the extent of secondary reactions. In this study, the temperature range was carefully selected in order to highlight the nitrogen release during secondary pyrolysis. The cumulative distributions of the coal nitrogen at various temperatures are presented in Figures 7.1 to 7.4. At the lowest temperature (1159 K), the secondary reactions just began as indicated by the initiation of HCN release. It is suggested that the initiation of HCN could be considered as a sign for the start of the gas-phase secondary reactions of the primary tar (Freihaut, et al. 1993). At the highest temperature (1858 K), the secondary reactions of the tar were near completion, as evidenced by the H/C ratio of the soot.

The distribution of the nitrogen from the parent coal was determined from the char and tar/soot yields coupled with elemental analysis. Gaseous nitrogen species were determined independently from the results of FTIR measurement. Except for the Illinois #6 coal, the nitrogen balance is within 10% at temperatures higher than 1500 K, but deteriorates at low temperatures. Below 1300 K, 10-20% of the nitrogen in the parent coal is not accounted for in the measurements. A similar trend was also observed in Chen's experiment, where about 10% of the coal nitrogen is not accounted for in the early phase of secondary pyrolysis (Chen, 1991). Haussmann also reported a nitrogen balance of 90% when pyrolyzing a Pittsburgh #8 coal in an arc-jet fired entrained-flow

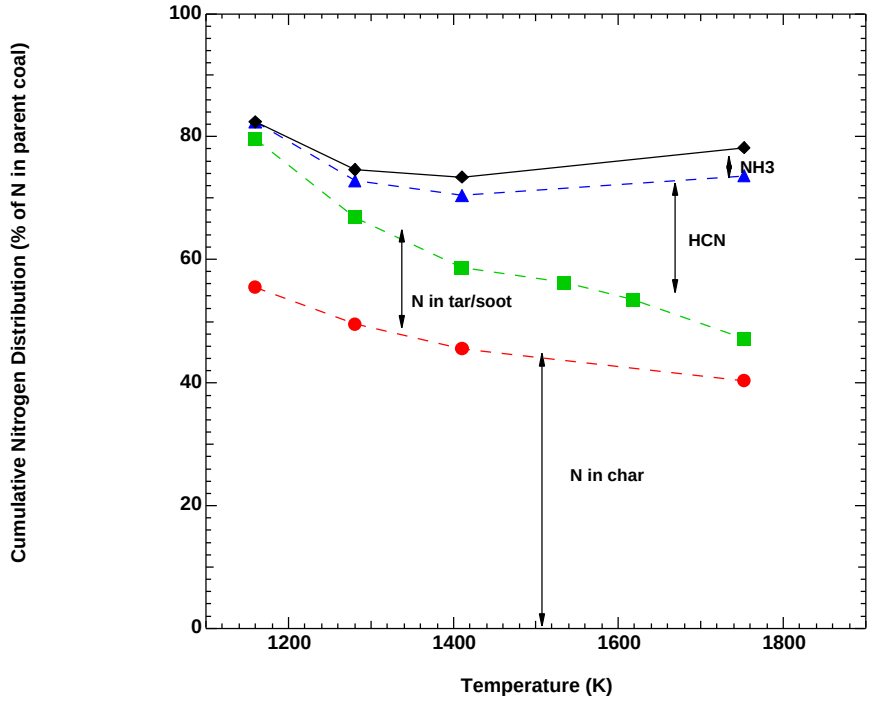

Figure 7.1. Cumulative distribution of the coal nitrogen for the Illinois #6 coal at the 7 inch location.

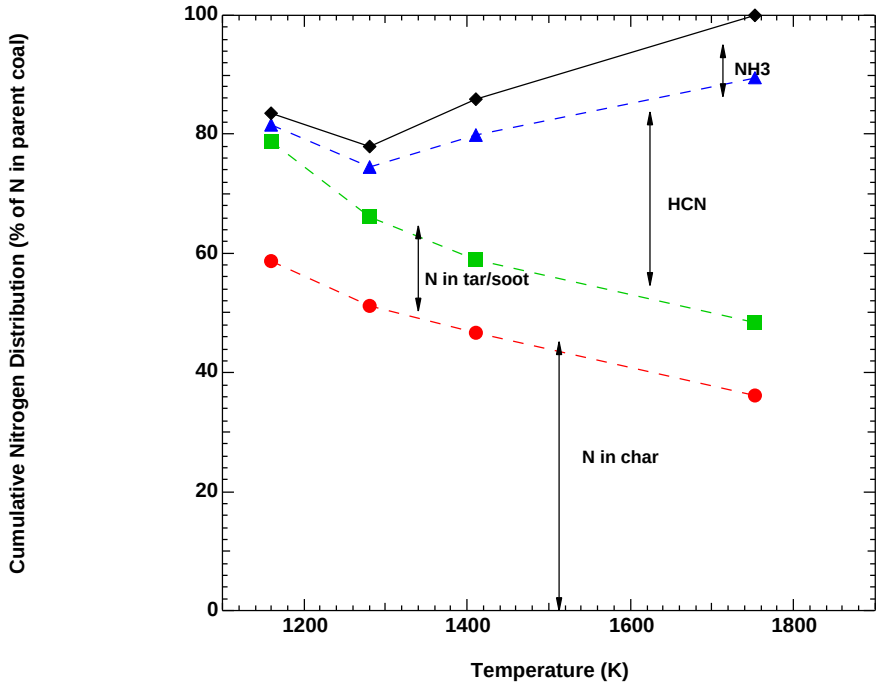

Figure 7.2. Cumulative distribution of the coal nitrogen for the Utah coal at the 7 inch location.

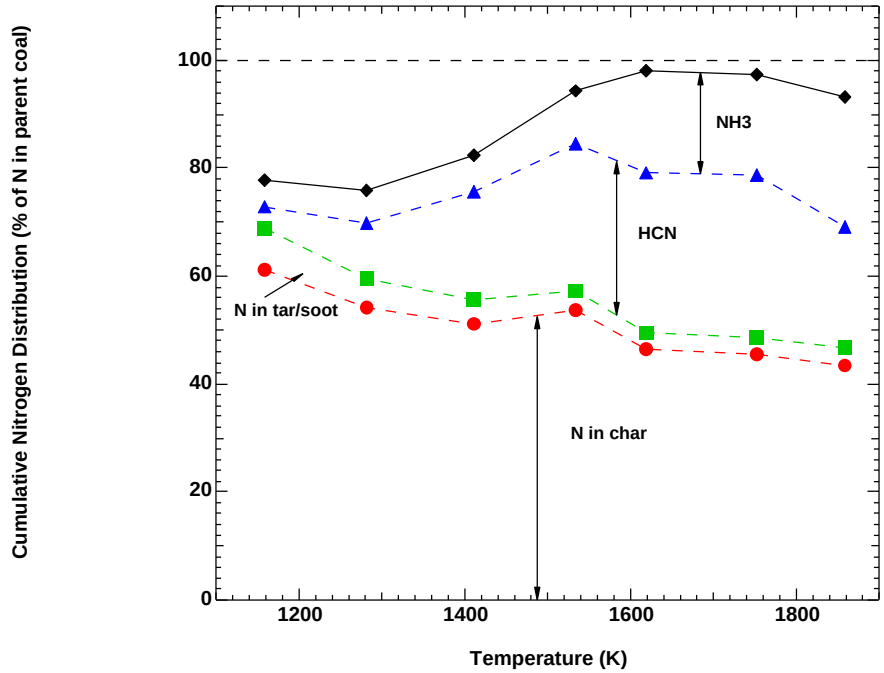

Figure 7.3. Cumulative distribution of the coal nitrogen for the Black Thunder coal at the 7 inch location.

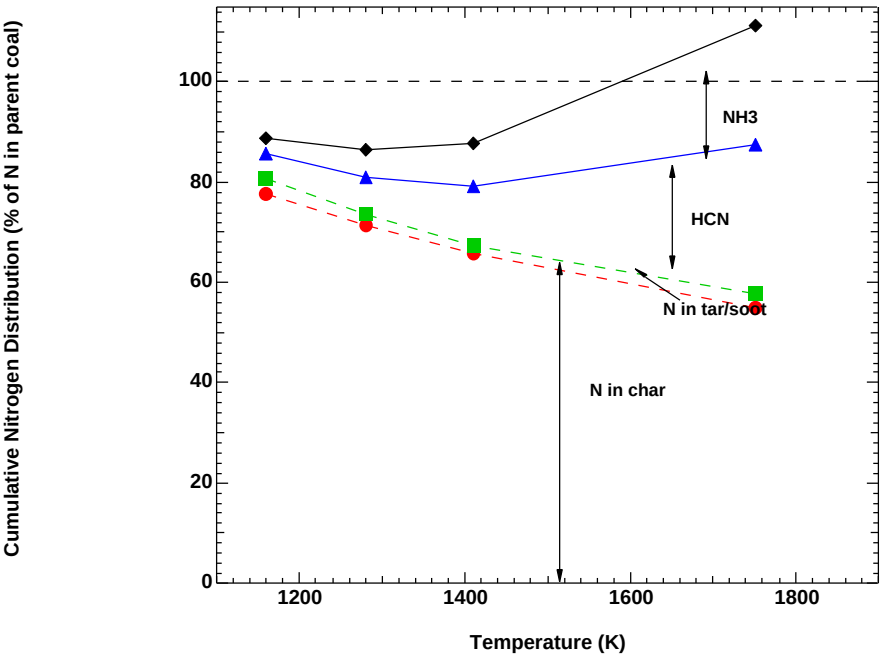

Figure 7.4. Cumulative distribution of the coal nitrogen for the Knife River coal at the 7 inch location.

reactor (Haussmann, 1989). However, the missing nitrogen remained constant over the temperature range in his study (1200-1600 K). Therefore, Haussman labeled the missing nitrogen as N_2.

Repeated FTIR analysis in the gas phase showed that the release of HCN and NH_3 at temperatures below 1300 K was insignificant. The small nitrogen-containing aromatics (1-2 rings) commonly found in coal tar (Nelson, et al. 1990) could possibly account for the missing nitrogen. However, no significant peaks associated with these nitrogen-containing species are identified in FTIR spectra. These species are also never reported in substantial amount in previous studies. Molecular nitrogen (N_2) may be responsible for the missing nitrogen during the pyrolysis of the Illinois #6 coal, possibly caused by reburning type reactions. However, it should not be a significant source of error for the other three coals, since the nitrogen balance improved and was close to 100% at high temperatures. Therefore, the gap in nitrogen balance is most likely due to inaccuracy of the nitrogen fraction in the solid phase and perhaps some unknown nitrogen species not mentioned above.

In Chapter 5, the tar and soot yields measured in this study are compared with those reported from literature. For coals of similar rank, systematic lower tar yields were observed in this study, especially at low temperatures. This may partially reconcile the failure of the nitrogen closure at low temperatures. For Illinois #6, the missing nitrogen (as much as 20%) even at high temperatures is unclear.

Modeling of Nitrogen Evolution during Secondary Reactions

Nitrogen evolution is the major topic in this study. Two major processes of nitrogen evolution have been identified during secondary pyrolysis. First, thermal cracking of tar causes ring opening reactions, releasing nitrogen as HCN (Chen, 1991).

Second, at high temperatures, when polymerization reactions of tar are sufficiently rapid, certain portions of the tar nitrogen will be integrated into soot. However, nitrogen can also be released directly from char at elevated temperatures. The measured HCN and NH_3 were the sum of those released from tar and those released directly from char. No distinction can be made between these two mechanisms in the current study. In addition, some researchers believe that NH_3 maybe a secondary product formed from HCN. This makes the model of HCN and NH_3 even more complicated, since the reaction pathways for HCN-NH_3 conversion are not fully understood.

In this study, only the nitrogen evolution in the tar and soot was modeled. Nitrogen release from char has already been modeled using the revised CPD model with adequate accuracy for high temperature, high heating rate pyrolysis (Perry, 1999). The fraction of the coal-N incorporated in tar or soot can be calculated by

$$N_{tar} = \frac{m_{N,tar}}{m_{N,coal}} = \frac{[N]_{tar} m_{tar}}{[N]_{coal} m_{coal}} \tag{7.1}$$

where [N] and m are the nitrogen content and mass of tar or coal, respectively. It should be noted that the mass of tar over the mass of coal gives the tar yield, as in (6.10)

$$\frac{m_{tar}}{m_{coal}} = y_{tar} \tag{7.2}$$

then

$$N_{tar} = \frac{[N]_{tar}}{[N]_{coal}} y_{tar} = R_N \quad y_{tar} \tag{7.3}$$

Since the tar and soot yield can be calculated using the model in the previous section, only the nitrogen ratio needs to be modeled. By careful examination of the experimental data, it was found that the ratio of the nitrogen content in tar or soot over that in the parent coal (daf) follows a similar trend for all the coals at long residence

times (Figure 7.5). The nitrogen ratio drops very quickly between 1300–1500 K, then decreases at a much slower rate at temperatures higher than 1600 K. An empirical first-order reaction mechanism was devised to fit the data in this study (also shown in Figure 7.5).

$$\frac{dR_N}{dt} = -A_N \exp(-\frac{E_N}{RT})(R_N - R_\infty) \qquad (7.4)$$

where A_N, E_N and R_∞ are the empirical pre-exponential factor, activation energy and ultimate nitrogen ratio, respectively. The coal-independent (for the coals in this study) kinetic parameters are shown in Table 7.1. The calculated amounts of coal nitrogen incorporated into tar and soot versus temperature using these parameters are shown in Figure 7.6. There is generally excellent agreement between the data and model predictions. The model does not agree with the data from the high temperature experiments on the Utah and Knife River coals (1752 K); these two points are thought to be in error, since nitrogen addition to soot is unlikely at this temperature.

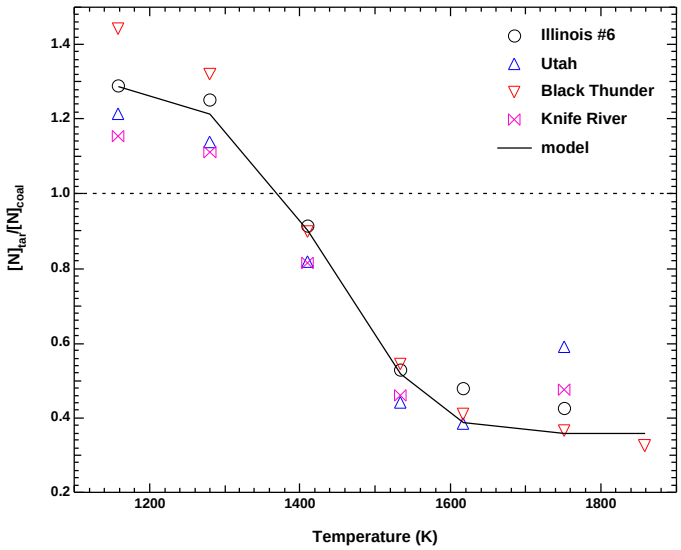

Figure 7.5. $[N]_{tar}/[N]_{coal}$ versus temperature for all the coals in this study. The line is the model prediction using the best-fit parameters in Table 7.1.

Table 7.1. Best-Fit Kinetic Parameters Used in the Simulation.

A_N (sec^{-1})	E_N (kJ/mol)	R_∞ (unitless)
5.90E8	220	0.36

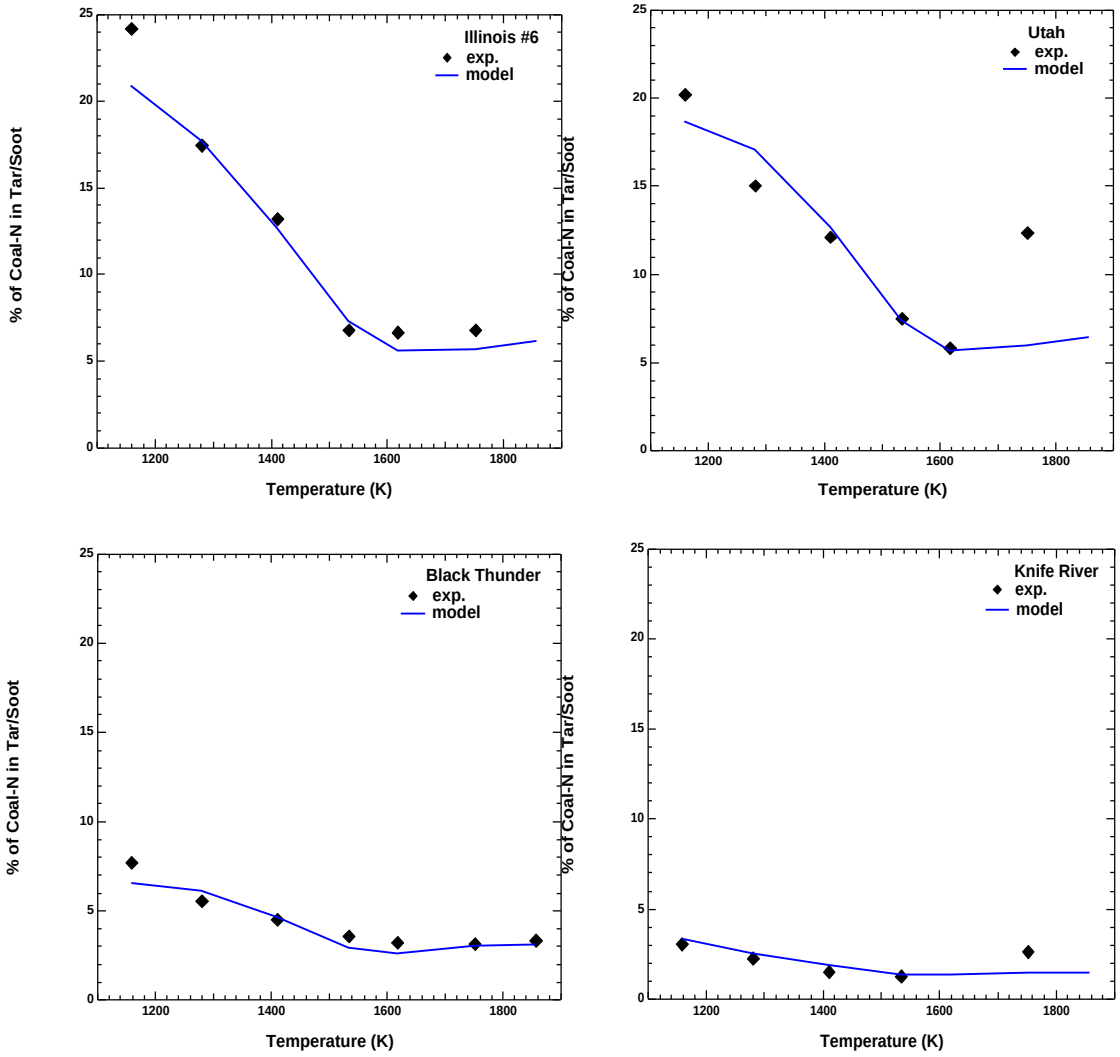

Figure 7.6. Predicted decay of the fraction of coal nitrogen in the tar and soot (N_{tar}) compared with the measured values (for the longest residence time at each temperature condition).

Nitrogen Release during Coal Pyrolysis

Total Nitrogen Release

As discussed in Chapter 1, only the nitrogen released to the gas phase can be reduced by effective methods such as air staging. Therefore, the fraction of volatile nitrogen somewhat determines the overall NO_x reduction efficiency for coal combustion. Figures 7.1 to 7.4 showed that about 40% of the coal nitrogen was released rapidly during the primary pyrolysis at 1159 K. However, the nitrogen release during secondary pyrolysis was at a much slower rate. At least 40% of the coal nitrogen remained in the char even at the most severe conditions. Pohl and Sarofim (1977) showed that all of the nitrogen in the char would be released if treated at 2100 K for 20 minutes. However, since typical residence times in industrial furnaces are about 2 s for pulverized coal, significant nitrogen remains in the char after pyrolysis.

During the pyrolysis process, nitrogen release is inherently related to mass release. In Figure 7.7a, the total nitrogen release versus mass release data obtained in this study are compared with the results reported by Baxter (1996) for an Illinois #6 coal and by Haussmann (1989) for a Pittsburgh #8 coal. This figure shows that the results in the current study are comparable with those in the literature. For bituminous coals, the nitrogen release is comparable with the mass release during the early stage of pyrolysis (0-30% mass release), followed by a slower nitrogen release than mass release in the 30-55% mass release stage. In the final stage (higher than 55% mass release), the nitrogen release was found to continue when the mass release was nearly completed.

The nitrogen release pattern for low rank coals is shown in Figure 7.7b and exhibits a different pattern from that observed for the bituminous coals in Figure 7.7a. In Figure 7.7b, the total nitrogen release versus mass release data for the Black Thunder coal

and Knife River lignite are compared with the results from Haussmann (1989) for a Montana subbituminous coal and from Baxter (1996) for a Beulah lignite. In the early phase of devolatilization, the fractional nitrogen release rates for the low rank coals are much slower than the normalized overall mass release. The slower nitrogen release during early pyrolysis is even more significant for the Montana subbituminous and the Beulah lignite operated in entrained-flow systems. As the pyrolysis proceeds, the particle temperatures rise and the nitrogen is released when the aromatic ring structures are volatilized or ruptured. During the late stages of pyrolysis, the nitrogen release catches up with the mass release. The continued slow nitrogen release after the completion of the mass release is less pronounced for low rank coals.

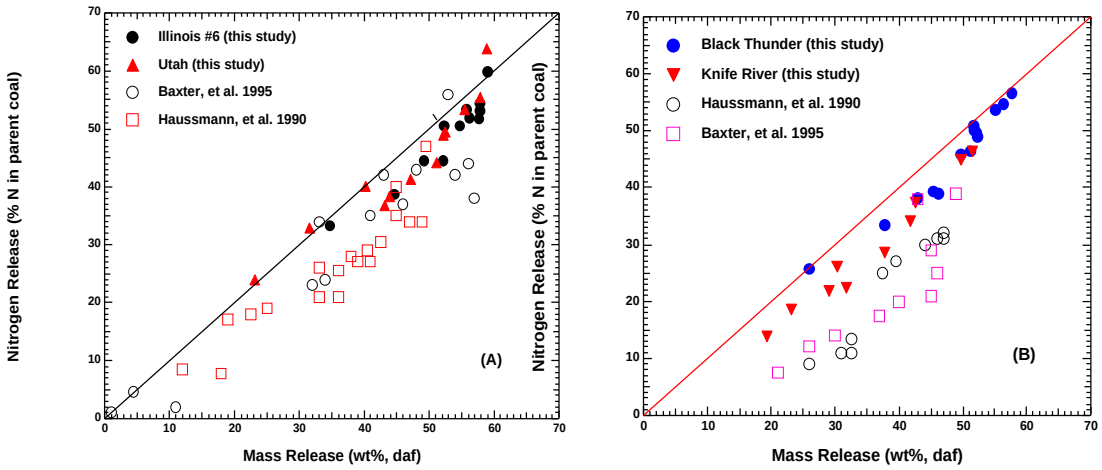

Figure 7.7. (A) Nitrogen release vs. mass release for the bituminous coals. Also shown are values reported by Baxter for an illinois #6 coal and by Haussmann for a Pittsburgh #8 coal; (B) nitrogen release vs. mass release for low rank coals. Also shown are values reported by Haussmann for a Montana subbituminous coal and by Baxter for a Beulah lignite.

Nitrogen Evolution in Tar and Soot

Under rapid heating conditions, tar is virtually the only carrier for nitrogen release when secondary reactions are eliminated. Almost all the nitrogen in coal exists in tightly bound aromatic ring structures, which are among the most thermally stable structures in the coal. These ring structures are transported essentially intact to form tar during primary pyrolysis. However, different types of coals are observed to exhibit different patterns of primary nitrogen release, indicating a strong rank dependence.

The nitrogen ratio in tar, defined as the nitrogen content in the tar or soot divided by the nitrogen content in the parent coal (daf), is a convenient gauge to monitor the rank dependence of nitrogen release:

$$R_N = \frac{[N]_{tar/soot}}{[N]_{coal,daf}} \tag{7.5}$$

Since the nitrogen content in the parent coal is a constant, the ratio actually reflects the change of nitrogen evolution in tar or soot. Freihaut et al. (1993) reported that bituminous coal tars display an almost constant R_N, irrespective of extent of tar evolution during the early phase of devolatilization. Values of R_N close to unity suggest that tar is a collection of random samples from the coal. This is also observed by Solomon and coworkers (1978) in a pyrolysis experiment involving 12 bituminous coals. They found that the amount of nitrogen released was proportional to the amount of tar released during the initial stage of devolatilization. However, low rank coal tars have a much smaller R_N, and R_N was found to increase with increasing temperature. The smaller R_N in low rank coal tars means the non-polar PAH are *preferentially* released as tar during pyrolysis of low rank coals. This is confirmed by the greater char nitrogen fraction in the Knife River lignite than other coals at 1159 K in this study. The exact

nature of the delayed nitrogen release in low rank coal tars is not obvious, but it may be related to the early crosslinking reaction that occurs only in low rank coals. Some nitrogen-containing PAH (PAHN) are trapped in the large clusters during the early crosslinking, making them too large to vaporize as tar during pyrolysis.

After the tar escapes the coal matrix, nitrogen release will take different routes of release in the tar and in the remaining char. The tar nitrogen evolution is presented in the following discussion. Further nitrogen release from char will be discussed in the next section.

Figure 7.5 shows the nitrogen ratio (R_N) versus temperature for the four coals used in this study. A similar trend is observed for all coals: the nitrogen ratios were higher than unity below 1300 K, followed by a rapid decay between 1300-1600 K, finally decreasing at a much slower rate at temperatures above 1600 K. The striking similarity of the nitrogen release from tars of different coal types indicates that reactivity of the tar nitrogen functionalities during secondary pyrolysis is largely rank independent.

It is interesting that the nitrogen content in tar is initially higher than the nitrogen content in coal, i.e., R_N is higher than unity, at the early stage of secondary pyrolysis. Such enrichment of nitrogen at the early phase of secondary pyrolysis can be explained by examining the chemical structure data of the tar and soot. From the chemical structure analysis, it was found that the first set of secondary reactions of tar was loss of side chains and functional groups (relatively free of nitrogen). The tar nitrogen release is delayed since nitrogen usually exists in aromatic ring structures that react at higher temperatures. Therefore, since the tar releases carbon, hydrogen and oxygen but not nitrogen, high nitrogen ratios are observed during the early stages of secondary pyrolysis.

At later stages of secondary pyrolysis, ring opening reactions became significant, where the tightly bound nitrogen in aromatic rings was released (usually as HCN). The nitrogen ratio, R_N, therefore dropped due to the nitrogen loss from tar.

Nitrogen in Soot

Polymerization of the ring structures in tar becomes more pronounced at more severe pyrolysis conditions. A portion of the nitrogen is incorporated into the young soot particles. Recently, the evolution of the nitrogen-containing compounds in tar during secondary pyrolysis was examined. It was found that the initial depletion of nitrogen in tar is mainly attributed to direct conversion into soot (Yu, et al. 1999). This implies that the young soot should have a higher nitrogen ratio than the primary tar, which is confirmed by examining Chen's (1991) soot data. Figure 7.8 shows Chen's nitrogen ratio (R_N) data for tar and soot during the secondary pyrolysis for a Pittsburgh #8 coal. In his experiment, the aerosols collected on the glass filters were first extracted with tetrahydrofuran (THF), followed by filtration through a Teflon membrane. The membrane residue was denoted as soot and the sample going through the membrane was deemed tar. As seen from the figure, nitrogen is concentrated in the soot during the early stage of secondary pyrolysis. However, the nitrogen ratio decreased rapidly due to the fast soot growth at more severe conditions. Haussmann and Chen reported that the fraction of coal nitrogen incorporated into the soot is constant during secondary pyrolysis, even though soot yields increase dramatically at the same time. The nitrogen analysis in this study supports this idea. In Figure 7.6, the fraction of coal nitrogen in tar and soot versus the temperature was shown. At temperatures above 1600 K, the nitrogen fraction in soot (there is almost no tar at these conditions) reaches an asymptotic value

which is coal-dependent. The observed constant nitrogen fraction in soot can be reconciled by the following arguments. As Yu pointed out, the incorporation of tar nitrogen into soot occurs during the early stages of secondary pyrolysis. As pyrolysis proceeds, the clusters in the soot become larger and more interconnected (see Figures 6.3 and 6.4), which serve as a barrier that hinders the further release of nitrogen by ring rupture. Direct addition of nitrogen-free hydrocarbons is an important soot growth mechanism at high temperatures, as discussed earlier. Soot growth by hydrocarbon addition lowers the nitrogen ratio in soot. Therefore, the amount of coal nitrogen integrated into soot in largely determined by the early soot formation process.

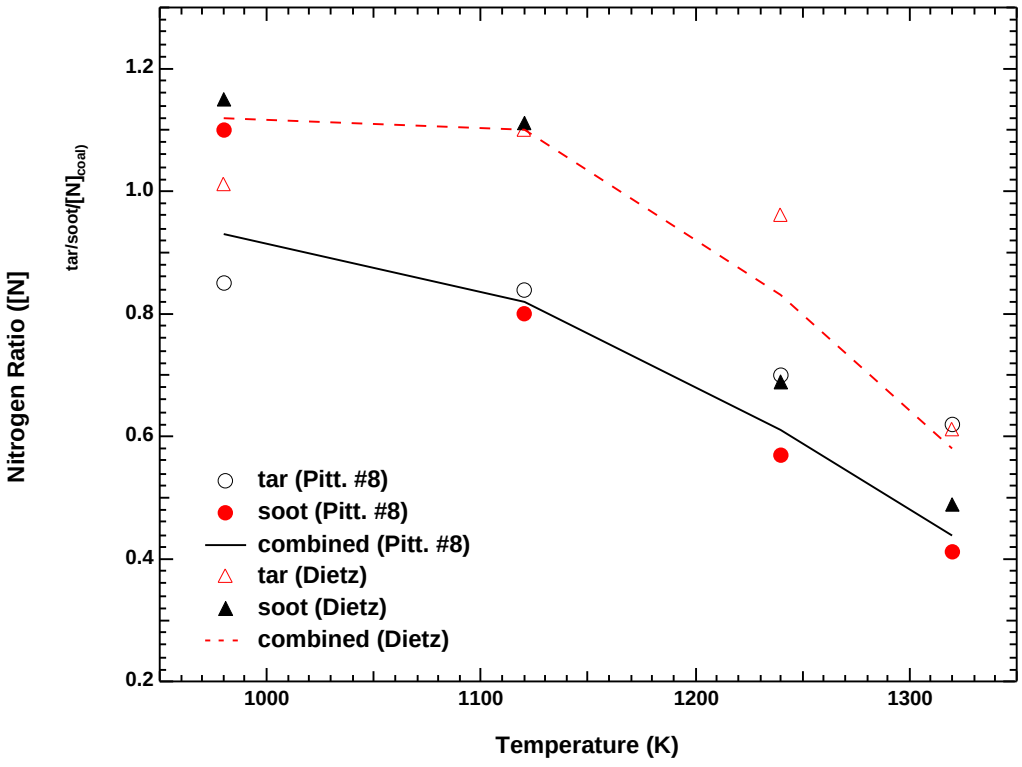

Figure 7.8. Nitrogen ratio of a Pittsburgh #8 tar and soot during secondary pyrolysis (adapted from Chen, 1991). Temperatures in the figure denote the maximum particle temperatures.

Reactivity of Nitrogen Functionalities in Tar

The decay in the nitrogen ratio is similar for all the coals in this study. Therefore, it is reasonable to suspect that the reactivity of the tar nitrogen shows little rank dependence. Analysis already showed that the nitrogen functionalities in coal tar are very similar for coals ranging from brown to bituminous (Nelson, et al. 1990). One or two ring nitrogen-containing aromatics such as pyrrole, pyridine, quinoline, indole and some nitriles are the major components. The observed nitrogen decay in tar would reflect the combined effect of all these compounds. As a homogeneous gas reaction, the nitrogen decay in tar is expected to be less dependent on the original coal properties.

Nitrogen in the Gas Phase

FTIR measurements in this study showed that HCN and NH_3 are the dominant nitrogen-containing gas species evolved during secondary pyrolysis (Figure 7.1 to 7.4). This is consistent with previous studies on coal nitrogen release under rapid heating conditions. Other important nitrogen species, reported previously in literature, were also examined. HNCO, found in fluidized-bed experiments (Ledesma, 1998), was not measured due to the significant overlap of the CO_2 and CO peaks in the spectral range 2200-2400 cm^{-1}. Scoping pyrolysis experiments were performed on a South Banko lignite in pure N_2 at 1000 K in the BYU drop tube reactor (Perry, 1999). No HNCO was detected in the gas phase. It is possible that HNCO formed through interaction with the fluidized particles. Therefore, measurements were focused on HCN and NH_3.

The relative amount of HCN and NH_3 formed during coal pyrolysis is very important in determining the final fuel-N conversion. While NH_3 is mainly converted to NO, HCN can either be converted to NO or N_2O (Schafer, 2000). The nitrogen partitioning in the gas phase during pyrolysis is therefore important in predicting NO_x

formation in coal-fired furnaces. However, it is still not clear whether HCN and NH_3 are released independently from different functionalities in the coal, or whether, and to what degree, NH_3 is a secondary product of HCN hydrogenation (Ledesma, 1998).

By examining the nitrogen distribution in this study, it was found that the sum of HCN and NH_3 at 1858 K is much higher than the fraction of coal nitrogen incorporated in the early tar. This observation indicates that secondary reaction of tar is not the only source of nitrogen release into the gas phase. Actually, the fraction of nitrogen released as tar is almost insignificant for low rank coals. The coal nitrogen in the early tars is only 8% for Black Thunder and 3% for Knife River. In contrast, the final amounts of HCN plus NH_3 can account for as much as 50% of the parent coal nitrogen. Thermal decomposition of char plays a significant role in nitrogen release during coal pyrolysis. Although XPS analysis showed that similar nitrogen functionalities are found in both tar and char (Kelemen, et al. 1998), the rate and mechanism of nitrogen release from these two sources are quite different. However, it was impossible to distinguish the separate contribution of char vs. tar to the HCN and NH_3 formation in the current study.

Thermal cracking of tar vapor without the interference of char was conducted in a tubular flow reactor from 600-1000^{o}C (Ledesma, 1998). HCN was found to be dominant in the gas phase, with a small amount of NH_3 and HNCO. The source of HCN is thought to be the nitriles found in coal tar. Nitrile functionality, absent in the parent coal and primary tar (at 600^{o}C), was identified in coal tar at high temperatures (800^{o}C) using XPS (Li, et al. 1997). However, amino nitrogen peaks, rather than nitriles, were found in low rank coal tars in another study (Kelemen, et al. 1998). It should be pointed out that it is difficult to distinguish these two functionalities, due to the overlap of these peaks in the

XPS spectra. Model compounds studies showed that the release of HCN from coal through nitriles is more plausible. Laskin and coworkers (1997) studied the decomposition of indole and quinoline (two nitrogen functionalities common found in coal tar) in a shock-tube reactor. Four major species were identified in the reaction system: acetylene, HCN, benzene and nitriles. Nitriles were formed by breaking the carbon-nitrogen bond in the compounds (Figures 7.9 and 7.10). HCN can be formed by breaking the weak carbon-carbon bond from nitriles, confirming that ring opening is the

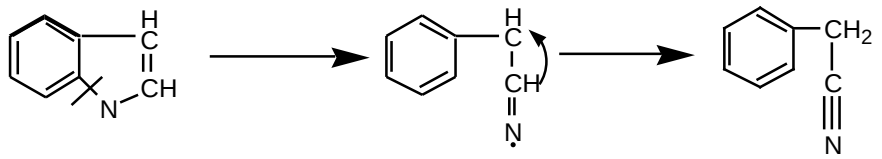

Figure 7.9. The reaction scheme of the formation of nitrile from indole (adapted from Laskin, 1997).

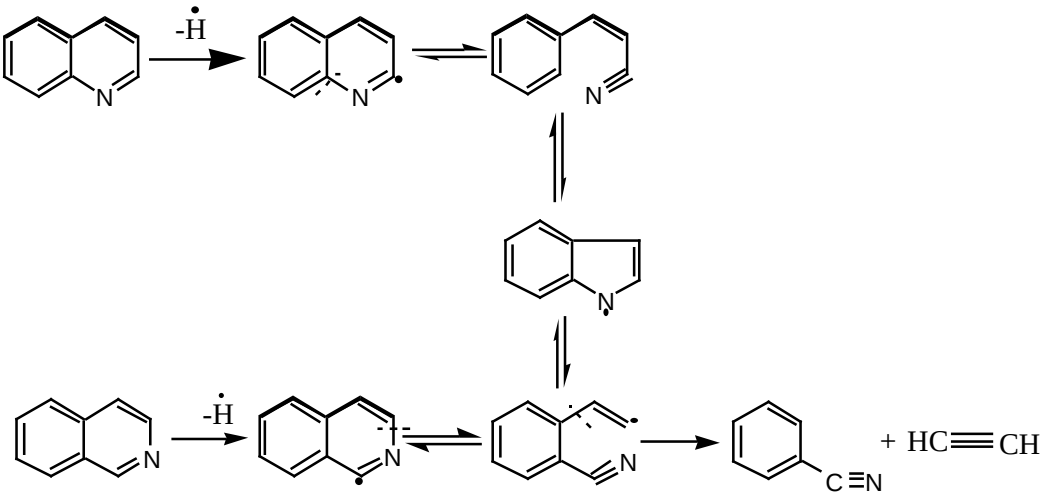

Figure 7.10. The reaction scheme of the formation of nitrile from quinoline and isoquinoline (adapted from Laskin, 1998).

major mechanism for nitrogen release from coal tar. No NH_3 was detected in their analysis. Actually, HCN is the only nitrogen species reported in model compound studies, except that reported by Axworthy where a small amount (less than 5%) of NH_3 was detected (Axworthy, et al. 1978). Coal tar contains the same nitrogen compounds that have been examined in model compounds studies. In addition, tar cracking is also a homogeneous gas phase reaction. Therefore, it is reasonable to believe that the amount of NH_3 formed *directly* from coal tar is small.

Coal tar is not merely a mixture of pure aromatic nitrogen-containing compounds. It is more complex and contains aliphatic side chains and oxygen functional groups. It is believed that these attachments play an important role in tar nitrogen release. First, these side chains, when detached to form radicals (having lower selectivity and activation energy), tend to attack the ring structures, resulting in an early release of nitrogen. Previous studies show that HCN usually emerges between 1250-1350 K for model compounds such as pyrrole (Mackie, et al. 1991), pyridine (Mackie, et al. 1990), indole (Laskin, 1997), quinoline (Laskin, 1998) and 2-picoline (Terentis, et al. 1992). However, HCN release in coal pyrolysis occurs at about 1000 K, which is much lower. Second, the existence of oxygen in coal tar makes the conversion from HCN to NH_3 possible. Van der Lans and co-workers suggested that NH_3 is formed from other nitrogen compounds (like HCN) by reaction with oxygen-derived radicals, since more NH_3 has been found in experiments with larger amounts of oxygen (Van der Lans, et al. 1997). The higher NH_3 formation in pyrolysis of low rank coals is also attributed to the higher oxygen content. In addition, more NH_3 was always detected in peat (having a higher oxygen and hydrogen content) than in coal in the same pyrolysis condition (Aho, et al. 1993; Leppalahti, 1995).

The current study, to a certain degree, also seems to support this idea. Figures 7.1 to 7.4 show that the NH_3 yield increased with increasing temperature. However, as temperature increased in the current experiments, the equivalence ratio became lower (see Table 4.2). The equivalence ratio is 1.45 at 1159 K but only 1.09 at 1858 K condition. The higher concentration of oxygen-derived radicals (resulting from both the high temperature and initial high oxygen concentration) may be *partially* responsible for the observed increase of NH_3 in the current study.

The main reaction pathway for the conversion of HCN to NH_3 can be summarized as (adapted from Van der Lans, et al. 1997):

$$HCN / C N \xrightarrow{oxygen} NCO \xrightarrow{H} NH_i \qquad (7.5)$$

The oxygen can be O_2, OH or O radicals. In a post flame environment, OH is more important (Fenimore, 1979). However, NCO seems to be the intermediate for the conversion at all cases.

NH_3 can also be formed directly from coal pyrolysis. Figures 7.11 and 7.12 show the HCN and NH_3 yields as a function of temperature, collected at 1 inch above the burner. For bituminous coals, the formation of NH_3 commenced at the same temperature as HCN. For low rank coals, NH_3 was released at a lower temperature than HCN. It is unlikely that the NH_3 was formed from HCN, due to the low temperature and the high equivalence ratio. The early occurrence of NH_3 from low rank coals strongly suggests a unique source of NH_3 that is significant only in low rank coals.

Two types of nitrogen functionalities are possible origins for NH_3. One type is the amine-containing functional groups. Amine is thought to be the source of NH_3 in coal pyrolysis by many researchers (Leppalahti, 1995; Kelemen 1998). However, amines

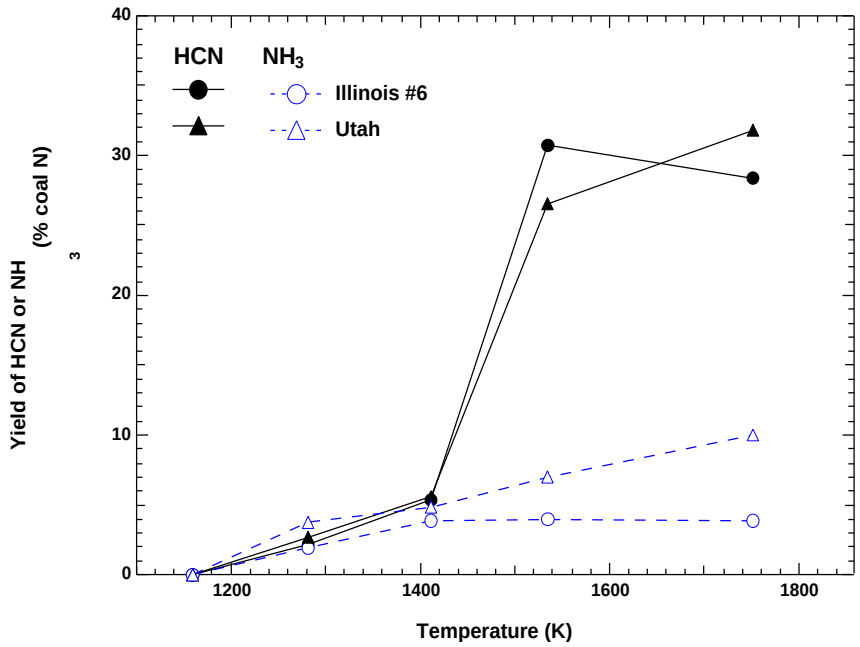

Figure 7.11. Yields of HCN and NH_3 versus temperature for high rank coals (collected at 1 inch above the burner).

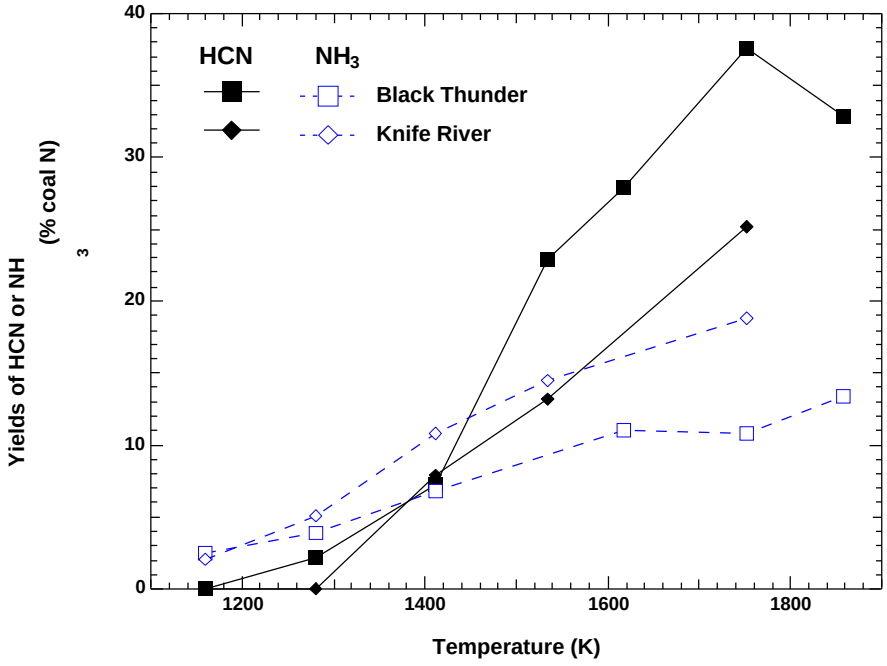

Figure 7.12. Yields of HCN and NH_3 versus temperature for low rank coals (collected at 1 inch above the burner).

only exist in very small amounts in coal and usually thermally decompose between 500 and 600°C, a temperature range much lower than the lowest temperature in the current study. The other type is quaternary nitrogen. The exact nature of quaternary nitrogen is still controversial. Some investigators think quaternary nitrogen is a distinct nitrogen functionality. Others believethat quaternary nitrogen is formed due to the oxidation of pyridinic nitrogen (Nelson, et al. 1992) or association with nearby or adjacent hydroxyl groups (Kelemen, et al. 1994). Quaternary nitrogen is more likely to be the source for the early release of NH_3 in this study, since quaternary nitrogen shows strong rank dependence and can only be found in significant amount in low rank coals. It should be emphasized that quaternary nitrogen may only be responsible for the early release of NH_3 seen in many studies. It is unlikely that quaternary nitrogen is the source of the large quantities of NH_3 formed at more severe conditions.

Previous studies show that nitrogen release during coal pyrolysis is a complicated process. The relative amount of HCN and NH_3 formed is not only determined by coal properties, but also dependent strongly on reactor configuration and local environment. Therefore, more data are needed before an attempt can be made to correlate the release of HCN and NH_3 with coal properties (i.e., certain functional groups or elemental compositions).

Nitrogen in Char

Nitrogen release from char is quite different from that of tar, although the nitrogen functionalities in the tar and char are similar. Figure 7.13 shows the corrected N/C ratio versus temperature for the coals in this study. The corrected N/C ratio is obtained from the N/C ratio in tar or char divided by the N/C ratio in the parent coal. A striking

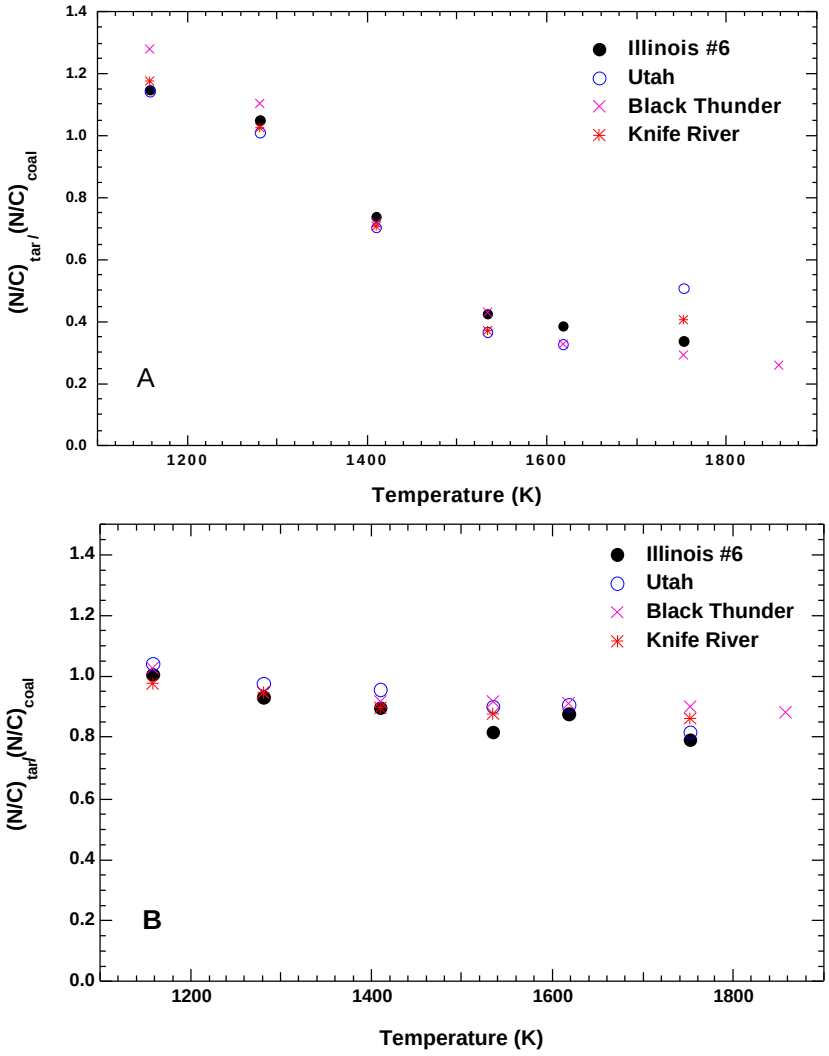

Figure 7.13. Corrected nitrogen/carbon ratio versus temperature (A) for the tar and soot and (B) for the char for the four coals in this study (collected at 7 inch above the burner).

similarity of the profiles of the nitrogen decay for the four coals is noticed in both tar and char. However, the N/C ratio in the char only decreased slightly from 1159 K to 1858 K. Chen (1991) suggested that the extensive, aromatic ring structures built up in char retarded the release of heteroatoms at elevated temperatures, a similar mechanism to that previously discussed for tar at the late stage of secondary reaction. A recent ^{13}C NMR

analysis on the tar-char pair collected at increasingly severe conditions indicated that the ring buildup reaction rate is comparable in the tar and in the char (Perry, 1999). Therefore, the much slower rate of nitrogen release from char cannot be solely attributed to the chemical structure change during coal pyrolysis. The large difference of nitrogen release rate from char and tar makes it reasonable to believe that differences in reactivity for the nitrogen functionalities in the char and tar may be also responsible. That is to say, the nitrogen functionalities trapped in char are less reactive than their counterparts in tar. These functionalities may either be transformed to more refractory types induced by heat during pyrolysis or stabilized by nearby functional groups, making them extremely resistant to thermal decomposition. More research is needed to verify the validity of this hypothesis.

It is thought that both HCN and NH_3 can be evolved from char during pyrolysis (Li, et al, 1996; Leppalahti, 1995). They may be released independently from different functionalities in char, or else NH_3 may be formed from HCN in the pores and surfaces of the char (Bassilakis, et al. 1993). Unfortunately, the exact reaction mechanism of char nitrogen cannot be examined due to the limits of the current study. In this study, the contributions to the total HCN and NH_3 release from the char and the tar cannot be distinguished. More research on high temperature char pyrolysis is needed to clarify the exact contribution of each mechanism.

8. Summary and Conclusions

The major objective of this study is to investigate the mechanisms of secondary reactions of coal volatiles, including nitrogen evolution and distributions among different products. Furthermore, soot formation during secondary pyrolysis was examined, and its effect on nitrogen chemistry was evaluated. These information help understand the nitrogen transformations at typical coal firing conditions, and is essential to the development of a comprehensive nitrogen release model for the coal-utilization processes.

Accomplishments

A $CO/H_2/O_2/N_2$ flame was operated under fuel-rich conditions in a flat flame reactor to provide a high temperature, oxygen-free post-flame environment to study secondary reactions of coal volatiles. Temperature, residence time, and coal rank were chosen as the major test variables to examine the nitrogen evolution and soot formation mechanism during secondary pyrolysis. Temperatures in the reactor were adjusted from 1159 K to 1858 K, where secondary reactions were highlighted. Four coals, ranging from high volatile bituminous to lignite, were used to study the influence of coal properties on nitrogen release. The results were reasonable, repeatable and comparable with published data from the literature.

The major accomplishments achieved in this study can be summarized as:

1) Low temperatures in a post-combustion environment were achieved using a CO flame, which facilitated the study of secondary pyrolysis.

2) A set of eighty pyrolysis experiments, including four coals, seven temperature conditions, and four residence times was completed. The resulting char and tar/soot samples were analyzed to provide the elemental compositions, mass release and product yields for each test.

3) Noncondensible gases produced during pyrolysis were accurately quantified by FTIR coupled with a multi-reflection, long-path gas cell. The results were reliable and reproducible, representing the first extensive gas analysis data of coal pyrolysis in a post-combustion environment. A detection limit as low as 50 ppb was achieved for some gases.

4) The chemical structure changes of tar and soot samples from a coal and two aromatic model compounds were derived from ^{13}C NMR analysis. This is the first data set of ^{13}C NMR analysis on tars and soots from model compounds.

5) A hypothetical secondary reaction mechanism of coal volatiles was developed. Three major processes were identified and modeled using first-order reactions. The nitrogen evolution from tar was also modeled as a first-order reaction and the corresponding rate expression was derived.

Summary of Results

Mass Release and Tar/Soot Yield

The ultimate mass release from coal pyrolysis in this study exhibited strong rank dependence and showed similar trends to those reported by other investigators. The tar

and soot yields measured in this study are much lower than those reported in the literature at similar temperatures and heating rates, especially for low rank coals. Two major reasons may be responsible for the observed lower tar/soot yields including A) unaccounted semivolatile species; and B) gasification of the nascent tar by the oxidizing species in the post flame environment. Of these two reasons, gasification is thought to be more important.

Chemical Structures of Tar and Soot

Changes in the chemical structure of tars and soots from an Illinois #6 coal and two model compounds, biphenyl and pyrene, were analyzed using solid state ^{13}C NMR spectroscopy. This is the first time tars and soots from coals pyrolyzed at increasingly severe conditions from 1250 K to 1600 K have been analyzed by ^{13}C NMR. Since transition from tar to soot usually occurs between 1300 K and 1450 K, this study provided a unique opportunity to examine the early soot formation mechanisms. This is also the first data set containing chemical structure analysis where two model compounds have been included, which gives insight into the evolution of soot from hydrocarbons.

The coal-derived soots exhibited loss of aliphatic and oxygen functional groups prior to significant growth in average aromatic ring size. This is evidenced by the dramatic loss of side chains per cluster at temperatures from 1160 K to 1280 K, while the aromatic carbons per cluster as well as bridges and loops per cluster remained roughly constant. Ring opening reactions started to dominate beginning at 1280 K. PAH containing oxygen functional groups seems to have a higher reaction rate than the non-polar PAH, as seen by the early disappearance of oxygen attached functional groups (carbonyl carbon, phenolic carbon and oxygen bonded to aliphatic or aromatic carbon) at

1400 K. At 1400 K, no aliphatic side chains were evident, but the number of bridges and loops increased dramatically, suggesting that ring polymerization reactions may have begun. Between 1411 K and 1534 K, polymerization reactions accelerated and became dominant; the clusters grew bigger and were more aromatic as well. The molecular weight per cluster increased more than three times and the aromaticity was very close to unity at 1534 K. Finally, at 1858 K, an extraordinarily large cluster size (greater than 100 carbons) was observed, indicating that soot growth is favored at high temperatures.

The data obtained for the model compounds exhibit a different pathway for pyrolysis and soot growth from that for the coal. For biphenyl, aliphatic carbon was absent in the starting compound, but was observed in the pyrolyzed samples. Therefore, it is believed that ring opening reaction is an early step in the soot formation process for biphenyl. Next, the decrease of the fraction of aliphatic carbon (from 0.09 to 0.02) with increasing temperature indicates that major structural rearrangements were occurring following the initial ring opening reactions. The number of bridges and loops, which is 1 in unreacted biphenyl, doubled to 2.2 and 2.5 at 1365 K and 1410 K and then doubled again to 4.7 at 1470 K. The cluster size, which started at 6 in the parent molecule, grew to 9, 11, 20 aromatic carbon, respectively. Hence, soot growth consists not only the ring size growth but also cluster crosslinking which results in the formation of large, interconnected structures.

The evolution of pyrene soot follows another path. First, little evidence is observed for ring opening reactions. Second, ring growth of only approximately 10% has occurred at 1410 K compared to nearly 100% in the case of the corresponding biphenyl soot. However, data on this 1410 K soot sample indicate that the relatively small cluster

size has been augmented by an average of 2.6 crosslinking sites per cluster. The data obtained from this study is inconclusive regarding the exact mechanism for ring growth in the pyrene soots between 1410 K and 1460 K, since different analysis methods on the broadened aromatic band of pyrene soots generated different results. Clearly, this is an area for future work.

Mechanism of Secondary Reactions of Coal Volatiles

A simple reaction mechanism of secondary reactions of nascent coal volatiles was proposed based on the tar/soot yields and chemical structure data. Two competitive reactions, cracking and polymerization, were assumed for primary tars. At low temperatures (below 1300 K), the cracking reaction is predominant, causing the release of secondary gases. At high temperatures, ring polymerization reaction accelerated, leading to substantial soot growth. It is further assumed that the fraction of primary tar that can be directly converted to soot is constant and dependent on coal rank. At temperatures higher than 1600 K, an additional soot growth mechanism from gas-phase hydrocarbon addition was also included.

The three reaction pathways were modeled as first-order reactions. Kinetic parameters were obtained by fitting the experimental data in the current study and those reported in literature. By using a single activation energy for each reaction, very good agreement was achieved between calculated tar/soot yields and measured yields. The early decrease of the tar plus soot yield with temperature, due to fast tar decay and slow soot growth, is clearly shown in the simulation.

Nitrogen Release during Coal Pyrolysis

Nitrogen release is inherently related to mass release during the early stage of devolatilization. In addition, a strong rank dependence of the total nitrogen release is also

observed. For bituminous coals, nitrogen release is proportional to mass release at first, followed by a delay during the middle stage, and then proceeding at a slow rate even after mass release is largely completed. For low rank coals, the fractional nitrogen release rates are much slower than the fractional release of overall mass during the early stage of pyrolysis. A delayed nitrogen release during the middle stage and a much slower nitrogen release from char after the majority of mass release ceases (at a prolonged time scale) is also observed.

Tar is virtually the only carrier of coal nitrogen during the early phase of pyrolysis. For bituminous coals, these ring structures in coal are transported essentially intact to tar during the early pyrolysis. Non-polar PAH are preferentially released as tar during the early pyrolysis for low rank coals, probably due to the early crosslinking in coal.

During secondary pyrolysis, an enrichment of nitrogen in tar is first observed, followed by a subsequent fast nitrogen release. The fraction of coal nitrogen in tar/soot reaches an asymptote during the late stages of pyrolysis. The enrichment of nitrogen in tar clearly shows that nitrogen exists in tightly-bound ring structures, which only react at more severe conditions. Subsequent nitrogen release, in the form of HCN, is caused by ring rupture at high temperatures. Incorporation of a portion of nitrogen into soot occurs during the early stages of soot formation. As pyrolysis proceeds, the clusters in soot become larger and more interconnected, which retard the further release of nitrogen. Therefore, the fraction of coal nitrogen incorporated into the soot remains constant while the soot yield increases rapidly. In addition, the nitrogen functionalities in tar seem to have a higher reactivity than their counterparts in the char.

It is thought that tar nitrogen is exclusively released as HCN from nitriles. NH_3 can be formed through the interactions of HCN and other oxygen radicals in the gas phase or on a specific surface. Direct release of nitrogen in char as both HCN and NH_3 is possible. The data in the current study by themselves are not conclusive regarding the complicated reaction pathways among the nitrogen species during coal pyrolysis. However, it proves that the relative amount of HCN and NH_3 formed is strongly dependent on reactor configuration and local environment.

Principal Conclusions

This study of nitrogen evolution during secondary coal pyrolysis and soot formation mechanism from coal tar and model compounds at high temperature, high heating rate conditions has given rise to the following conclusions:

1) Both temperature and residence time have significant effects on volatile release from coal during secondary coal pyrolysis.
2) Secondary reactions of coal tar are influenced more by thermal history than by chemical structure, based on similar behavior of tar decay from a broad range of coal types.
3) Addition of gas phase hydrocarbons to existing soot particles is necessary to explain the slight increase in soot yield at temperatures above 1600 K, but is not the principal soot formation mechanism in a coal system. C_2H_2 is the major species participating in the soot surface growth, while benzene and other species make much less contribution.
4) The sooting mechanism was dependent on the chemical structure of the parent aromatic molecules. For coal tar, loss of aliphatic side chains and

oxygen functional groups was the first step in soot formation, followed by rapid ring growth above 1400 K. For biphenyl, significant ring opening reactions occurred prior to ring growth. For pyrene, little evidence of ring opening reactions was found.

5) The reactivity of nitrogen functionalities in coal tar shows little rank dependence.

6) For low rank coals, NH_3 is released earlier than HCN; for high rank coals, NH_3 is released at the same time as HCN. Some types of quaternary nitrogen are responsible for the earlier release of NH_3 than HCN at low temperatures. However, quaternary nitrogen is not the source of the large quantities of NH_3 formed at more severe conditions.

7) Tar nitrogen is exclusively released as HCN. NH_3 can subsequently be formed from HCN and other nitrogen species.

Limitations and Recommendations

The current study offered a unique opportunity to examine the secondary reactions of coal volatiles, with an emphasis on nitrogen species. The results confirm much of what has been reported in previous studies. At the same time, new phenomena have been observed and new ideas have been developed. Unfortunately, it is not possible to address all the questions regarding nitrogen evolution during secondary pyrolysis due to the limitations of the current study. The limitations in this study are presented and recommendations are proposed here which would be valuable for future work in this area.

1) The current tar and soot collection system should be reconstructed to improve the collection efficiency. Significant amounts of tar or soot (10-

15%) were deposited on the walls of the collection system, which is hard to collect and measure. Although a correction is made to the tar/soot yields by weighing those deposits after wiping them off using kimwipes, a more accurate method is needed because the tar/soot yields are one of the most important measurements. Perhaps a porous wall could be used throughout the collection system to minimize tar or soot deposition.

2) Products collected at different residence times provide the detailed kinetics for secondary pyrolysis. However, the residence times in the current study are not long enough to further examine the additional soot formation from hydrocarbons and nitrogen evolution from soot, especially at high temperatures. Using a longer reactor is an option to obtain longer residence times.

4) A better closure on the nitrogen balance is desired, especially at low temperatures in this study. A further investigation is needed to resolve this problem. Since the nitrogen balance is very good at high temperatures, it is possible that some nitrogen species that are significant at low temperatures but converted to other species at more severe conditions were not measured.

3) N_2 and oxygen containing species (CO, CO_2, H_2O etc.) could not be measured in the current study. Accurate quantification of N_2 could help secure a better nitrogen balance and shed light on another possible pathway of nitrogen evolution during secondary pyrolysis. If air was replaced by pure oxygen and dilution/quench nitrogen was replaced by an inert gas such

as argon or helium, N_2 could be measured using a high resolution gas chromatograph.

4) The collected tar and soot deposits should be split and examined separately. The soot percentage in the total deposit is a convenient gauge for the extent of secondary reactions of tar. It is essential to track the soot formation rate from tar and nitrogen evolution during different stages of secondary pyrolysis. It is also useful to test the validity of the current secondary reaction mechanism of tar.

5) The secondary reactions of coal volatiles and nitrogen release are modeled as empirical, first-order reactions in this study. All the kinetic data are derived from experimental data. No chemical structure data are involved in the model, therefore, it is not expected to be valid for conditions too far away from those adopted in the current study. A detailed, "intrinsic" model that incorporates changes of chemical structure and nitrogen functionalities is desirable in order to predict accurately the nitrogen release for coals from different origins and at a broad range of conditions.

6) It is demonstrated in the current study that nitrogen decay from tar is roughly independent of coal rank. Pyrolysis of nitrogen-containing model compounds (such as pyridine, pyrrole, quinoline, nitriles, etc.) in the flat flame reactor will provide useful clues regarding the nitrogen transformations within tar and the subsequent release as gas species. The gas phase should be carefully examined to verify the interactions of the nitrogen species with other species in the gas phase. The chemical structure

analysis of the resulting soot will help understand the nitrogen evolution from soot at elevated temperatures.

7) The secondary reaction model should be incorporated into a general devolatilization model (such as the CPD model) so that the whole process of coal pyrolysis can be evaluated.

References

Aho, M. J., J. P. Hamalainen, and J. L. Tummavuori, “Conversion of Peat and Coal Nitrogen through HCN and NH_3 to Nitrogen Oxides at 800°C.” Fuel **72**: 837-841 (1993).

Austin, J., "Revised Comprehensive Reaction Mechanism for $CO/H_2/O_2$ kinetics." (1999), World Wide Web Homepage through http://web.galcit.caltech.edu/EDL/mechanisms/library/library.html

Axworthy, A. E., V. H. Dayan and G. B. Marin, “Reactions of Fuel-Nitrogen Compounds under Conditions of Inert Pyrolysis.” Fuel **57**: 29-35 (1978).

Badger, G. M., J. K. Donnelly and T. M. Spotswood, “The Formation of Aromatic Hydrocarbons at High Temperatures XXIII The Pyrolysis of Anthracene.” Australian Journal of Chemistry. **17**: 1147-1156 (1964).

Bassilakis, R., Y. Zhao, P. R. Solomon and M. A. Serio, “Sulfur and Nitrogen Evolution in the Argonne Coals: Experiment and Modeling.” Energy & Fuels **7**: 710-720 (1993).

Baxter, L. L., R. E. Mitchell, T. H. Fletcher and R. H. Hurt, “Nitrogen Release during Coal Combustion.” Energy & Fuels **10**: 188-196 (1996).

Bittner, J. D. and J. B. Howard, "Composition Profiles and Reaction Mechanisms in a Near-Sooting Premixed Benzene/Oxygen/Argon Flames." 18th Symposium (International) on Combustion **18**: 1105-1116 (1981).

Blair, D. W., J. O. L. Wendt and W. Bartok, "Evolution of Nitrogen and Other Species during Controlled Pyrolysis of Coal." 16th Symposium (International) on Combustion **16**: 475-489 (1976).

Breton, H., "Multi-Component Analysis Using Established Techniques." Proceedings of SPIE **1717**: 76-91 (1992).

Brill, T. B., P. J. Brush, K. J. James, J. E. Shepherd and K. J. Pfeiffer, “T-Jump/FTIR Spectroscopy: A New Entry into the Rapid, Isothermal Pyrolysis Chemistry of Solids and Liquids.” Applied Spectroscopy **46**: 900-911 (1992).

Brown, A. L. and T. H. Fletcher, “Modeling Soot Derived from Pulverized Coal.” Energy & Fuels **12**: 745-757 (1998).

Cai, H. Y., A. J. Guell, D. R. Dugwell and R. Kandiyoti, “Heteroatom Distribution in Pyrolysis Products as a Function of Heating Rate and Pressure.” Fuel **72**: 321-327 (1992).

Chen, S. L., J. A. Cole, J.C. Kramlich, J. M. McCarthy and D. W. Pershing, "Advanced NO_x Reduction Process using -NH and -CN Compounds in Conjunction with Staged Air Addition." 22nd Symposium (International) on Combustion **22**: 1135-1145 (1988).

Chen, J. C., "Effects of Secondary Reactions on Product Distribution and Nitrogen Evolution from Rapid Coal Pyrolysis", Ph. D. Dissertation, Mechanical Engineering Department, Stanford University, Stanford, CA (1991).

Chen, J. C. and S. Niksa, “Coal Devolatilization during Rapid Transient Heating 1. Primary Devolatilization.” Energy & Fuels **6**: 254-264 (1992a).

Chen, J. C. and S. Niksa, “Suppressed Nitrogen Evolution from Coal-Derived Soot and Low-Volatility Coal Chars.” 24th Symposium (International) on Combustion **24**: 1269-1276 (1992b).

Cliff, D. I., K. R. Doolan, J. C. Mackie and R. J. Tyler, “Products from Rapid Heating of a Brown Coal in the Temperature range 400-2300^{o}C.” Fuel **63**: 394-400 (1984).

Compton, S. V. and D. A. C. Compton, Practical Sampling Techniques for Infrared Analysis, Chapter 8: Quantitative Analysis-Avoiding Common Pitfalls. CRC Press, Ann Arbor, MI (1993).

Doolan, K. R., J. C. Mackie, R. J. Tyler, “Coal Flash Pyrolysis: Secondary Cracking of Tar Vapours in the Range 870-2000 K.” Fuel **66**: 572-578 (1986).

Fenimore, C. P., "Studies of Fuel-Nitrogen Species in Rich Flame Gases." 17th Symposium (International) on Combustion, **17**: 661-670 (1979).

Fletcher, T. H., M. S. Solum, D. M. Grant, S. Critchfield and R. J. Pugmire, “Solid State ^{13}C and ^{1}H NMR Studies of the Evolution of the Chemical Structures of Coal Char and Tar during Devolatilization.” 23rd Symposium (International) on Combustion **23**: 1231-1237 (1990).

Fletcher, T. H. and D. R. Hardesty, "Milestone Report" for DOE's Pittsburgh Energy Technology Center, Sandia Report SAND92-8209 (1992).

Fletcher, T. H., A. R. Kerstein, R. J. Pugmire, M. S. Solum and D. M. Grant, “A Chemical Model of Coal Devolatilization 3. Direct Use of ^{13}C NMR Data to Predict Effects of Coal Type.” Energy & Fuels **6**: 414 (1992).

Fletcher, T. H., J. Ma, J. R. Rigby, A. L. Brown and B. W. Webb, “Soot in Coal Combustion Systems.” Progress in Energy and Combustion Science **23**: 283-301 (1997).

Freihaut, J. D. and D. J. Seery, “An Investigation of Yields and Characteristics of Tars Released During the Thermal Decomposition of Coal.” ACS Division of Fuel Chemistry, Preprints **26**(2): 133-149 (1981).

Freihaut, J. D., W. M. Proscia and D. J. Seery, “Chemical Characteristics of Tars Produced in a Novel Low-Severity, Entrained-Flow Reactor.” Energy & Fuels **3**: 692-703 (1989).

Freihaut, J. D., W. M. Proscia and J. C. Mackie, “Chemical and Thermochemical Properties of Heavy Molecular Weight Hydrocarbons Evolved During Rapid Heating of Coal of Varying Rank Characteristics.” Combustion Science and Technology **93**: 323-347 (1993).

Frenklach, M., D. W. Clary, W. C. Gardiner and S. E. Stein, "Effect of Fuel Structure on Pathways to Soot." 21st Symposium (International) on Combustion **21**: 1067-1076 (1986).

Frenklach, M. and H. Wang, "Detailed Modeling of Soot Particle Nucleation and Growth." 23rd Symposium (International) on Combustion **23**: 1559-1566 (1990).

Friebel, J. and R. F. W. Kopsel, “The Fate of Nitrogen during Pyrolysis of German Low Rank Coals- A Parameter Study.” Fuel **78**: 923-932 (1999).

Genetti, D. B., "An Advanced Model of Coal Devolatilization Based on Chemical Structure", M. S. Thesis, Department of Chemical Engineering, Brigham Young University, Provo, UT (1999).

Glarborg, P. and J. A. Miller, "Mechanism and Modeling of Hydrogen Cyanide Oxidation in A Flow Reactor." Combustion and Flame **99**: 475-483 (1994).

Glassman, I., "Soot Formation in Combustion Processes." 22nd Symposium (International) on Combustion **22**: 295-311 (1988).

Glassman, I., Chapter 8: Environmental Combustion Considerations, Combustion, 3rd edition. Academic Press, Inc., New York (2000).

Hambly, E. M., "The Chemical Structure of Coal Tar and Char During Devolatilization", M. S. Thesis, Department of Chemical Engineering, Brigham Young University, Provo, UT (1998).

Hanst, P. L., QASoft User's Mannual. Anaheim, CA, Infrared Analysis, Inc. (1999a).

Hanst, P. L., QASOFT Version-32. Anaheim, CA, Infrared Analysis, Inc (1999b).

Haussmann, G. J. and C. H. Kruger, "Evolution and Reaction of Fuel Nitrogen During Rapid Coal Pyrolysis and Combustion." Presented at the Spring meeting of the Western State Section of The Combustion Institute, Livermore, CA. (1989).

Hayashi, J., K. Nakagawa, K. Kusakabe and S. Morooka, “Change in Molecular Structure of Flash Pyrolysis Tar by Secondary Reaction in a Fluidized Bed Reactor.” Fuel Processing Technology **30**: 237-248 (1992).

Haynes, B. S., Chapter 5: Soot and Hydrocarbons in Combustion, Fossil Fuel Combustion. Editor: W. Bartok and A. F. Sarofim, John Wiley & Sons, Inc., New York. (1991).

Homann, K. H. and H. G. Wagner, "Some New Aspects of The Mechanism of Carbon Formation in Premixed Flames." 11th Symposium (International) on Combustion **11**: 371-379 (1967).

Homann, K. H., "Formation of Large Molecules, Particulates and Ions in Premixed Hydrocarbon Flames; Progress and Unresolved Questions." 20th Symposium (International) on Combustion **20**: 857-870 (1984).

Ingle, J. D., Jr. and S. R. Crouch, Spectrochemical Analysis Prentice Hall, New Jersey, (1988).

Kallonen, R., “Smoke Gas Analysis by FTIR Method, Preliminary Investigation.” Journal of Fire Science **8**: 343-360 (1990).

Kambara, S., T. Takarada, M. Toyoshima and K. Kato, “Relations Between Functional Forms of Coal Nitrogen and NO_x Emissions from Pulverized Coal Combustion.” Fuel **74**: 1247-1253 (1995).

Kassman, H., M. Abul-Milh and L. E. Amand, "Measurement of NH_3 and HCN Concentrations in a CFB Boiler, A Comparison Between A Conventional Absorption and FTIR Technique." 13th International Conference on Fluidized Bed Combustion **2**: 1447-1454 (1995).

Kee, R. J., J. F. Grcar, M. D. Smooke and J. A. Miller, "A Fortran Program for Modeling Steady Laminar One-Dimensional Premixed Flame", Sandia Report SAND85-8240 (1985).

Kelemen, S. R., M. L. Gorbaty, S. N. Vaughn and P. J. Kwiatek, “Quantification of Nitrogen Forms in Argonne Premium Coals.” ACS Division of Fuel Chemistry Preprint 384-392 (1993).

Kelemen, S. R., M. L. Gorbaty, S. N. Vaughn and P. J. Kwiatek, “Quantification of Nitrogen Forms in Argonne Premium Coals.” Energy & Fuels **8**: 896-906 (1994).

Kelemen, S. R., M. L. Gorbaty, P. J. Kwiatek, T. H. Fletcher, M. Watt, M. S. Solum and R. J. Pugmire, “Nitrogen Transformations in Coal During Pyrolysis.” Energy & Fuels **12**: 159-173 (1998).

Ko, G. H., D. M. Sanchez, W. A. Peters and J. B. Howard, "Correlations for Effects of Coal Type and Pressure on Tar Yields from Rapid Devolatilization." 22nd Symposium (International) on Combustion **22**: 115-124 (1988).

Kremer, H. and W. Schulz, "Influence of Temperature on the Formation of NOx during Pulverized Coal Combustion." 21st Symposium (International) on Combustion **21**: 1217-1222 (1986).

Laskin, A. and A. Lifshitz, "Isomerization and Decomposition of Indole. Experimental Results and Kinetic Modeling." Journal of Physical Chemsitry **101**(A): 7787-7801 (1997).

Laskin, A. and A. Lifshitz, "Thermal Decomposition of Quinoline and Isoquinoline. The Role of 1-Indene Imine Radical." Journal of Physical Chemistry **102**(A): 928-946 (1998).

Ledesma, E. B., "Investigation of the Rates of Evolution and Distribution of Products During the Pyrolysis and Combustion of Coal Volatiles," Ph. D. Dissertation, Department of Physical and Theoretical Chemistry, University of Sydney, Sydney, Australia (1998).

Ledesma, E. B., C. Z. Li, P. F. Nelson and J. C. Mackie, "Release of HCN, NH_3, and HNCO from the Thermal Gas-Phase Cracking of Coal Pyrolysis Tars." Energy & Fuels **12**: 536-541 (1998).

Leppalahti, J., "Formation of NH_3 and HCN in slow-heating-rate Inert Pyrolysis of Peat, Coal and Bark." Fuel **74**: 1363-1368 (1995).

Leppalahti, J. and T. Koljonen, "Nitrogen Evolution from Coal, Peat and Wood during Gasification: Literature Review." Fuel Processing Technology **43**: 1-45 (1995).

Li, C. Z., P. F. Nelson, E. B. Ledesma and J. C. Mackie, "An Experimental Study of the Release of Nitrogen from Coals Pyrolyzed in Fluidized-Bed Reactors." 26th Symposium (International) on Combustion **26**: 3205-3211 (1996).

Li, C. Z., A. N. Buckley and P. F. Nelson, "Effects of Temperature and Molecular Mass on the Nitrogen Functionality of Tars Produced under High Heating Rate Conditions." Fuel **77**: 157-164 (1997).

Ma, J., "Soot Formation From Coal Pyrolysis," Ph. D. Dissertation, Department of Chemical Engineering, Brigham Young University, Provo, UT (1996).

Mackie, J. C., M. B. Colket and P. Nelson, "Shock Tube Pyrolysis of Pyridine." Journal of Physical Chemistry **94**: 4009-4106 (1990).

Mackie, J. C., M. B. Colket, P. Nelson and M. Esler, "Shock Tube Pyrolysis of Pyrrole and Kinetic Modeling." International Journal of Chemical Kinetics **23**: 733-760 (1991).

Man, C. K., N. V. Russell, J. R. Gibbins and J. Williamson, "A Kinetic Study of Secondary Volatile Nitrogen Release from Coal." ACS Division of Fuel Chemistry **43**(3): 1139-1142 (1998).

McLean, W. J., D. R. Hardesty and J. H. Phol, "Direct Observations of Devolatilizing Pulverized Coal Particles in a Combustion Environment." 18th Symposium (International) on Combustion **18**: 1239-1248 (1981).

Miller, J. A. and C. T. Bowman, "Mechanism and Modeling of Nitrogen Chemistry in Combustion." Progress in Energy and Combustion Science **15**: 287-338 (1989).

Miller, J. A. and P. Glarborg, Springer Series Physical Chemistry **61**: 318 (1996).

Mullins, O. C., S. Mitra-Kirtley, J. V. Elp and S. P. Cramer, "Molecular Structure of Nitrogen in Coal from XANES Spectroscopy." Applied Spectroscopy **47**: 1268-1275 (1993).

Nelson, P. F. and R. J. Tyler, "Formation of Light Gases and Aromatic Species During the Rapid Pyrolysis of Coal." 21st Symposium (International) on Combustion **21**: 427-435 (1986).

Nelson, P. F., I. W. Smith, R. J. Tyler and J. C. Mackie, "Pyrolysis of Coal at High Temperatures." Energy & Fuels **2**: 391-400 (1988).

Nelson, P. F., M. D. Kelly and M. J. Wornat, "Conversion of Fuel Nitrogen in Coal Volatiles to NOx Precursors Under Rapid Heating Conditions." Fuel **70**: 403-407 (1990).

Nelson, P. F., A. N. Buchley and M. D. Kelly, "Functional Forms of Nitrogen in Coals and the Release of Coal Nitrogen as NO_x Precursors (HCN and NH_3)." 24th Symposium (International) on Combustion **24**: 1259-1267 (1992).

Nenniger, R. D., "Aerosols Produced From Coal Pyrolysis." Ph. D. Dissertation, Department of Chemical Engineering, MIT, Cambridge, MA (1986).

Niksa, S., "Predicting the Evolution of Fuel Nitrogen from Various Coals." 25th Symposium (International) on Combustion **25**: 537-544 (1994).

Niksa, S., "FLASHCHAIN Theory for Rapid Coal Devolatilization Kinetics. 6. Predicting the Evolution of Fuel Nitrogen from Various Coals." Energy & Fuels **9**: 467-478 (1995).

Niksa, S. and S. Cho, "Conversion of Fuel-Nitrogen in the Primary Zones of Pulverized Coal Flames." Energy & Fuels **10**: 463-473 (1996).

Peck, R. E., K. C. Midkiff and R. A. Altenkirch, "The Evolution of Nitrogen from Pulverized Subbituminous Coal Burnt in a One-Dimensional Flames." 20th Symposium (International) on Combustion **20**: 1373-1380 (1984).

Perry, S. T., "A Global Free-Radical Mechanism for Nitrogen Release during Coal Devolatilization Based on Chemical Structure.", Ph. D. Dissertation, Department of Chemical Engineering, Brigham Young University, Provo, UT (1999).

Pershing, D. W. and J. O. Wendt, "Pulverized Coal Combustion: The Influence of Flame Temperature and Coal Composition on Thermal and Fuel NO_x." 16th Symposium (International) on Combustion **16**: 389-399 (1977).

Phong-Anant, D., L. J. Wibberley and T. F. Wall, "Nitrogen Oxide Formation from Australian Coals." Combustion and Flame **62**: 21-30 (1985).

Pohl, J. H. and A. F. Sarofim, "Devolatilization and Oxidation of Coal Nitrogen.", 16th Symposium (International) on Combustion **16**: 491-501 (1977).

Pugmire, R. J., M. S. Solum, D. M. Grant, S. Critchfield and T. H. Fletcher, "Structural Evolution of Matched Tar-Char Pairs in Rapid Pyrolysis Experiments." Fuel **70**: 414-423 (1990).

Pugmire, R. J., Personal Communication, (1999).

Rees, D. P., L. D. Smoot and P. O. Hedman, "Nitrogen Oxide Formation Inside A Laboratory Pulverized Coal Combustor." 18th Symposium (International) on Combustion **18**: 1305-1311 (1981).

Rigby, J. R., "Experimentally Determined Optical Properties and Chemical Compositions of Coal-Derived Soot.", Ph. D. Dissertation, Department of Mechanical Engineering, Brigham Young University, Provo, UT (1996).

Rudiger, H., U. Greul, H. Spliethoff and K. R. G. Hein, "Distribution of Fuel Nitrogen in Pyrolysis Products Used for Reburning." Fuel **76**: 201-205 (1997).

Schafer, S. and B. Bonn "Hydrolysis of HCN as An Important Step in Nitrogen Oxide Formation in Fluidized Combustion. Part 1. Homogeneous Reactions." Fuel **79**: 1239-1246 (2000).

Seeker, W. R., G. S. Samuelsen, M. P. Heap and J. D. Trolinger, "The Thermal Decomposition of Pulverized Coal Particles.", 18th Symposium (International) on Combustion **18**: 1213-1226 (1981).

Serio, M. A., W. A. Peters and J. B. Howard, "Kinetics of Vapor-Phase Secondary Reactions of Prompt Coal Pyrolysis Tars." Ind. Eng. Chem. Res. **26**: 1831-1838 (1987).

Smith, K. L., L. D. Smoot, T. H. Fletcher and R. J. Pugmire, The Structure and Reaction Processes of Coal. Plenum Press, New York (1994).

Smoot, L. D., Editor, Fundamentals of Coal Combustion for Clean and Efficient Use. Elsevier, New York (1993).

Solomon, P. R. and M. B. Colket, “Evolution of Fuel Nitrogen in Coal Devolatilization.” Fuel **57**: 749-755 (1978).

Solomon, P. R., D. G. Hamblen, R. M. Carangelo, M. A. Serio and G. V. Deshpande, “General Model of Coal Devolatilization.” Energy & Fuels **2**: 405-422 (1988).

Solomon, P. R., M. A. Serio, R. M. Carangelo and R. Bassilakis, “Analysis of the Argonne Premium Coal Samples by Thermogravimetirc Fourier Transform Infrared Spectroscopy.” Energy & Fuels: 319-333 (1990).

Solomon, P. R., M. A. Serio and E. M. Suuberg, “Coal Pyrolysis: Experiments, Kinetic Rates and Mechanisms.” Progress in Energy and Combustion Science **18**: 133-220 (1992).

Solum, M. S., R. J. Pugmire and D. M. Grant, “^{13}C Solid-State NMR of Argonne Premium Coals.” Energy & Fuels **3**: 187-193 (1999).

Solum, M. S., A. Sarofim, R. J. Pugmire, T. H. Fletcher and H. Zhang, “C-13 NMR Analysis of Soot Produced from Model Compounds and A Coal.” In Press (2000).

Takagi, H., T. Isoda, K. Kusakabe and S. Morooka, “Effects of Coal Structures on Denitrogenation during Flash Pyrolysis.” Energy & Fuels **13**: 934-940 (1999).

Terentis, A., A. Doughty and J. C. Mackie, “Kinetics of Pyrolysis of A Coal Model Compound, 2-Picoline, the Nitrogen Heteroaromatic Analogue of Toluene. 1. Product Distributions.” Journal of Physical Chemistry **96**: 10334-10339 (1992).

Tyler, R. J., “Flash Pyrolysis of Coals. Devolatilization of Bituminous Coals in a Small Fluidized-Bed Reactor.” Fuel **59**: 218-226 (1979).

Van der Lans, R. P., P. Glarborg and K. Dam-Johansen, “Influence of Process Parameters on Nitrogen Oxide Formation in Pulverized Coal Burners.” Progress in Energy and Combustion Science **23**: 349-377 (1997).

Veranth, J. M., T. H. Fletcher, D. W. Pershing and A. F. Sarofim, "Measurements of Soot and Char in Pulverized Coal Fly Ash.", Fuel **79**: 1067-1075 (2000).

Watt, M., "The Chemical Structure of Coal During Devolatilization.", M. S. Thesis, Brigham Young University, Provo, UT (1996).

Watt, M., T. H. Fletcher, S. Bai, M. S. Solum and R. J. Pugmire, "Chemical Structure of Coal Tar during Devolatilization.", 26th Symposium (International) on Combustion **26**: 3153-3160 (1996).

White, J. U., “Long Optical Paths of Large Aperture.” J. Opt. Soc. Amer. **32**: 285-289 (1942).

Wornat, M. J., A. F. Sarofim and J. P. Longwell, "Pyrolysis-Induced Changes in the Ring Number Composition of Polycyclic Aromatic Compounds form a High Volatile Bituminous Coal.", 22nd Symposium (International) on Combustion, **22**: 135-143 (1988a).

Wornat, M. J., A. F. Sarofim, J. P. Longwell and A. L. Lafleur, "Effect of Pyrolysis Conditions on the Composition of Nitrogen-Containing Polycyclic Aromatic Compounds from a Bituminous Coal." Energy & Fuels: 775-782 (1988b).

Xu, W. C. and A. Tomita, "Effect of Coal Type on the Flash Pyrolysis of Various Coals." Fuel **66**: 627-636 (1986).

Xu, W. C. and A. Tomita, "The Effects of Temperature and Residence Time on the Secondary Reactions of Volatiles from Coal Pyrolysis." Fuel Processing Technology **21**: 25-37 (1989).

Yetter, R. A., F. L. Dryer and H. Rabits, "A Comprehensive Reaction Mechanism for Carbon Monoxide/Hydrogen/Oxygen Kinetics." Combustion Science and Technology **79**: 97-128 (1991).

Yu, L. E., L. M. Hildemann and S. Niksa, "Characteristics of Nitrogen-Containing Aromatic Compounds in Coal Tars during Secondary Pyrolysis." Fuel **78**: 377-385 (1999).

Zhang, H., "Nitrogen Release during Secondary Coal Pyrolysis", ACERC Annual Report 1998, ACERC, Brigham Young University, Provo, UT (1998).

Zhang, H. and T. H. Fletcher, "Nitrogen Transformations during Secondary Coal Pyrolysis", ACERC Annual Report 1999, ACERC, Brigham Young University, Provo, UT (1999).

Appendices

Appendix A Tabulation of Experimental Data

Table A.1 Summary of Mass Release and Tar/Soot yields for the FFB Tests

Illinois #6 (Bituminous)

Temperature (K)	Collection height (inch)	Residence time (ms)	Tar/soot yields (daf, wt%)	Mass release (daf, wt%)
1159	1.0	46	17.03	37.63
1159 (rep.)	1.0	46	14.04	34.74
1281	1.0	38	15.80	44.71
1411	1.0	33	12.87	49.26
1534	1.0	19	11.63	56.22
1618	1.0	18	13.18	57.62
1752	1.0	19	17.80	55.76
1281	3.0	88	13.60	49.82
1411	3.0	74	14.77	56.31
1534	3.0	44	10.96	56.30
1534 (rep.)	3.0	44	13.32	58.52
1618	3.0	38	14.28	53.32
1858	3.0	39	10.08	53.78
1281	5.0	119	12.46	54.40
1534	5.0	66	15.44	55.59
1618	5.0	58	15.14	56.72
1159	7.0	182	18.77	52.19
1281	7.0	153	13.93	54.79
1411	7.0	130	14.44	57.89
1534	7.0	88	19.35	52.34
1618	7.0	76	13.98	57.87
1752	7.0	84	16.05	59.02

Utah (Bituminous)

Temperature (K)	Collection Height (inch)	Residence time (ms)	Tar/soot yields (daf, wt%)	Mass Release (daf, wt%)
1159	1.0	46	9.03	23.17
1281	1.0	38	9.14	31.65
1411	1.0	33	9.80	40.20
1534	1.0	19	12.09	43.11
1618	1.0	18	11.55	43.91
1752	1.0	19	17.26	52.56

1281	3.0	88	13.97	52.42
1411	3.0	74	12.99	54.65
1534	3.0	44	12.05	42.19
1618	3.0	38	13.67	49.30
1858	3.0	39	17.82	55.52
1281	5.0	119	14.89	51.00
1534	5.0	66	14.93	50.59
1618	5.0	58	12.79	53.97
1159	7.0	182	16.64	47.11
1281	7.0	153	13.19	52.19
1411	7.0	130	14.83	55.44
1534	7.0	88	17.09	51.21
1618	7.0	76	15.09	57.86
1752	7.0	84	20.94	58.90

Black Thunder (Subbituminous)

Temperature (K)	Collection Height (inch)	Residence time (ms)	Tar/soot yields (daf, wt%)	Mass Release (daf, wt%)
1159	1.0	46	5.17	25.94
1281	1.0	38	4.35	37.79
1411	1.0	33	4.48	42.98
1534	1.0	19	4.09	45.30
1618	1.0	18	4.67	51.72
1752	1.0	19	7.67	51.87
1858	1.0	17	8.11	52.22
1281	3.0	88	4.10	47.91
1411	3.0	74	4.84	50.54
1534	3.0	44	5.42	51.37
1618	3.0	38	7.51	53.88
1752	3.0	43	9.73	55.25
1858	3.0	39	8.48	55.33
1281	5.0	119	4.29	48.66
1534	5.0	66	5.98	51.10
1159	7.0	182	5.32	46.19
1281	7.0	153	4.17	49.73
1411	7.0	130	4.99	52.41
1534	7.0	88	6.50	51.25
1618	7.0	76	7.77	55.03
1752	7.0	84	8.59	56.42
1858	7.0	78	10.26	57.76

Knife River (Lignite)

Temperature (K)	Collection Height (inch)	Residence time (ms)	Tar/soot yields (daf, wt%)	Mass Release (daf, wt%)
1159	1.0	46	2.32	19.35

1281	1.0	38	2.34	23.17
1411	1.0	33	1.84	28.98
1534	1.0	19	0.84	30.26
1752	1.0	19	3.54	42.69
1281	3.0	88	1.42	37.30
1411	3.0	74	1.55	43.69
1534	3.0	44	1.89	45.12
1858	3.0	39	3.81	40.44
1281	5.0	119	1.76	38.58
1534	5.0	66	2.37	47.92
1159	7.0	182	2.62	31.84
1281	7.0	153	1.99	37.79
1411	7.0	130	1.82	41.77
1534	7.0	88	2.65	51.52
1752	7.0	84	5.49	49.79

Table A.2 Summary of Ultimate Analysis of Tar/soot and Char Samples (on dry, ash free basis)

Illinois #6 (tar and soot)

Temperature (K)	Collection Height (inch)	C%	H%	N%	S%	O%
1159	1.0	81.42	5.19	1.76	2.51	9.12
1159 (rep.)	1.0	80.61	5.00	1.65	2.48	10.25
1281	1.0	84.00	4.67	1.90	2.65	6.78
1411	1.0	88.43	4.16	1.76	2.30	3.35
1534	1.0	94.09	1.09	0.73	1.25	2.84
1618	1.0	96.49	0.92	0.71	1.07	0.81
1752	1.0	95.12	1.20	0.78	1.53	1.37
1281	3.0	87.82	4.06	1.79	2.26	4.07
1411	3.0	92.08	3.25	1.41	1.67	1.59
1534	3.0	90.41	2.17	0.85	1.81	4.76
1534 (rep.)	3.0	93.63	1.73	0.77	1.66	2.21
1618	3.0	93.88	1.43	0.77	1.31	2.61
1858	3.0	93.71	0.79	0.63	1.50	3.38
1281	5.0	90.89	3.892	1.622	2.208	1.388
1534	5.0	95.3	1.26	0.697	1.517	1.226
1618	5.0	96.39	1.2	0.611	0.234	1.565
1159	7.0	85.01	4.367	1.937	2.28	6.406
1281	7.0	90.25	4.065	1.882	2.085	1.718
1411	7.0	93.61	3.195	1.374	1.515	0.306
1534	7.0	93.71	1.67	0.792	1.628	2.2
1618	7.0	94.02	0.81	0.7185	1.061	3.391
1752	7.0	95.87	0.738	0.637	1.814	0.941

Illinois #6 (char)

Temperature (K)	Collection Height (inch)	C%	H%	N%	S%	O%
1159	1.0	80.95	4.14	1.61	4.23	9.07
1159 (rep.)	1.0	78.93	4.08	1.53	4.32	11.13
1281	1.0	82.14	3.74	1.67	4.35	8.09
1411	1.0	84.74	3.37	1.65	3.57	6.67
1534	1.0	94.67	3.23	1.65	3.23	-2.78
1618	1.0	95.59	1.73	1.71	2.30	-1.33
1752	1.0	91.37	2.11	1.59	2.95	1.98
1281	3.0	87.63	3.08	1.66	3.16	4.46
1411	3.0	90.39	2.39	1.57	2.96	2.68
1534	3.0	91.17	1.97	1.63	3.17	2.06
1534 (rep.)	3.0	92.73	1.70	1.62	2.88	1.07
1618	3.0	92.52	1.86	1.61	2.70	1.32
1858	3.0	93.48	1.22	1.45	2.67	1.18

1281	5.0	90.47	2.55	1.65	2.70	2.62
1534	5.0	95.69	1.38	1.66	2.42	-1.15
1618	5.0	98.44	0.98	1.72	2.16	-3.31
1159	7.0	87.47	3.09	1.75	2.92	4.78
1281	7.0	88.80	2.72	1.64	2.92	3.92
1411	7.0	91.08	2.19	1.63	2.79	2.32
1534	7.0	96.24	1.57	1.56	2.54	-1.91
1618	7.0	96.10	1.07	1.67	1.47	-0.30
1752	7.0	93.81	1.20	1.48	2.69	0.82

Utah (tar and soot)

Temperature (K)	Collection Height (inch)	C%	H%	N%	S%	O%
1159	1.0	82.99	5.55	1.71	0.39	9.368
1281	1.0	85.68	5.04	1.77	0.38	7.134
1411	1.0	88.15	4.73	1.77	0.41	4.944
1534	1.0	98.16	1.67	0.81	0.26	-0.895
1618	1.0	96.57	1.17	0.69	0.21	1.368
1752	1.0	96.81	1.78	0.85	0.26	0.302
1281	3.0	90.00	4.37	1.89	0.43	3.31
1411	3.0	93.50	3.44	1.44	0.29	1.34
1534	3.0	96.94	1.52	0.74	0.34	0.46
1618	3.0	96.13	1.18	0.62	0.28	1.79
1858	3.0	97.25	0.77	0.57	0.29	1.12
1281	5.0	90.10	4.26	1.85	0.36	3.44
1534	5.0	90.73	1.95	0.76	0.37	6.18
1618	5.0	96.39	1.20	0.61	0.23	1.57
1159	7.0	86.68	4.65	1.99	0.38	6.30
1281	7.0	91.53	4.18	1.86	0.34	2.08
1411	7.0	94.49	3.30	1.34	0.24	0.63
1534	7.0	97.44	1.48	0.72	0.34	0.02
1618	7.0	95.13	1.17	0.63	0.29	2.78
1752	7.0	94.74	0.89	0.97	0.24	3.16

Utah (char)

Temperature (K)	Collection Height (inch)	C%	H%	N%	S%	O%
1159	1.0	82.20	5.12	1.62	0.50	10.56
1281	1.0	83.80	4.73	1.61	0.45	9.41
1411	1.0	83.51	4.29	1.64	0.47	10.10
1534	1.0	87.44	3.40	1.82	0.43	6.91
1618	1.0	96.36	2.39	1.89	0.37	-1.01
1752	1.0	91.67	2.99	1.75	0.38	3.22

1281	3.0	90.91	3.37	1.86	0.45	3.41
1411	3.0	91.41	2.68	1.78	0.41	3.72
1534	3.0	90.54	3.10	1.79	0.36	4.20
1618	3.0	94.09	1.87	1.72	0.32	2.00
1858	3.0	97.48	1.32	1.78	0.36	-0.95
1281	5.0	87.41	3.23	1.73	0.43	7.20
1534	5.0	99.18	2.12	1.94	0.37	-3.61
1618	5.0	96.93	1.43	1.73	0.29	-0.38
1159	7.0	86.65	3.30	1.82	0.40	7.83
1281	7.0	89.23	2.91	1.75	0.36	5.76
1411	7.0	89.27	2.37	1.72	0.35	6.28
1534	7.0	103.49	1.89	1.88	0.38	-7.64
1618	7.0	94.93	1.58	1.73	0.31	1.45
1752	7.0	87.45	1.32	1.44	0.33	9.46

Black Thunder (tar and soot)

Temperature (K)	Collection Height (inch)	C%	H%	N%	S%	O%
1159	1.0	78.91	5.43	1.20	0.45	14.01
1281	1.0	82.57	4.96	1.36	0.43	10.68
1411	1.0	88.14	4.65	1.34	0.48	5.40
1534	1.0	93.26	3.86	0.88	0.44	1.57
1618	1.0	95.40	2.76	0.50	0.55	0.80
1752	1.0	97.73	1.36	0.44	0.44	0.03
1858	1.0	98.02	0.90	0.41	0.35	0.32
1281	3.0	90.85	4.36	1.41	0.45	2.93
1411	3.0	94.90	3.81	1.02	0.38	-0.12
1534	3.0	95.01	2.09	0.43	0.36	2.11
1618	3.0	96.62	1.37	0.38	0.47	1.16
1752	3.0	97.24	0.81	0.44	0.48	1.03
1858	3.0	97.73	0.61	0.41	0.49	0.77
1281	5.0	91.28	4.284	1.397	0.396	2.643
1534	5.0	96.31	1.798	0.45	0.381	1.061
1159	7.0	86.12	4.583	1.529	0.422	7.346
1281	7.0	91.71	4.268	1.4	0.43	2.192
1411	7.0	95.75	3.62	0.954	0.299	-0.623
1534	7.0	96.27	1.783	0.576	0.367	1.004
1618	7.0	95.98	1.106	0.433	0.463	2.018
1752	7.0	96.1	0.695	0.387	0.528	2.29
1858	7.0	96.17	0.532	0.345	0.606	2.347

Black Thunder (char)

Temperature (K)	Collection Height (inch)	C%	H%	N%	S%	O%
1159	1.0	76.34	4.32	1.07	0.39	17.88
1281	1.0	79.03	3.84	1.14	0.34	15.65
1411	1.0	82.15	3.51	1.15	0.32	12.86
1534	1.0	86.50	2.94	1.18	0.38	9.00
1618	1.0	84.80	2.68	1.08	0.35	11.10
1752	1.0	86.67	2.20	1.11	0.35	9.67
1858	1.0	87.55	1.76	1.14	0.35	9.20
1281	3.0	85.74	2.88	1.17	0.23	9.99
1411	3.0	88.89	2.41	1.18	0.26	7.26
1534	3.0	91.81	1.74	1.15	0.30	5.00
1618	3.0	87.96	1.66	1.11	0.35	8.92
1752	3.0	88.29	1.46	1.09	0.34	8.83
1858	3.0	89.90	1.28	1.12	0.32	7.38
1281	5.0	86.80	2.70	1.18	0.24	9.09
1534	5.0	92.99	1.50	1.19	0.30	4.02
1159	7.0	84.75	3.09	1.21	0.27	10.69
1281	7.0	86.97	2.57	1.14	0.28	9.03
1411	7.0	89.56	1.97	1.14	0.30	7.03
1534	7.0	92.17	1.39	1.17	1.05	4.21
1618	7.0	88.08	1.45	1.11	0.37	8.99
1752	7.0	88.55	1.27	1.11	0.34	8.73
1858	7.0	89.30	1.11	1.09	0.39	8.12

Knife River (tar and soot)

Temperature (K)	Collection Height (inch)	C%	H%	N%	S%	O%
1159	1.0	67.74	4.33	1.05	0.92	25.95
1281	1.0	62.34	3.66	1.01	1.01	31.97
1411	1.0	62.42	3.42	0.97	0.90	32.29
1534	1.0	83.11	3.30	0.69	1.38	11.53
1752	1.0	85.88	1.70	0.56	1.03	10.83
1281	3.0	75.20	3.31	1.12	1.15	19.23
1411	3.0	81.46	3.16	0.85	0.87	13.67
1534	3.0	87.94	2.84	0.61	1.47	7.14
1858	3.0	85.98	0.74	0.51	0.50	12.27
1281	5.0	73.85	3.34	1.07	1.10	20.64
1534	5.0	87.71	2.26	0.48	1.66	7.89
1159	7.0	69.34	3.76	1.19	1.11	24.60
1281	7.0	76.67	3.41	1.15	1.20	17.57
1411	7.0	81.30	3.27	0.84	0.90	13.68
1534	7.0	87.14	2.00	0.47	1.74	8.65

1752	7.0	82.24	0.77	0.49	2.19	14.31

Knife River (char)

Temperature (K)	Collection Height (inch)	C%	H%	N%	S%	O%
1159	1.0	75.20	4.18	1.11	1.42	18.09
1281	1.0	77.73	4.04	1.10	1.36	15.77
1411	1.0	80.94	3.71	1.14	1.30	12.90
1534	1.0	83.17	2.93	1.10	0.99	11.81
1752	1.0	87.64	2.26	1.13	1.07	7.89
1281	3.0	85.92	2.78	1.21	1.06	9.03
1411	3.0	89.69	2.32	1.20	0.54	6.25
1534	3.0	87.73	2.40	1.11	1.04	7.71
1858	3.0	93.21	1.21	1.29	0.62	3.67
1281	5.0	87.05	2.68	1.19	1.08	7.99
1534	5.0	89.01	1.90	1.15	1.10	6.85
1159	7.0	82.54	3.38	1.18	1.17	11.72
1281	7.0	85.93	2.73	1.19	1.19	8.97
1411	7.0	89.16	2.06	1.17	0.96	6.65
1534	7.0	89.72	1.80	1.15	1.09	6.24
1752	7.0	89.80	1.60	1.14	1.15	6.31

Table A.3 Distribution of Noncondensible Hydrocarbon Gases in the FFB (wt% of daf coal)

Illinois #6

Temperature (K)	Collection Height (inch)	CH_4	C_2H_2	C_2H_4	C_6H_6	Propylene	1,3-butadiene
1159	1.0	0.75	0.12	1.09	0	0.24	0.16
1281	1.0	1.52	0.60	2.17	0	0.29	0.33
1411	1.0	2.26	2.00	2.77	1.05	0.16	0.24
1534	1.0	1.95	7.17	1.09	2.03	N.M.	N.M.
1618	1.0	N.M.	N.M.	N.M.	N.M.	N.M.	N.M.
1752	1.0	0.59	4.76	0.24	0	0	0
1281	3.0	2.96	1.38	2.75	1.47	0.13	0.27
1411	3.0	2.77	3.13	1.65	2.03	0	0
1534	3.0	0.67	4.39	0.07	0.76	0	0
1618	3.0	N.M.	N.M.	N.M.	N.M.	N.M.	N.M.
1858	3.0	0.03	0.69	0	0	0	0
1281	5.0	4.01	2.31	3.64	1.71	0.11	0.13
1534	5.0	0	0	0	0	0	0
1618	5.0	N.M.	N.M.	N.M.	N.M.	N.M.	N.M.
1159	7.0	2.01	0.62	2.42	0	0.21	0.32
1281	7.0	2.55	1.34	2.63	0	0.08	0.2
1411	7.0	2.20	2.75	1.19	1.43	0	0
1534	7.0	1.63	7.69	0.12	0.61	0	0
1618	7.0	N.M.			N.M.	N.M.	N.M.
1752	7.0	0.17	2.94	0	0	0	0

Utah

Temperature (K)	Collection Height (inch)	CH_4	C_2H_2	C_2H_4	C_6H_6	Propylene	1,3-butadiene
1159	1.0	0.84	0.14	1.31	0	0.35	0.17
1281	1.0	1.74	0.78	2.70	0	0.43	0.39
1411	1.0	2.60	2.23	3.66	0	0.37	0.41
1534	1.0	3.84	11.73	4.03	2.67	0.22	N.M.
1618	1.0	N.M.	N.M.	N.M.	N.M.	N.M.	N.M.
1752	1.0	0.91	6.16	1.24	0	0.16	0.14
1281	3.0	4.63	2.38	6.33	1.74	0.62	0.69
1411	3.0	5.03	6.32	4.67	2.53	0.12	0.21
1534	3.0	2.60	2.23	3.66	0	0.37	0.41
1618	3.0	N.M.	N.M.	N.M.	N.M.	N.M.	N.M.
1858	3.0	0.31	1.83	0.12	0	0	0
1281	5.0	4.94	2.99	6.24	1.79	0.36	0.46

1534	5.0	N.M.	N.M.	N.M.	N.M.	N.M.	N.M.
1618	5.0	N.M.	N.M.	N.M.	N.M.	N.M.	N.M.
1159	7.0	2.89	0.64	4.22	0	0.74	0.83
1281	7.0	3.94	2.08	4.79	1.47	0.23	0.41
1411	7.0	4.34	4.62	3.50	1.88	0	0
1534	7.0	2.62	10.06	0.52	1.24	0	0
1618	7.0	N.M.	N.M.	N.M.	N.M.	N.M.	N.M.
1752	7.0	0.59	4.57	0	0	0	0

Black Thunder

Temperature (K)	Collection Height (inch)	CH_4	C_2H_2	C_2H_4	C_6H_6	Propylene	1,3-butadiene
1159	1.0	0.72	0.17	1.55	0	0.37	0.19
1281	1.0	1.40	0.73	3.01	0	0.51	0.41
1411	1.0	2.08	2.49	3.35	1.66	0.22	0.28
1534	1.0	2.56	5.96	2.51	2.61	N.M.	N.M.
1618	1.0	1.72	7.91	1.26	0.79	N.M.	N.M.
1752	1.0	0.76	6.84	0.55	0	N.M.	N.M.
1858	1.0	0.30	3.13	0.31	0	N.M.	N.M.
1281	3.0	3.17	2.04	4.60	1.15	0.30	0.49
1411	3.0	2.98	4.28	2.82	2.45	0	0
1534	3.0	2.47	7.98	0.95	2.04	0	0
1618	3.0	1.09	7.02	0.26	0.25	N.M.	N.M.
1752	3.0	0.35	4.02	0.14	0	N.M.	N.M.
1858	3.0	0.13	1.66	0.12	0	N.M.	N.M.
1281	5.0	3.32	2.05	4.62	2.06	0.24	0.45
1534	5.0	1.59	4.98	0.38	1.57	N.M.	N.M.
1618	5.0	N.M.	N.M.	N.M.	N.M.	N.M.	N.M.
1159	7.0	2.39	0.70	3.72	0	0.49	0.57
1281	7.0	3.19	2.10	4.37	2.11	0.20	0.39
1411	7.0	3.14	4.88	2.42	2.39	0	0
1534	7.0	1.38	4.55	0.19	1.06	N.M.	N.M.
1618	7.0	0.81	5.81	0.09	0	N.M.	N.M.
1752	7.0	0.37	3.21	0.06	0	N.M.	N.M.
1858	7.0	0.09	0.86	0	0	N.M.	N.M.

Knife River

Temperature (K)	Collection Height (inch)	CH_4	C_2H_2	C_2H_4	C_6H_6	Propylene	1,3-butadiene
1159	1.0	0.45	0.11	0.81	0	0.17	0.08
1281	1.0	0.91	0.47	1.64	0	0.19	0.21

1411	1.0	1.81	1.83	2.27	0	0.12	0.32
1534	1.0	1.11	3.08	0.93	1.18	NM	NM
1752	1.0	0.44	2.46	0.32	0	0	0
1281	3.0	2.09	1.25	2.10	1.22	0.11	0.16
1411	3.0	2.51	3.74	2.05	2.06	0	0
1534	3.0	2.27	5.28	1.21	1.47	NM	NM
1858	3.0	0.25	1.32	0.04	0	0	0
1281	5.0	2.61	1.77	2.88	1.19	0.13	0.20
1534	5.0	1.40	4.30	0.33	0	NM	NM
1159	7.0	1.46	0.46	2.13	0	0.25	0.34
1281	7.0	1.52	1.03	1.96	0	0	0
1411	7.0	1.42	2.12	1.11	0	0	0
1534	7.0	1.40	4.38	0.26	0	0	0
1752	7.0	0.19	2.00	0	0	0	0

Table A.4 Nitrogen Distribution Among Various Products
Illinois #6 (Bituminous)

Temperature (K)	Collection height (inch)	Residence time (ms)	HCN	NH_3	N_{tar}	N_{char}
1159	1.0	46	0.00	0.00	17.61	66.72
1281	1.0	38	2.14	1.90	19.97	61.39
1411	1.0	33	5.39	3.92	15.03	55.58
1534	1.0	19	30.73	4.02	5.63	48.17
1618	1.0	18	N. M.	N. M.	6.18	48.27
1752	1.0	19	28.42	3.86	9.22	46.77
1281	3.0	88	7.69	3.91	16.22	55.45
1411	3.0	74	16.06	4.12	13.80	45.60
1534	3.0	44	30.50	5.62	6.80	44.73
1618	3.0	38	N. M.	N. M.	7.31	49.89
1858	3.0	39	28.14	20.85	4.23	44.47
1281	5.0	119	12.57	4.94	13.44	50.03
1534	5.0	66	30.73	4.02	7.16	49.02
1618	5.0	58	N. M.	N. M.	6.15	49.50
1159	7.0	182	2.73	0.00	24.17	55.55
1281	7.0	153	5.99	1.73	17.43	49.44
1411	7.0	130	11.71	2.97	13.19	45.58
1534	7.0	88	N. M.	4.40	6.82	49.50
1618	7.0	76	N. M.	N. M.	6.68	46.81
1752	7.0	84	26.70	4.60	6.80	40.22

Utah (Bituminous)

Temperature (K)	Collection Height (inch)	Residence time (ms)	HCN	NH_3	N_{tar}	N_{char}
1159	1.0	46	0.00	0.00	9.40	76.03
1281	1.0	38	2.73	3.71	9.88	67.12
1411	1.0	33	5.54	4.89	10.57	59.92
1534	1.0	19	26.60	7.04	5.94	63.19
1618	1.0	18	N. M.	N. M.	4.84	61.72
1752	1.0	19	31.86	10.03	8.96	50.54
1281	3.0	88	7.18	5.51	16.13	53.99
1411	3.0	74	20.91	8.79	11.39	49.30
1534	3.0	44	bad data	bad data	5.41	63.31
1618	3.0	38	N. M.	N. M.	5.17	53.11
1858	3.0	39	22.91	33.18	6.17	48.28
1281	5.0	119	9.68	5.18	16.78	51.87
1534	5.0	66			6.92	58.48
1618	5.0	58	N. M.	N. M.	4.76	48.59

1159	7.0	182	2.74	1.79	20.20	58.68
1281	7.0	153	8.39	3.52	15.00	51.14
1411	7.0	130	21.05	6.02	12.11	46.78
1534	7.0	88	bad data	bad data	7.51	55.93
1618	7.0	76	N. M.	N. M.	5.79	44.61
1752	7.0	84	41.16	10.37	12.34	36.08

Black Thunder (Subbituminous)

Temperature (K)	Collection Height (inch)	Residence time (ms)	HCN	NH_3	N_{tar}	N_{char}
1159	1.0	46	0.00	2.53	5.88	74.37
1281	1.0	38	2.14	3.84	5.61	66.64
1411	1.0	33	7.28	6.83	5.68	61.87
1534	1.0	19	22.97	8.93	3.42	60.76
1618	1.0	18	27.92	11.02	2.19	49.19
1752	1.0	19	37.67	10.82	3.16	49.92
1858	1.0	17	32.82	13.36	3.17	50.41
1281	3.0	88	9.11	6.28	5.49	57.22
1411	3.0	74	16.44	8.09	4.68	54.79
1534	3.0	44	28.43	bad data	2.22	52.61
1618	3.0	38	33.27	23.21	2.68	48.22
1752	3.0	43	30.53	27.85	4.04	45.97
1858	3.0	39	25.64	22.58	3.31	47.00
1281	5.0	119	10.14	6.12	5.68	56.81
1534	5.0	66	21.23	1.70	2.55	54.92
1159	7.0	182	4.04	4.77	7.70	61.14
1281	7.0	153	10.30	5.86	5.53	54.11
1411	7.0	130	19.92	6.75	4.51	51.16
1534	7.0	88	27.40	9.68	3.54	53.68
1618	7.0	76	29.51	19.01	3.19	46.37
1752	7.0	84	30.04	18.67	3.15	45.43
1858	7.0	78	22.45	24.11	3.35	43.38

Knife River (Lignite)

Temperature (K)	Collection Height (inch)	Residence time (ms)	HCN	NH_3	N_{tar}	N_{char}
1159	1.0	46	0.00	2.05	2.36	86.25
1281	1.0	38	0.00	5.09	2.29	81.38
1411	1.0	33	7.91	10.79	1.72	78.21
1534	1.0	19	13.20	14.44	0.56	73.86
1752	1.0	19	25.19	18.79	1.89	62.51
1281	3.0	88	7.89	11.34	1.53	72.97
1411	3.0	74	17.68	17.45	1.27	65.45
1534	3.0	44	22.37	15.55	1.11	58.81
1858	3.0	39	30.21	bad data	1.89	bad data

1281	5.0	119	10.89	22.00	1.90	70.5
1534	5.0	66	8.98	12.34	1.40	57.7
1159	7.0	182	5.16	2.91	3.02	77.64
1281	7.0	153	7.19	5.64	2.21	71.45
1411	7.0	130	11.78	8.76	1.48	65.82
1534	7.0	88	22.00	14.83	1.21	53.68
1752	7.0	84	29.82	23.59	2.60	55.09

Appendix B Kinetic Scheme For Carbon Monoxide/Hydrogen/Air Combustion

The following Chemkin format mechanism was used in the simulation of the flat flame burner

```
! Data from Yetter R.A., Dryer F.L. and Rabitz H., " A comprehensive
! reaction mechanism for carbon monoxide/hydrogen/oxygen kinetics",
! Combust. Sci. Tech. v79, pp97-128, 1991
! J. Austin 6/24/99
! Two reactions were refitted to Arrhenius expression

ELEMENTS H   C   O   N  AR END

SPECIES  H2 H O2 O OH H2O HO2 H2O2 CO CO2 HCO N2 AR END

REACTIONS  KCAl/MOLE
! H2-O2 Chain Reactions
   H+O2=O+OH               1.900E14      0.00  16.44
   O+H2=H+OH               5.13E4        2.67  6.29
   OH+H2=H+H2O             2.14E8        1.51  3.43
   OH+OH=O+H2O             5.00E11       0.00  16.29
! refitted to Arrhenius expression
!H2-O2 Dissociation/Recombination Reactions
   H2+N2= H+H+N2           4.57E19       -1.40  104.38
   H2+AR=H+H+AR            5.89E18       -1.10  104.38
   O+O+N2=O2+N2            6.17E15       -0.50   0.00
   O+O+AR=O2+AR            1.91E13        0.00  -1.79
   O+H+M=OH+M              4.68E18       -1.00   0.00
   H+OH+N2=H2O+N2          2.24E22       -2.00   0.00
   H+OH+AR=H2O+AR          8.32E21       -2.00   0.00
! Formation and Consumption of HO2
   H+O2+N2=HO2+N2          6.76E19       -1.42   0.00
   H+O2+AR=HO2+AR          1.15E15        0.00  -1.00
   HO2+H=H2+O2             6.61E13        0.00   2.13
   HO2+H=OH+OH             1.70E14        0.00   0.87
   HO2+O=OH+O2             1.74E13        0.00  -0.40
   HO2+OH=H2O+O2           1.45E16       -1.00   0.00
! Formation and Consumption of H2O2
   HO2+HO2=H2O2+O2         3.02E12       0.00    1.39
   H2O2+N2=OH+OH+N2        1.20E17       0.00   45.50
   H2O2+AR=OH+OH+AR        8.51E16       0.00   45.50
   H2O2+H=H2O+OH           1.00E13       0.00    3.59
   H2O2+H=H2+HO2           4.79E13       0.00    7.95
   H2O2+O=OH+HO2           9.55E6        2.00    3.97
   H2O2+OH=H2O+HO2         7.08E12       0.00    1.43
! Oxidation of CO
   CO+O+N2=CO2+N2          2.51E13       0.00   -4.54
   CO+O+AR=CO2+AR          2.19E13       0.00   -4.54
```

```
   CO+O2=CO2+O             2.51E12       0.00   47.69
   CO+OH=CO2+H             5.00E12       0.00    9.91
!refitted to Arrhenius expression
   CO+HO2=CO2+OH           6.03E13       0.00   22.95
! Formation and Consumption of HCO
   HCO+N2=H+CO+N2          1.86E17      -1.00   17.00
   HCO+AR=H+CO+AR          1.86E17      -1.00   17.00
   HCO+O2=CO+HO2           7.59E12       0.00    0.41
   HCO+H=CO+H2             7.24E13       0.00    0.00
   HCO+O=CO+OH             3.02E13       0.00    0.00
   HCO+OH=CO+H2O           3.02E13       0.00    0.00
END
```

Appendix C Gas Temperature Correction

A type-B thermocouple was used to measure the centerline gas temperature profiles at different temperature settings in the flat flame burner. The measured temperature (bead temperature) was then corrected to account for radiation losses between the bead and the wall of the reactor. The correction is based on the energy balance on the thermocouple bead.

Assume the thermocouple bead has attained equilibrium and conduction along the bead wires is neglected, an energy balance can be established on the bead.

$$Q_{convection} = Q_{radiation} \tag{C.1}$$

$$hA_b(T_g - T_b) = A_b\sigma\varepsilon(T_b^4 - T_w^4) \tag{C.2}$$

so the actual gas temperature can be calculated by

$$T_g = T_b + \frac{\sigma\varepsilon(T_b^4 - T_w^4)}{h} \tag{C.3}$$

where h is the convective heat transfer coefficient, ε is the thermocouple bead emissivity, σ is the Stefan-Boltzmann constant, T_b is the bead temperature, T_w is the wall temperature and T_g is the actual gas temperature. Emissivity is assumed as 0.4, obtained from silica coating. A value of 500 K is used for the wall temperature. h can be calculated from the Nusselt number:

$$h = Nu(T_f)\ \frac{k_f(T_f)}{D_b} \tag{C.4}$$

where T_f is the film temperature in the boundary layer, k_f is the thermal conductivity of the gas evaluated at T_f, and D_b is the diameter of the bead. A value of 0.9 mm for D_b is used in the correction, as measured under a microscope. T_f is estimated by averaging the gas temperature and the bead temperature. k_f is calculated by weighing thermal conductivity of the three major components in the gas, namely CO_2, N_2 can CO. The individual thermal conductivity is estimated using a correlation developed by Mitchell [Mitchell, 1997 #121].

$$k_f = \sum_{i=1}^{3} x_i \quad k_i(T_f) = \sum_{i=1}^{3} x_i \quad a_i \quad 10^{-7} \quad T_f^{b_i} \tag{C.5}$$

The Nusselt number is estimated by a correlation with Reynolds number and Prandtl number in equation C.6.

$$Nu(T_f) = 2.0 + 0.6 \quad Re(T_f)^{1/2} \quad Pr(T_f)^{1/3} \tag{C.6}$$

$$Re(T_f) = \frac{D_b \nu_\infty \rho_f(T_f)}{\mu_f(T_f)} \tag{C.7}$$

$$Pr(T_f) = \frac{C_p(T_f) \quad \mu_f(T_f)}{k_f(T_f)} \tag{C.8}$$

where ν_∞ is the terminal velocity of the flowing gas, ρ is the density, C_p is the heat capacity and μ is the viscosity. ν_∞ is calculated using mass conservation and measured gas temperature. Density is estimated by assuming ideal gas behavior. Heat capacity is obtained using a polynomial correlation based on published gas properties . Finally, Viscosity is calculated using Mitchell's correlation. The coefficients used in the correlation are presented in Table C.1.

$$C_p = \sum_{i=1}^{3} x_i \quad C_{p,i}(T_f) = \sum_{i=1}^{3} x_i \quad \frac{(m_{i,1} \quad T_f^{\,2} + m_{i,2} \quad T_f + m_{i,3}) \quad 10^3}{M_i} \tag{C.9}$$

$$\mu_f = \sum_{i=1}^{3} x_i \quad \mu(T_f) = \sum_{i=1}^{3} x_i \; c_i \; 10^{-7} \; T_f^{d_i} \tag{C.10}$$

The bead temperature is first used to evaluate the gas properties in the boundary layer. Then the gas temperature is calculated iteratively using equation C.3 until a certain convergence criterion is reached. The corrected centerline gas temperature profiles can be found in Figure 4.4.

Table C.1 Coefficients Used in Equations

	CO_2	N_2	CO
a	2.3291	7.6893	7.3710
b	3.6078	3.6974	3.7486
c	3.6078	3.6974	3.7486
d	0.6756	0.6756	0.6756
m_1	-4E-6	0.0185	40.15
m_2	-2E-6	0.0093	25.449
m_3	-2E-6	0.009	26.211

Appendix D Ash Content in the Tar or Soot Samples

Table D.1. Ash Content in the Tar or Soot Samples.

sample	temperature (K)	sampling location (inch)	residence time (ms)	ash content
biphenyl	1365	3		76.5%
	1410	3		70.0%
pyrene	1410	3		10.1%
	1460	3		7.94%
	1470	3		35.4%
Illinois #6	1159	1	46	0
	1752	1	19	0.52%
	1752	3	43	0.85%
Utah	1411	7	130	-1.56%
	1752	7	84	-0.49%
Black Thunder	1159	1	46	-4.14%
	1752	7	84	-0.68%
	1858	7	78	1.25%
Knife River	1281	3	88	14.43%
	1752	7	84	11.90%
	1858	3	39	8.58%

Appendix E Error Analysis

Since nitrogen evolution during coal pyrolysis was the major topic in this study, the error analysis was focused on the nitrogen measurements in the experiment. Variations of the nitrogen measurements were caused by the following three reasons:

1. Sample to sample variations

Variations of tar/soot yields and char yields under a pyrolysis condition can be estimated by replicate pyrolysis experiments.

2. Sample characterization techniques on solid samples

Variability associated with sample characterization techniques can be assessed by replicate analysis on a single sample. Elemental analysis and ICP are the two major analysis techniques that introduce errors in the nitrogen measurements in the solid samples. Elemental analysis directly gives the variations of the nitrogen content in the tar/soot and in the char. Uncertainty of the nitrogen fraction in the char was introduced indirectly by the ICP measurements, since the char yield was determined by ICP.

3. Gas analysis using FTIR

Replicate FTIR analyses give some indication of the repeatability of the nitrogen concentrations in the gas phase.

An error analysis was performed on each the above three categories to assess the uncertainty of the nitrogen measurements in the experiment. In order to compare the

variability associated with each category, relative standard deviation (σ_r) defined in equation (E.1) is used in the discussion.

$$\sigma_r = \frac{\sqrt{\frac{1}{n-1}\sum_{i=1}^{n}\left(x_i - \bar{x}\right)^2}}{\bar{x}} \qquad \text{(E.1)}$$

where n is the total number of replicates, x_i is the value of the ith replicate, and $\bar{x}$ is the mean value of all replicates.

Sample to Sample Variations

Table E.1 shows the tar/soot yields and the char yields from two replicate pyrolysis experiments using the Illinois #6 coal. The first two columns represent the measured tar/soot yields and char yields collected at 1 inch height in the 1159 K condition, while the last two columns represent the corresponding results collected at 3 inch height in the 1534 K condition. A large amount of variation associated with tar/soot yields is observed from the table. The relative standard deviation of the tar/soot yields is

Table E.1. Replicate Sample Collection in the Flat Flame Burner using the Illinois #6 coal.

	Replicate 1	Replicate 2	Replicate 1	Replicate 2
sample collection date	10/18/99	1/15/00	6/16/98	12/9/99
temperature (K)	1159	1159	1534	1534
residence time (ms)	46	46	44	44
tar/soot yields (wt% of daf coal)	17.03	14.04	10.96	13.32
char yields (wt% of daf coal)	62.37	65.26	43.69[#]	41.48
Relative standard deviation				
tar/soot yields	13.6%		13.7%	
char yields	3.20%		3.67%	

[#]: The original char yield is incorrect due to the break down of the ICP, the value reported here is the char yield of the closet condition at 1411 K.

as high as 14%, while the relative standard deviation of the char yields is less than 4%. The variations in char yield is the combined effects of the ICP analysis and experiment replication. The large uncertainty in the tar/soot yields is thought to be caused by the significant tar or soot loss in the sample collection system. Ma (1996) reported a 15% soot loss in the sample collection system in the FFB at higher temperatures (above 1650 K). In this study, the tar or soot loss is expected to be even higher for the low temperature pyrolysis experiments, as described in Chapter 8. Although extreme care has been taken to collect all the tar or soot samples in the experiments, an accurate estimation of the tar or soot loss due to deposition on the walls of the collection tube is almost impossible.

Elemental Analysis of the Solid Samples

Table E.2 shows the variations associated with elemental analysis of the Illinois #6 coal, char and soot, respectively. The char and soot samples collected at 44 ms in the 1534 K condition were chosen for the error analysis due to the long period (nearly two years) between the two replicate sample collection and elemental analysis. The first two columns show the CHNS analysis on the parent coal. The first columns present the results performed at BYU and the second column present the results performed at Galbraith Laboratories in Knoxville, Tennessee. The variations caused by the CHNS analysis are really small for the parent coal. For carbon, hydrogen and nitrogen, the relative standard deviations are less than 1%. In addition, the relative differences between the measurements of C, N, and S performed at BYU and those determined at Galbraith laboratory are less than 2%; for oxygen, the difference is less than 4%. The difference is a little bit high for hydrogen, at about 6%. The elemental analysis

Table E.2. Replicate CHNS analysis on the Illinois #6 parent coal, char and soot.

Sample	Coal	Coal	Char	Char	Soot	Soot
	Rep. 1 (BYU)	Rep. 2 (Galb. lab.)	Rep. 1	Rep. 2	Rep. 1	Rep. 2
Analysis date	4/30/98	7/13/00	6/18/98	4/21/00	6/18/98	4/21/00
temperature (K)			1534	1534	1534	1534
residence time (ms)			44	44	44	44
mean value						
C%	76.00±0.46[a]	75.68	91.17±0.55	92.73±0.06	90.41±1.01	93.63±0.52
H%	5.48±0.05	5.16	1.97±0.05	1.70±0.02	2.17±0.14	1.73±0.05
N%	1.52±0.01	1.50	1.63±0.01	1.62±0.03	0.85±0.01	0.77±0.02
S%	4.68±0.08	4.64	3.17±0.19	2.88±0.03	1.81±0.25	1.66±0.02
O%	12.32	12.78	2.06	1.07	4.76	2.21
relative standard deviation						
C%	0.61%		0.75%	0.08%	1.11%	0.55%
H%	0.91%		3.12%	0.01%	6.52%	2.78%
N%	0.66%		0.89%	0.02%	1.46%	1.96%
S%	1.71%		7.36%	0.01%	13.6%	1.25%

[a] Uncertainty measurements represent the standard deviation as calculated from 5 replicate elemental determinations of a single sample.

procedures performed at BYU and Galbraith laboratory are similar. The only difference is that the samples were dried under vacuum overnight before the analysis at Galbraith laboratory, while the samples were dried in an oven at 105°C for two hours at BYU, therefore, the difference between the hydrogen analysis is how moisture is measured. The ^{13}C NMR analysis on the coal samples showed that the procedure used in Galbraith laboratory is better for the determination of the hydrogen content (Solum, et al. 2000).

Columns 3 and 4 in Table E.2 show the elemental analysis on the char samples, and columns 5 and 6 show the results on the soot samples. These results show an excellent repeatability during the CHNS analysis performed on the same day. The relative standard deviation for samples analyzed consecutively in the analyzer is usually

less than 3% for carbon, hydrogen and nitrogen. As seen from the table, the elemental composition is also similar for char or soot samples collected on different days. For the char, the difference is less than 1% (relative) for nitrogen; for the soot, the difference is about 10% (relative) for nitrogen. The relative difference between the measurements in the char and soot is about 20% for hydrogen and 50% for oxygen. It should be noted that oxygen is determined by subtracting the summation of carbon, hydrogen, nitrogen and sulfur in this study. This practice is subject to a lot of errors, therefore it cannot be used to obtain accurate results for oxygen for severely pyrolyzed samples where the oxygen content is small. The reason for the large difference in hydrogen content for samples collected at different date is unclear at this time. However, the results did show that the uncertainty introduced by the elemental analyzer is much smaller than that caused by sample collections.

Gas Phase Analysis Using FTIR

The replicate HCN and NH_3 concentrations measured in the FFB during pyrolysis of the Utah and Black Thunder coals are presented in Table E.3. The two conditions presented here were chosen randomly and represented the average variations in the gas phase analysis using the FTIR system. The relative standard deviation was calculated from the seven replicates measurements performed on the same day. The relative standard deviation is about 10% for HCN and about 15% for NH_3. Possible sources of the variations of the measured concentrations include variations in a) coal heterogeneity; b) coal feed rate; and c) FTIR analysis, including calibration and quantitative analysis. Considering the extremely low concentrations of HCN and NH_3 (ppb-level) and large amounts of burning gases (strong IR absorbers that significantly interfere with the

measurements of other weakly absorbed species) in the FFB, the results are considered excellent.

Table E.3. Replicate FTIR Measurements of HCN and NH_3 in the FFB.

	HCN (ppm)	NH_3 (ppm)	HCN (ppm)	NH_3 (ppm)
coal	Utah	Utah	Black Thunder	Black Thunder
sample collection date	10/2/99	10/2/99	11/24/99	11/24/99
temperature (K)	1752	1752	1281	1281
residence time (ms)	84	84	119	119
Rep. 1	2.087	0.522	0.376	0.216
Rep. 2	2.139	0.443	0.357	0.242
Rep. 3	2.151	0.518	0.453	0.202
Rep. 4	2.365	0.704	0.419	0.215
Rep. 5	2.466	0.656	0.378	0.262
Rep. 6	2.263	0.570	0.347	0.251
Rep. 7	1.921	0.461	0.458	0.294
mean value	**2.199**	**0.553**	**0.398**	**0.240**
relative standard deviation	**8.28%**	**17.5%**	**11.3%**	**13.3%**

Summary

The error analysis shows that three major reasons caused the variations in the nitrogen measurements in this study. Replicate sample collection introduced about 15% (relative) uncertainties in tar/soot yields. ICP analysis combined with replicate sample collection introduced about 4% (relative) uncertainties in char yields. Elemental analysis is the most accurate sample characterization techniques used in the current study, with only 2% relative standard deviation for nitrogen in the tar/soot and char. Gas phase measurements by FTIR are accurate to within 10% (relative) for HCN and 15% (relative) for NH_3.